



The University of
Nottingham

UNITED KINGDOM • CHINA • MALAYSIA

**Redox Mediators for Thermoelectrochemical
Cells and Electroanalysis of Quinones in Protic
Ionic Liquids**

By:

Peter A Greatorex-Davies

Supervisors:

Dr. Darren A Walsh, Prof. Jairton Dupont

Thesis submitted to the University of Nottingham for the degree
of Doctor of Philosophy

September 2021

Abstract

Thermoelectrochemical cells offer promising prospects for future harvesting of waste heat in many areas, such as; power stations, geothermal energy and in devices utilising human body heat. There are two main sets of devices currently used in these areas. The most widely used devices are solid-state thermoelectric cells, but these suffer from low Seebeck coefficients, expensiveness of parts and lack of flexibility. Thermoelectrochemical devices utilising aqueous electrolytes are also used, however, under normal conditions these are limited to operating temperatures below 75°C.

In this report investigations have been conducted for several redox mediators dissolved in aqueous or ionic liquid electrolyte for use in thermoelectrochemical cells. Both aqueous $[\text{Fe}(\text{CN})_6]^{3-/4-}$ and $\text{I}^-/[\text{I}_3]^-$ redox couples showed reasonably similar results to the literature, and in both cases a good power output was obtained similar to that found in the literature. The Results for the non-aqueous $\text{I}^-/[\text{I}_3]^-$ solutions showed a decreased performance both in terms of Seebeck coefficient and maximum power output.

For the Q/QH_2 redox couple this trend was the same with the aqueous results again providing a better performance than for the IL solutions. This is in spite of the lower analyte concentration due to the limit in solubility of Q in water.

Investigations for $\text{Fe}(\text{acac})_{2/3}$, $\text{V}(\text{acac})_3/\text{VO}(\text{acac})_2$ have also been carried out in triethylammonium trifluoroacetate ($[\text{tea}][\text{TFAc}]$). The $\text{Fe}(\text{acac})_{2/3}$ solution showed the best S_e of 1.53 mV K⁻¹ at temperatures up to 30 °C, which is comparable to that of the benchmark system, aqueous $[\text{Fe}(\text{CN})_6]^{3-/4-}$, at the

same concentrations. However, instabilities of the species led to very poor performance when attempting to generate useful power outputs.

The electrochemistry of quinones has been investigated in a wide variety of solutions and even in water, shows significant complexity. The variation in voltammetric response lies in the key role of protons in the reduction of Q to QH₂. In well buffered water this reduction reaction is a simple reversible two electron wave. However, in unbuffered water and other non-aqueous media insufficient protons in the system result in other deprotonated forms becoming present.

Here investigations of the Q/QH₂ mechanism in Protic Ionic Liquids (PILs) reveal different processes occurring in PILs synthesised with a strong acid, such as diethylmethylammonium triflate ([dema][TfO]) and PILs synthesised with a weaker acid, such as [tea][TFAc]. In [dema][TfO] the several Q/QH₂ redox waves are observed corresponding to different electrochemical processes. These separate waves are concluded to be due the protons being sourced from the acid, hydronium ions, and the base, with QH₂ and QH⁻ being products of the Q reductions. By adding acid, the waves eventually merge to form a single, two-electron reduction of Q to QH₂.

For [tea][TFAc], the results behave as a buffered aqueous system, and when adding either acid or base the voltammetry does not change significantly and remains a two-electron reduction to QH₂.

These results demonstrate the usefulness of Q/QH₂ voltammetry in characterising the acid content in various PILs with even small changes in the systems resulting in significant observable changes in the observed redox reactions.

Declaration

This thesis is the result of my own investigations, and is not being concurrently submitted in candidature for any degree

Signed _____

Date _____

Acknowledgements

Firstly, I would like to thank my supervisor Dr. Darren Walsh for giving me the opportunity to work on this project and for his guidance along the way. I would also like to thank Prof. Jairton Dupont for his help in the early stages of this project.

I would like to thank all the members of the Walsh group and friends who have been fantastic to work with and always supportive. Andinet, Sayyar, Saddam, Helena, Fiona, Matt, Cath, Thais, Pedro, Grace, Astrid, Neelam, Lais, Josh, Rosie, Lyndsey, Marco, Carlos, Justine, Conrad, Rory, Kostas, Bhaskar and Sue. A particular thank you to Sean and Dan, who's support, and discussions of various topics have been invaluable and have helped me through the more difficult and frustrating times.

I would like to thank the many friends who have supported me throughout this and helped me get through it. Particularly to Paul and Steve, who have supported me through various points of my PhD and have always been encouraging.

I would like to thank my family, particularly my mum and dad who have been so supportive for me and helped me throughout my PhD. To my wife, Sarah, who's endless support and love has been incredible.

Finally, to my God who has helped me through this experience, I don't know where I would be without my faith and trust in him.

Abbreviations and Symbols

Abbreviation	Meaning	Units
<i>A</i>	Electrode area	cm^2
acac	Acetylacetone	
AIL	Aprotic Ionic Liquid	
a_{ox}	Activity of oxidised species	
a_{red}	Activity of reduced species	
[BMPy][NTf ₂]	1-butyl-3-methylpyrrolidinium bis(trifluoromethanesulfonyl) imide	
<i>C</i>	Concentration of redox species	mol dm^{-3}
[C ₁₀₁ C ₁ Im] [NTf ₂]	1-(2-methoxyethyl)-3-methyl imidazolium bis(trifluoromethanesulfonyl) imide	
CE	Counter Electrode	
<i>D</i>	Diffusion coefficient	$\text{cm}^2 \text{s}^{-1}$
<i>d</i>	Electrode diameter	cm
	<i>or</i>	
	Density	g cm^{-3}
DCM	Dichloromethane	
[dema][TfO]	Diethylmethylammonium triflate	
DiBoyFc	Dibutanoyl ferrocene	
[dmba][TfO]	Dimethylbutylammonium triflate	
DMF	Dimethylformamide	
DMSO	Dimethylsulfoxide	
D_{ox}	Diffusion coefficient of oxidised species	$\text{cm}^2 \text{s}^{-1}$
D_{red}	Diffusion coefficient of reduced species	$\text{cm}^2 \text{s}^{-1}$
<i>E</i>	Measured electrode potential	V
E°	Standard electrode potential	V
ΔE	Potential difference	V

$E_{1/2}$	Half wave potential	V
E_f	Formal potential	V
E_{Fer}	Fermi level	V
E_{mid}	Midpoint potential between redox peaks	V
ΔE_p	Peak-to-peak potential separation	V
[EMIm][BF ₄]	1-ethyl-3-methylimidazolium tetrafluoroborate	
F	Faraday constant	C mol ⁻¹
Fc	Ferrocene	
ΔG°	Gibbs free energy	J mol ⁻¹
GC	Glassy-Carbon	
ΔH°	Enthalpy change	J mol ⁻¹
HTFAc	Trifluoroacetic acid	
HTfO	Triflic acid	
i	Current	A
IL	Ionic Liquid	
i_p	Peak current	A
i_{ss}	Steady-state current	A
j	Current density	$\mu\text{A cm}^{-2}$
MeCN	Acetonitrile	
n	Stoichiometric number of electrons	
NMR	Nuclear Magnetic Resonance	
OCP	Open circuit potential	V
P	Power	W
[P _{2,2,2} (101)] [NTf ₂]	Triethylmethoxymethylphosphonium bis(trifluoromethanesulfonyl) imide	
PC	Propylene carbonate	
P_D	Power density	$\mu\text{W cm}^{-1}$
PIL	Protic ionic liquid	

P_{max}	Maximum power density	$\mu\text{W cm}^{-1}$
ppm	Parts per million	
Pyr	Pyridine	
Q	1,4-benzoquinone	
QH ₂	Hydroquinone	
R	Gas constant	$\text{J K}^{-1} \text{mol}^{-1}$
r	Electrode radius	cm
RE	Reference Electrode	
ΔS°	Entropy change	$\text{J K}^{-1} \text{mol}^{-1}$
SCE	Standard Calomel Electrode	
S_e	Seebeck coefficient	mV K^{-1}
SSTC	Solid-State Thermocell	
T	Absolute Temperature	K
ΔT	Temperature difference	K
T_C	Temperature of cold electrode	$^\circ\text{C}$
T_H	Temperature of hot electrode	$^\circ\text{C}$
TEC	Thermoelectrochemical Cell	
t	Time	s
[tea][TFAc]	Triethylammonium trifluoroacetate	
WE	Working Electrode	
Z	Figure of merit	K^{-1}
α	Transfer coefficient	
δ	Chemical shift	ppm
η	Viscosity	mPa s
κ	Thermal conductivity	$\text{W m}^{-1} \text{K}^{-1}$
ν	Scan rate	V s^{-1}
σ	Electrical conductivity	S m^{-1}
τ	Dimensionless time	

Table of contents

Chapter 1.....	1
1.1 Thermoelectrochemical Cells.....	1
1.2 Investigations of Thermoelectrochemical Cells.....	5
1.3 Electrochemistry of Quinones.....	13
1.3.1 Stability of Quinones in Solution.....	15
1.3.2 Quinones in Buffered or Acidic Aqueous Solution.....	16
1.3.3 Quinones in Unbuffered Aqueous Media.....	19
1.3.4 Quinones in non-aqueous systems.....	22
1.4 Ionic Liquids.....	25
1.5 Project Objectives.....	27
1.6 References.....	29
Chapter 2.....	34
2.1 Electrochemical Theory.....	34
2.2 Electroanalysis.....	35
2.2.1 Cyclic Voltammetry.....	39
2.2.2 Chronoamperometry.....	44
2.3 The Seebeck Effect.....	47
2.3.1 Thermoelectrochemical measurements.....	48

2.4 References.....	50
Chapter 3.....	51
3.1 Introduction.....	51
3.2 Ionic Liquid Synthesis	51
3.2.1 Proton Nuclear Magnetic Resonance	53
3.2.2 Fourier-Transform Infrared Spectroscopy	56
3.2.3 Cyclic Voltammetry of the Protic Ionic Liquids	57
3.2.4 Viscosity and Density Measurements	60
3.3 Thermoelectrochemical Setup	61
3.4 Potassium Ferri/ferrocyanide	63
3.4.1 Electrochemical studies.....	64
3.4.2 Thermoelectrochemical studies.....	64
3.4.3 Power measurements	65
3.5 Conclusions.....	68
3.6 References.....	69
Chapter 4.....	70
4.1 Background.....	70
4.2 Experimental	72
4.2.1 Chemicals	72

4.2.2 Electrochemical measurements.....	73
4.3 Results and Discussion	75
4.3.1 Electrochemistry of Q and QH ₂ in [dema][TfO]	75
4.3.2 Effect of Excess Acid on the [dema][TfO] solutions.....	83
4.3.3 Effect of excess base on the [dema][TfO] solutions	89
4.3.4 Effect of additional water on the [dema][TfO] solutions.....	92
4.3.5 Electrochemistry of Q and QH ₂ in [tea][TFAc]	93
4.3.6 Electrochemistry of Q and QH ₂ in [tea][TfO]	96
4.4 Conclusions.....	99
4.5 References.....	100
Chapter 5.....	102
5.1 Background.....	102
5.2 Experimental	105
5.2.1 Chemicals	105
5.2.2 Electrochemical measurements.....	106
5.3 Electrochemical studies.....	107
5.4 Thermochemical studies.....	113
5.4.1 Power measurements	117
5.5 Conclusions.....	122

5.6 References.....	123
Chapter 6.....	124
6.1 Background.....	124
6.2 Experimental	126
6.2.1 Chemicals	126
6.2.2 Electrochemical measurements.....	126
6.3 Results and discussion.....	127
6.3.1 Electrochemical Studies	127
6.3.2 Thermochemical studies.....	130
6.3.3 Power Measurements	132
6.4 Conclusions.....	134
6.5 References.....	135
Chapter 7.....	136
7.1 Background.....	136
7.2 Experimental	138
7.2.1 Chemicals	138
7.2.2 Electrochemical studies.....	138
7.3 Results and discussion.....	139
7.3.1 Electrochemical Studies of Iron acetylacetonates.....	139

7.3.2 Electrochemical Studies of Vanadium acetylacetonates	142
7.3.3 Thermoelectrochemical studies of acetylacetonates	143
7.4 Conclusions.....	147
7.5 References.....	147
Chapter 8.....	149
8.1 Conclusions.....	149
8.2 Future Work	153

Chapter 1

Introduction and Literature Review

1.1 Thermoelectrochemical Cells

Every year vast amounts of energy is lost as low grade waste heat, which is typically quoted as waste heat below 150°C.¹ There is huge potential, therefore, in devices that can convert this heat into useful energy. Thermoelectric devices are of particular scientific interest because of their ability to directly convert this thermal energy into electrical energy under continuous operation and because of their lack of moving parts.^{2, 3} In recent years research in this area has been primarily focused on Solid-State Thermocells (SSTCs).⁴ These devices utilise differences in applied heat between p and n-type semiconductor materials.¹ Energy is output as a consequence of the Seebeck effect. This effect states that a temperature difference between two electrodes induces a potential difference between these electrodes. When connected to an external circuit this generates a current output. This relationship between the potential and the temperature of these devices is described by the Seebeck coefficient, S_e :²

$$S_e = \frac{\partial E(T)}{\partial T} = \frac{\Delta S^\circ}{nF} \quad (\text{Eq. 1.1})$$

Where $E(T)$ is the potential difference as a function of the temperature, T . ΔS is the entropy of the reaction, n is the number of electrons transferred and F is the faraday constant. The efficiency of such devices can be evaluated using the dimensionless figure of merit, ZT :⁵

$$ZT = \frac{S_e^2 T \sigma}{\kappa} \quad (\text{Eq. 1.2})$$

Where σ and κ are the electrical and thermal conductivities respectively of the materials. Eq. 1.1 shows the efficiency of these devices has a high dependence on S_e . Finding systems with high S_e values is therefore one of the key components to maximising energy outputs.

SSTCs typically only have Seebeck coefficients of the order of 10s of $\mu\text{V K}^{-1}$, which is a major limiter to the maximum achievable efficiencies of such devices.⁶

⁷ In addition, large electrical conductivities have a tendency to be coupled with large thermal conductivities, and thus this further limits the efficiencies these devices can achieve.⁸

Thermoelectrochemical Cells (TECs), which use liquid electrolytes instead of solid-state semiconductors, show promise in overcoming some of these issues. These devices still utilise the Seebeck effect, however they can have S_e values of the order of mV K^{-1} , several orders of magnitude higher than for SSTCs.¹ TECs also

have lower thermal conductivities than their solid-state counterparts.⁸ This allows higher temperatures, and thus higher potential differences, to be maintained.^{3, 9} Since TECs use liquid electrolytes they also have the added advantages of being able to be designed with more flexibility and being more scalable, allowing for a wider range of applications.¹⁰ They also do not rely on expensive metalloids, such as Bi_2Te_3 , which are found in SSTCs.¹¹

The main drawback with TECs is that these devices have far lower electrical conductivities than SSTCs and ZT values often suffer as a result despite the larger Seebeck coefficients and lower thermal conductivities.

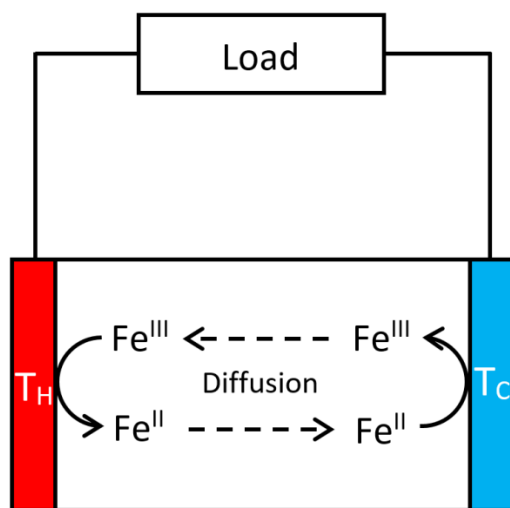


Fig. 1.1: Schematic of a TEC with a single redox couple, $\text{Fe}^{\text{II}}/\text{Fe}^{\text{III}}$, in solution. Two electrodes are held at different temperatures, T_H and T_C , leading to a potential difference building up between the two electrodes.

A schematic of a TEC is shown in Fig. 1.1. In a TEC, one side of the cell is connected to a heat source, while the other end is kept at a lower temperature (usually ambient). The most common setup in recent devices is a cell containing

two inert electrodes, such as Pt, and a single redox couple in solution. Since the chemical equilibrium at an electrode shifts with temperature, maintaining a temperature difference leads to a difference in equilibrium, and thus a potential difference, between these electrodes.

In the case of the Fe^{II/III} redox reaction, where the Seebeck is positive,^{12, 13} the reduction reaction is more favourable at the hot electrode and oxidation at the cold. This leads to a net build-up of Fe^{II} at the hot electrode and Fe^{III} at the cold. As the concentration of these species increases at the respective electrodes, the concentration gradient results in net diffusion of the species across the solution to the opposite electrodes. These two processes continue to occur and eventually an equilibrium is reached with a stable potential difference between the two electrodes.

Under discharge conditions the larger current output results in a reduction in this potential difference. The system then acts continuously to counteract this drop potential difference and will stabilise at a lower potential difference. The equilibrium potential difference at a set current output will depend largely on the rate of ion movement through the solution and the kinetics of the reaction at the electrodes.

For TECs involving inert electrodes and a single solution-based redox couple the main interaction between the solution and the electrodes is the exchange of electrons. Since there are also no moving parts in these devices it means these

cells can operate for long periods of time without a significant decrease in performance.¹²

1.2 Investigations of Thermoelectrochemical Cells

The earliest studies of TECs date back to 1825,¹⁴ just after the discovery of the Seebeck effect in 1821.⁶ However it was not until the 1960s and 70s when wider attention was paid to these devices.¹² Early research was primarily focused on TECs utilising high temperature molten salts,^{12, 15-23} these included AgNO_3 ,¹⁵ Bi-halides¹⁶ and AgCl .¹⁷ The high temperatures used in these early devices allows for high voltages to be obtained which lead to large energy outputs.¹² However, the high temperatures required, which include far higher than ambient temperatures at the colder electrode, limit the useful application of such devices and prevents them being useful for harvesting low-grade waste heat. Another key disadvantage in these systems is that the electrode materials are directly involved in the reactions and continuous use of the devices causes permanent alterations to the electrodes.¹² This creates problems for long term use.

More recent studies have primarily focused on the use of a redox couple dissolved in aqueous electrolytes with noble metals or carbon materials as electrodes.⁹ One of the earliest studies in this area was conducted by Burrows in 1975.¹² He investigated $[\text{Fe}(\text{CN})_6]^{3-/4-}$ dissolved in 0.5 M K_2SO_4 solution, which produced a Seebeck coefficient of -1.4 mV K^{-1} . This was higher than the system of $\text{Fe}^{\text{II/III}}$ dissolved in an HCl solution ($+0.6 \text{ mV K}^{-1}$) that he had previously

investigated. When testing the power output of a cell with an electrode separation of 25 cm, Burrows found that the power output increased linearly with increasing concentration of the redox couple and at 0.4 M $[\text{Fe}(\text{CN})_6]^{3-/4-}$ (concentration of each species = 0.2 M) the maximum power density was $93 \mu\text{W cm}^{-2}$ at $\Delta T = 50 \text{ K}$. The $\text{Fe}^{II/III}$ couple that he investigated was able to reach 4 M, far more soluble than $[\text{Fe}(\text{CN})_6]^{3-/4-}$. However, the lower S_e meant the maximum power obtained for the $\text{Fe}^{II/III}$ couple was just $42 \mu\text{W cm}^{-1}$ at $\Delta T = 50^\circ\text{C}$. This shows the high importance of selected species having higher S_e values, even if it occurs at the expense of a lower solubility.

The $[\text{Fe}(\text{CN})_6]^{3-/4-}$ system has since been widely studied in aqueous systems^{3, 5, 10, 18, 24-28} with calculated S_e values predominantly -1.4 mV K^{-1} but have been quoted in the range of -1.1 to -1.66 mV K^{-1} .^{5, 18} One major factor in these differences is the concentration of the active species. Dilute electrolytes generally show an increased S_e and the value of -1.66 mV K^{-1} was measured in a dilute solution of 15 mM of each species.¹⁸ However, above 0.2 M the value of S_e becomes more stable.¹⁸ Although higher values for S_e can be obtained, this affects the maximum current outputs for a cell and at these lower concentrations the maximum power, P_{max} , generally decreases.

The reasonably high S_e coupled with the good reversibility, stability and wide characterisation of this redox couple has led to a 0.4 M $[\text{Fe}(\text{CN})_6]^{3-/4-}$ solution being widely considered as the benchmark for aqueous TECs.^{5, 29}

Many other aqueous electrolytes have also been investigated for use in TECs. Common redox couples include Cu complexes,^{14, 18} $I^-/[I_3]^-$,^{1, 5, 30} and Br_2/Br^- .^{31, 32} Kuzminskii et al.¹⁸ studied several Cu complexes as well as $CuSO_4$ in aqueous solutions. They found that a $Cu(bipy)_2^{+2}$ (bipyridine ligand) couple gave the highest Seebeck coefficient of -2.5 mV K^{-1} , which was at $\Delta T = 27 \text{ K}$. However, the concentrations in this case were just 0.1 mM for both redox species and for the supporting electrolyte, which will mean the maximum power outputs will be relatively small. Alzahrani et al.⁵ investigated $I^-/[I_3]^-$ in two different cells. One cell contained Pt electrodes while the second utilised stainless-steel electrodes. The Pt cell produced a Seebeck coefficient of just $+0.26 \text{ mV K}^{-1}$. When using the stainless-steel cell this value increased dramatically, reaching a maximum of $+13.6 \text{ mV K}^{-1}$ at $\Delta T = 10^\circ\text{C}$. This value dropped considerably at higher temperatures and at $\Delta T = 50^\circ\text{C}$ it was $+1.8 \text{ mV K}^{-1}$. This effect appears to be due to the direct involvement of the stainless-steel electrodes in the reaction. The electrode corroded over time and the potential difference of the electrode dropped from 136 to 89 mV between these two temperatures. This suggests that this high S_e is only a short lived and long-term use would likely result in a decrease in the performance of the cell.

One of the main problems with aqueous electrolyte is that the boiling point of water limits the maximum achievable temperature difference, with optimal operating temperatures between 25 and 75°C .³ This restriction can be overcome by using high pressure systems such as the one used by Ikeshoji et al.,²⁷ however

this presents added problems such as the need for a specialised air tight cell to avoid leaking.

Several groups therefore moved towards studying organic solvents for use as TEC electrolytes.^{1, 6, 18, 33} Some of these liquids, such as γ -butyrolactone (204 °C) and 1-dodecanol (259 °C), can have boiling points >200°C. Kuzminskii et al.¹⁸ tested $\text{Cu}(\text{bipy})_2^{+/2+}$ in a solution of 1 M LiBF_4 dissolved in the γ -butyrolactone. They report $S_e = -4.17 \text{ mV K}^{-1}$ with 1 mM concentrations of each of the redox species, which is higher than that for the aqueous system. Bonetti et al.⁶ obtained $S_e = +7.16 \text{ mV K}^{-1}$ for a 0.1 M solution of tetrabutylammonium nitrate in 1-dodecanol which is one of the highest S_e values recorded to date. Despite the large Seebeck coefficient, the figure of merit calculated from this system was calculated to be an order of magnitude below that of the aqueous $[\text{Fe}(\text{CN})_6]^{4-/3-}$ system. This was mostly attributed to the lower electrical conductivity of the solution.

Despite the higher boiling points of some of these organic solvents they still generally have relatively high vapour pressures, which still presents a drawback.³ Ionic liquids (ILs) are another alternative to aqueous systems. These are salts that are liquid at below 100 °C and often have thermal stabilities of above 300°C and generally have low vapour pressures¹. This makes them a promising candidate for devices utilising higher temperature waste heat. An added advantage of ILs is that they have a good intrinsic conductivity, which means that no supporting electrolyte is necessary.³⁴

Many groups have therefore moved towards investigating ILs based electrolytes for this application.^{1, 2, 8, 11, 13, 29, 33, 35, 36} One of the earliest studies of S_e values in ILs was conducted by Migita et al.¹³ They study a range of Fe and Cr based redox couples in the IL 1-butyl-1-methylpyrrolidinium bis(trifluoromethanesulfonyl) imide ($[C_4C_1Py][NTf_2]$). The highest S_e in this liquid was for 0.1 M $[Fe(CN)_6]^{4-/3-}$ where the value was -1.49 mV K^{-1} , which is similar to the value in water. The $Fe^{2+/3+}$ system quoted shows a high improvement of $S_e = +0.96 \text{ mV K}^{-1}$, which is more than 50% larger than that for the couple in aqueous electrolyte investigated by Burrows.¹² Migita et al. observed that S_e depended highly on the ion size and the magnitude of the charge, which suggests that electrostatic interactions with the surrounding IL ions are responsible for these large changes in S_e with a high charge and low size generally being favourable.

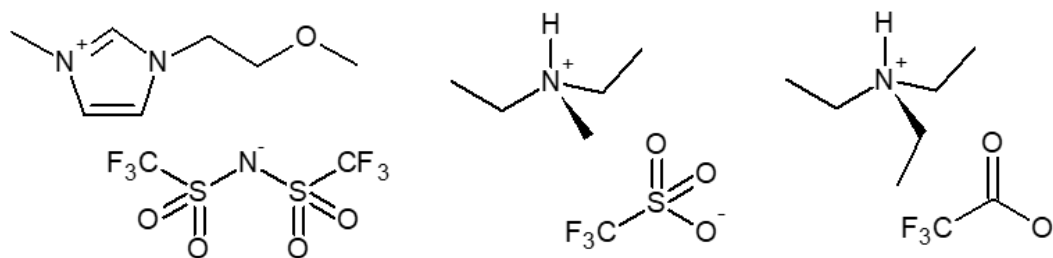


Fig. 1.2: Some ILs used in the present study. From left to right 1-(2-methoxyethyl)-3-methyl imidazolium bis(trifluoromethanesulfonyl)imide ($[C_{102}C_1Im][NTf_2]$), diethylmethylammonium triflate ($[dema][TfO]$) and triethylammonium trifluoroacetate ($[tea][TFAc]$).

The $I^-/[I_3]^-$ redox couple has been investigated by several groups for this application and has been shown to be soluble in a wide variety of solvents with reasonably reversible electrochemistry.^{1, 2, 5, 8, 11, 30, 37, 38} This widespread solubility

has made it suitable for analysis in many different ILs allowing for a comparison of the effect different ILs on the Seebeck coefficient of this species. Abraham et al.¹ investigated 0.4 M $I^-/[I_3]^-$ in a range of ILs, comparing them to values in water and in methoxypropionitrile. They found that the aqueous system produced the highest S_e of +0.53 mV K⁻¹. This was over double that of 1-ethyl-3-methylimidazolium tetrafluoroborate ($[C_2C_1Im][BF_4]$) (+0.26 mV K⁻¹), the highest S_e in any IL studied. This in turn was far higher than for the IL with the lowest S_e (+0.03 mV K⁻¹), which was $[P_{2,2,2,(101)}][NTf_2]$ (triethylmethoxymethylphosphonium cation). Siddique et al.³⁸ investigated the $I^-/[I_3]^-$ redox couple in a range of protic ILs, with the highest Seebeck coefficient being +0.42 mV K⁻¹ in tri(2-ethylhexyl)ammonium trifluoroacetate. Although still lower than for the aqueous system this value is significantly higher than for $[EMIm][BF_4]$.

Recently Anari et al.¹¹ have investigated combining redox couples in order to maximise S_e in the ionic liquid $[C_2C_1Im][NTf_2]$. They investigate various combinations of Ferrocene/Ferrocenium (Fc/Fc^+) and $I^-/[I_3]^-$ in this IL. A simple mixing of these two couples gave $S_e = +0.813$ mV K⁻¹. This is far higher than the values for either Fc/Fc^+ (+0.100 mV K⁻¹) or $I^-/[I_3]^-$ (+0.057 mV K⁻¹) in this IL. The highest value they gave was $S_e = +1.669$ mV K⁻¹, which was produced by adding a dibutanoyl chain onto Fc ($[DiBoylFc][I_3]$).

Aside from the electrolytes themselves, there have also been several studies investigating various electrode materials for these systems.^{4, 28, 29, 31, 32, 35, 39-41} Shindo et al.³¹ investigated an aqueous Br_2/Br^- system using non-graphitised

carbon electrodes. They report an S_e value of $+5.68 \text{ mV K}^{-1}$ for a saturated Br_2 solution at a temperature difference above 40°C . This value is 2.5 times that previously reported for this system when using graphite fibers.³⁹ This was also far higher than when lower concentrations of the redox species were used and at 1 wt. % Br_2 S_e was $+3.90 \text{ mV K}^{-1}$. The reason the system is so affected by the change in electrode materials is partly to do with the mechanism of such devices which involves the adsorption and desorption of the Br_2 species from the electrode surface.³² It was also noted that there was a large shift in the magnitude of S_e at 40°C (up from $+1.55 \text{ mV K}^{-1}$ when using the non-graphitised electrode) which was attributed to be due to the boiling point of Br_2 , which is close to this temperature. Qiao et al.⁴⁰ also quote a high value for this system of $S_e = +3.7 \text{ mV K}^{-1}$ when investigating electrode materials. The nanoporous carbons used are soaked in a NaCl solution which increases the ion charge density at the surface, leading to an increased conductivity in the solution.

Another important factor for maximising performance of TECs is optimising parameters such as electrode separation and utilisation of convection.^{3, 8, 12, 14, 25-27, 35} Multiple studies have found that the open circuit potential, and thus S_e , is unaffected by the separation of the electrodes,^{8, 25} orientation²⁶ and convection.^{26, 27} However, these parameters play a crucial role in maximising the power output of these cells. Mua et al.²⁵ investigate the effect of increasing electrode separation on the open circuit potential and power of aqueous $[\text{Fe}(\text{CN})_6]^{4-/3-}$ using two Pt electrodes. When increasing the separations from 0.1 cm to 150 cm, they

measured a drop in the steady-state current, i_{ss} , which resulted in the power dropping from $20 \mu\text{W cm}^{-2}$ to just $0.036 \mu\text{W cm}^{-2}$.

Burrows¹² investigated the effects of forced convection on a 0.1 M aqueous $[\text{Fe}(\text{CN})_6]^{4-/3-}$ solution. He observed a fourfold increase in the power density of this system. A similar increase in a 0.2 M solution, would lead to a power output of 0.4 mW cm^{-1} . However, this forced convection relies on an external power source which will reduce the net energy gain and potentially increase the need for maintenance for the device.¹⁴

Several studies have investigated different cell orientations in order to utilise natural convection rather than relying on forced convection.^{3, 14, 26} Quickenden and Mua²⁶ investigated three orientations with the hot side either above, below or at the same height as the cold side. They found that for the hot above cold system i_{sc} reduced to about 40% of the maximum after an hour of use, while for the other two orientations i_{sc} was almost unchanged. This suggests that convective flow in this case hindered the mass transport through solution. Gunawan et al.¹⁴ and Salazar et al.³ have also both investigated this effect and both concluded that cold above hot electrodes gave the best conversion efficiencies with Gunawan quoting a 100% increase in the maximum power within his cell.

1.3 Electrochemistry of Quinones

Quinones are a class of organic molecule that is widely found in nature. The simplest form of these is p-benzoquinone (Q) and hydroquinone (QH₂). The electrochemistry of these and other quinones have been widely studied with the earliest recorded study was conducted in 1904 by Haber and Russ.^{42, 43}

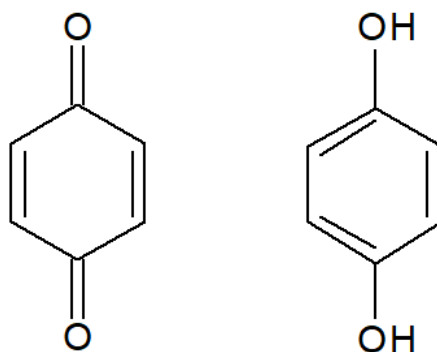


Fig. 1.3: The chemical structures of p-benzoquinone (left) and hydroquinone (right).

The interest in this reaction lies in the role of protons during the oxidation and reduction of the various species. The reactions proceed differently depending on the availability of protons for the reaction and the overall acidity of the system. The overall reaction pathways for a two-electron, two-proton reaction such as this can be summed up by a nine-membered scheme of squares.⁴⁴

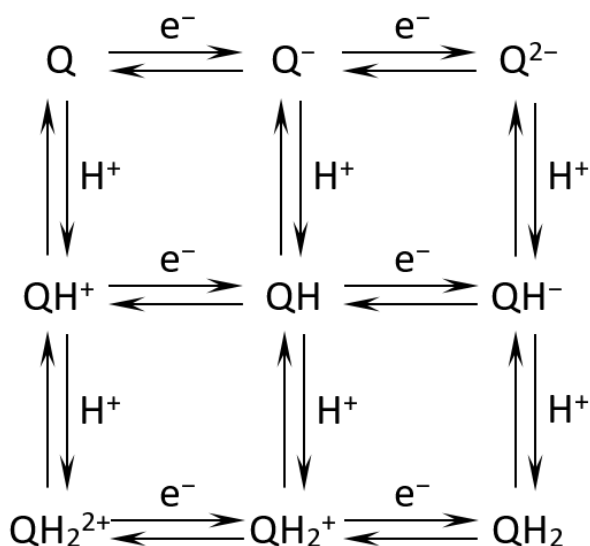


Fig. 1.3: Two-proton, two-electron scheme of squares showing the possible reaction pathways for the Q/QH₂ system.

For a reaction involving both protons and electrons the potential, E , of the reaction will shift with each pH unit according to the equation:

$$E = E^0 - 0.0592 \left(\frac{H^+}{e^-} \right) pH \quad (\text{Eq. 1.3})$$

Where E^0 is the standard potential, defined at pH = 0 and 1 atm and H^+ and e^- correspond to the number of protons and electrons transferred respectively per molecule.

There have been many studies on Q and QH₂ in aqueous media,^{42, 43, 45-72} as well as other Q derivatives.^{46, 66-81} However studies have also been conducted in many organic solvents including Acetonitrile (MeCN),⁸²⁻⁹³ Dimethylformamide (DMF),^{82, 94} Dimethylsulfoxide (DMSO),^{95, 96} Pyridine (Pyr),⁹⁷ Propylene carbonate (PC)⁸⁸ and dichloromethane (DCM).⁸⁹ More recently studies have investigated the properties of these species in ILs.⁹⁸⁻¹⁰⁵

1.3.1 Stability of Quinones in Solution

Quinones are well known to stick to electrode surfaces such as Pt.^{46, 47} This is often irreversible and can influence and hinder the electrochemical reactions at the surface.

White et. al.⁵⁴ conducted a detailed and systematic study into the influence of adsorbed species on the electrode surface. Their investigation included QH₂ and several derivatives, as well as iodine and cyanide. Their results reveal that the kinetics and reaction pathway depend on the nature and orientation of the adsorbed particles. Zeigerson and Gileadi¹⁰⁶ focused investigations of the self-inhibition effects of QH₂ on a Pt electrode surface. In an unbuffered pH 0 solution, they conclude that at concentrations below 0.1 M there was a very low surface coverage if QH₂, but this increases rapidly as the concentration reaches 0.2 M. However, at a pH 3 they observe that a lower concentration of below 0.05 M is required to ensure minimal QH₂ deposition.

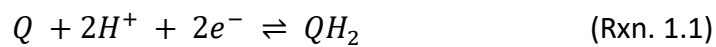
Soriaga and Hubbard⁴⁶ investigated the influence of I⁻ on the surface deposition of various aromatics, including QH₂. They found that even small quantities (0.5 mM) of I⁻ resulted in the displacement of some previously adsorbed aromatics.

In addition to significant influences of the electrodes on the quinone reaction, they are also prone to decomposition at high pH.⁵⁵ This decomposition begins to

occur in water as the pH is increased to 9. By pH 13 this leads to significant irreversibility in the electrochemistry with rapid decomposition of Q.

1.3.2 Quinones in Buffered or Acidic Aqueous Solution

The simplest case for the Q reaction occurs in acidic or well buffered aqueous media. In this case the reduction of Q occurs by a 2-electron, 2-proton process to form QH₂⁴⁵:



Yet even in this simplest case there have been disagreements over the exact reaction pathway. One of the earliest mechanistic studies of this reaction was conducted by Vetter.⁴⁵ He investigated the reactions of both Q and QH₂ at a Pt electrode and observed two different reaction pathways depending on the acidity of the solution. At a pH < 5 he established that the reaction began with a protonation and the reduction followed a CECE pathway (where 'C' represents the chemical step, a proton transfer, and 'E' represents an electron transfer). At higher pH levels the pathway altered with the reduction occurring before any protonation following an ECEC route instead. Shim and Park⁵⁷ found the pathway to be ECEC at a pH > 3.1. However, since this was an unbuffered system the pH at the electrode surface would change as the reaction progressed, which could account for this discrepancy.

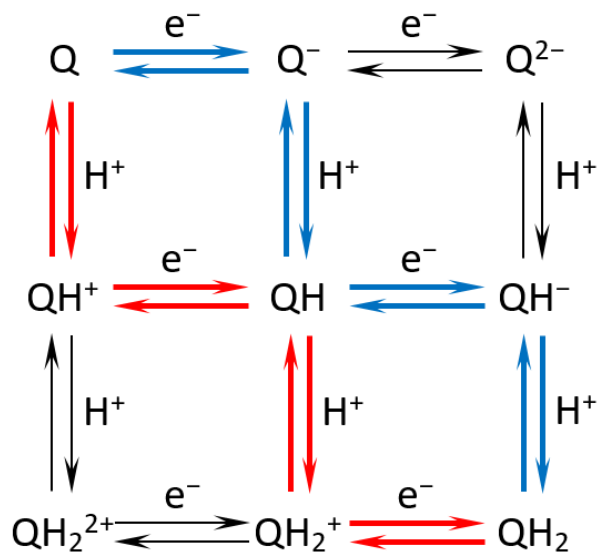


Fig. 1.4: Scheme of squares showing the CECE pathway (red) and the ECEC pathway (blue). Both reduction pathways ultimately result in the formation of QH₂.

Carrying on from this Hale and Parsons⁴³ went on to study the stabilities of various intermediate species. They suggested that the semiquinone species, QH, is stabilised by adsorption onto the Pt surface and they therefore used a Hg drop electrode in their investigations. Their conclusions were similar to those established by Vetter. However, they suggested a stronger acidity is required for QH₂⁺ to be involved in the reaction pathway. Hale and Parsons also observed that the rate constant of Q reduction was higher at a Hg electrode than at Pt, suggesting that this was due to the adsorption of Q onto the Pt surface which hindered the reaction. These findings are disputed by Loshkarev and Tomilov,⁵¹ who concluded that the kinetics of the reaction was independent of the pH of the solution with the reaction pathway always being EECC.

Laviron^{44, 47} used existing experimental data along with computational calculations to further analyse this reaction. He formed a model of the change of reaction pathway with change in pH. These results largely agreed with that previously established by Vetter⁴⁵ with the addition of an additional ECCE pathway that is dominant between a pH of 3.5 and 5.5. He also established that with the exception of extremes of pH the reaction involves two or more of the pathways from reactants to products and is never purely one pathway. The majority of investigations therefore support this change in mechanism as the pH increases, which is largely summed up by Laviron's work.

Bailey and Ritchie^{53,55} constructed a full pH diagram for the Q-QH₂ system from polarographic data in order to get a full analysis of the system. They found that at a pH < -1, Q was readily protonated to QH⁺, thus leading to a slope of -29.6 mV per pH level for the reduction reaction:



Above this pH, the reaction progresses according to Rxn. 1.1 until sufficiently high pH is achieved that deprotonated forms of QH₂ become the most stable. For an acid, AH, that dissociates according to the equation:

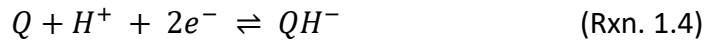


The pH and pka for dilute electrolyte are defined by equations 1.4 and 1.5, where a is the activity of each species which can be approximated to the concentrations of each species.

$$pH = -\log(a_{H^+}) \approx -\log([H^+]) \quad (\text{Eq. 1.4})$$

$$pka = -\log\left(\frac{a_{H^+}a_{A^-}}{a_{AH}}\right) \approx -\log\left(\frac{[H^+][A^-]}{[AH]}\right) \quad (\text{Eq. 1.5})$$

From this it follows that when the pH is equal to the pka there is a shift in reaction mechanism with the deprotonated species becoming favourable. The pka values for QH₂ and QH⁻ are 8.85 and 11.4 respectively. This therefore leads to a change in the major reaction products at these pH values according to reactions 1.4 and 1.5 respectively.



These give slopes of -29.6 mV per pH for Rxn. 1.4 and zero for Rxn. 1.5 due to the reduced number of protons transferred in the reactions. As well as constructing these diagrams using polarography they also used cyclic voltammetry in well buffered solutions to again construct pH diagrams.⁵⁵ By using the half wave potentials, $E_{1/2}$, they constructed a pH diagram for this system. As expected, the reaction was found to progress according to Rxn. 1.1 at lower pH.

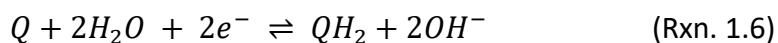
1.3.3 Quinones in Unbuffered Aqueous Media

In unbuffered media, the reduction of Q progressing via Rxn. 1.1 results in a decrease in the proton concentration near the electrode surface. This then leads

to an increase in the pH at the electrode surface.^{49, 50} Conversely for QH₂, the oxidation of this species leads to a decrease in the pH near the surface.

Muller et al.⁴⁹ found that these pH changes can be quite significant. They found that for a 1 mM solution of Q at pH 7 the surface pH increased to pH 10 as reduction occurred. Conversely for QH₂, they found that the pH of the solution increased to pH 3 after oxidation of the species. The magnitude of the pH change was also found to change with changing analyte concentration since a larger analyte concentration leads to the removal, or addition of more protons from the solvent.

The lack of protons at higher pH results in the emergence of a second Q reduction peak at further negative potentials.^{52, 55, 56} For simplicity, the more positive process will be referred to as process A, and the more negative as process B. An example of this is shown in Fig. 1.5 extracted from Tang et al.⁵⁸ This reaction change was investigated by Abbot and Collat,⁵² who found that process B began to appear when the concentration of Q was greater than that of the acid. They concluded that this peak also resulted in the formation of QH₂. In this case they suggested that the protons therefore had to come from neutral H₂O according to the equation:



Robertson and Pendley⁵⁶ investigated the system at a micro electrode. Their work suggests that both reactions are 2-electron processes and concluded that

process B involved the formation of QH_2 . However, they suggest that since QH_2 is a stronger acid than H_2O the protons likely come from the QH_2 .

Bailey and Ritchie⁵⁵ investigated the voltammetry of unbuffered aqueous Q and QH_2 across a range of pH values. They found that, as expected, process A was pH dependent. However, process B had an $E_{1/2}$ that did not change significantly with pH. This would rule out Rxn. 1.6 due to the change in solution pH that occurs in this case and therefore suggest that the reaction occurs without any transfer of protons as occurs in Rxn. 1.5.

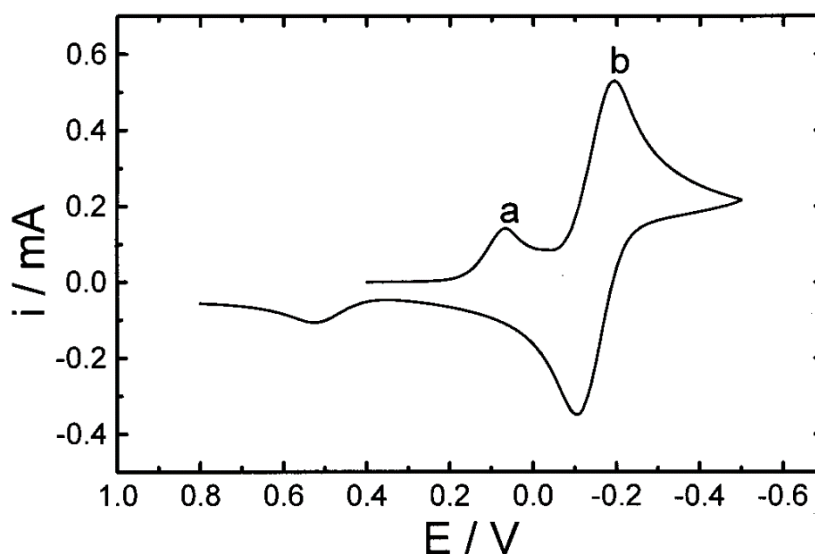


Fig. 1.5: Quinone reduction taken at a Pt electrode for 5 mM Q in 0.5 M KCl at pH 3.27. Taken from Tang et al.⁵⁸

Shim and Park⁵⁷ studied the Q reduction at various pH's in order to investigate the radicals formed in the reaction. They also conclude that process A is pH dependent, while process B is not. From their results they concluded that process B was in fact only a 1-electron process. They determined this using

chronoamperometric current functions, with the product being $Q^{\cdot-}$, which they detected through UV vis.

Tang et al.⁵⁸ followed on from this by using *in situ* Electron Spin Resonance (ESR) to detect radical ions. They used a rotating disk electrode to calculate that the number of electrons passed is 2 for all reactions. In addition, they also found that $E_{1/2}$ for process B was independent of the pH, in line with the previous investigations. They therefore conclude that the product was a simple 2-electron process producing Q^{2-} as in Rxn. 1.5. They also detected the $Q^{\cdot-}$ radical during the reduction of Q and observed that the concentration of this species continued to increase for a time after the electrochemical reaction had finished. Their conclusion was that the radical was formed from the comproportionation of the reactant and product by:

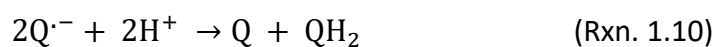


1.3.4 Quinones in non-aqueous systems

For many non-aqueous solvents there is a far lower proton availability than in neutral water. In these solvents the $Q^{\cdot-}$ ion is stabilised usually resulting in two single-electron transfers being observed. These correspond to the formation of the anion and dianion species respectively:⁸²



It is generally observed that the second reduction wave corresponding to Rxn. 1.9 is smaller than the first.⁸² The protonated radical species QH[•] has a higher electron affinity than Q which leads to the reduction potential of QH[•] being positive of Q.⁹⁵ Thus whenever Q^{•-} can be protonated it will then be reduced at the same potential as Q. This leads to the disproportionation reaction in Rxn. 1.10, which will be in favour of forming the products.¹⁰⁷



This results in an increase in the size of the first reduction wave, at the expense of the second wave.

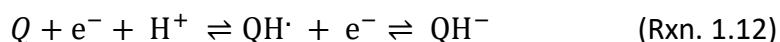
Wawzonek et al.⁸² investigated Q and other Q derivatives dissolved in MeCN and DMF at a mercury drop electrode. They used polarography to detect the presence of both the Q^{•-} and Q²⁻ species. Further to this they also added small amounts of water or acid as proton donors to investigate the effects of this on the Q electrochemistry. They found that the potential first reduction corresponding to Rxn. 1.8 was unaffected by the addition of these proton sources. However, the second reduction moved to more positive potentials. As the proton concentrations increased this eventually resulting in the two redox waves merging into a single peak.

They attributed this shift in peak potential to be the result of the rapid protonation of the dianion species to form QH₂. However, they also suggested it could be due to a single protonation reaction of the form:



Due to the electron affinity of QH^\cdot this would require the chemical step to occur first, otherwise the reduction should happen at the same potential as the first reduction.

Eggs and Chambers⁸³ looked at the oxidation reaction of QH_2 in MeCN. They observed a single relatively sharp oxidation wave for QH_2 in the absence of any proton donors, which they concluded was produced from Q according to Rxn. 1.1. The product in this case will be present as a mixture of Q and QH^+ . However, the reverse wave was a lot slower and broader. They attributed this to the formation of QH^- according to the equation:



In the presence of excess protons this then gets protonated to form QH_2 . They compared this to reactions of Q in the presence of weaker and stronger acids. With a weaker acid the Q reaction has a single reduction wave which they attribute to the single-electron reduction according to Rxn. 1.8. However, the positive going sweep shows three oxidation waves. The first was attributed to the reoxidation of this $Q^{\cdot-}$ species to Q. The next two were attributed to the oxidation of QH^- and QH_2 respectively. However, it is not specified where these doubly reduced species come from since the reduction is stated to be only a single-electron reduction. When using a stronger acid, a second, more positive reduction wave is seen. This is attributed to the reduction of a Q/H^+ mixture to QH^- as in Rxn.

1.12. As further acid is added the voltammetry then begins to resemble that of QH₂ with the most negative reduction disappearing.

Parker⁸⁴ investigated the gradual addition of base to QH₂ and an acidified Q solution. For the QH₂ oxidation he agreed with Eggins and Chambers that this produced Q according to Rxn. 1.1, with the added point that this was an ECEC mechanism. By comparing the voltammetric response of QH₂ with that of a 2:1 mixture of HClO₄ he noticed the same oxidation and reduction reactions occurred. An additional reaction in the latter attributed to proton reduction was also observed. As base was added in each case a second oxidation and reduction reaction were observed at more negative potentials. The oxidation was attributed to the reaction of QH⁻, in line with what Eggins and Chambers concluded. For the reductions Parker distinguished between QH⁺, with one of the oxygen atoms protonated, and the complex [Q]H⁺, with the proton not specifically attached to an oxygen atom. He concluded that both reduction reactions were 2-electron reactions and were the result of the reduction of QH⁺ for the positive reaction and [Q]H⁺ for the one at more negative potential.

1.4 Ionic Liquids

Ionic liquids (ILs) are defined as being salts that are liquid at temperatures of less than 100 °C.¹ Since these are salts they are composed entirely of ions meaning they have a good intrinsic conductivity and generally have low vapour pressures due to the strong ionic interactions. They are also generally characterised by

having wide potential windows, with this being particularly true for aprotic ILs. However they are also usually more viscous than water or other organic solvents.

ILs fall into two main categories. Protic Ionic Liquids (PILs) and Aprotic Ionic Liquids (AILs). PILs are generally produced by a neutralisation reaction between a Brønsted-Lowry acid and a Brønsted-Lowry base.² The resultant IL therefore consists of the conjugate base and conjugate acid respectively, which leads to a liquid with a labile proton. AILs on the other hand are not synthesised by an acid-base reaction and do not contain a labile proton. One common synthesis method is a simple ion exchange of two salts in solution.

In PILs the strength of the acid and bases involved in the PIL synthesis plays an important role in the nature of the resulting liquid. The acid-base reaction is a reversible reaction and at equilibrium will contain a low concentration of neutral species, it has been suggested that the liquid should contain 99% ions to be classed as a pure salt.³ The aqueous pK_a can be a good indicator of the strength of the bound proton in the resulting liquid, and it is widely accepted that a $\Delta pK_a > 10$ is required to ensure a highly ionised PIL.^{4, 5} It should be noted that pK_a values are defined in aqueous systems, so will not apply perfectly in the anhydrous systems such as for neat PIL. In addition other factors such as hydrogen bonding and structure will also play a part in the ionicity of the PIL.³

1.5 Project Objectives

In this report, thermoelectrochemical measurements have been conducted for $I^-/[I_3]^-$, Q/QH_2 , $Fe(acac)_{2/3}$ (acac is the acetylacetonate ligand) and $V(acac)_3/VO(acac)_2$ in solution. The investigations focus on using these analytes dissolved in ILs, although they have also been studied in water where they are sufficiently soluble. In addition to this, the commonly used redox couple, $[Fe(CN)_6]^{3-/4-}$, has been investigated for accurate comparison with literature data and enables the comparison of the power outputs of each system.

The overall aim of these investigations was to look into alternative redox couples to $[Fe(CN)_6]^{3-/4-}$, which is widely considered the benchmark of these devices. As well as looking for improved Seebeck coefficients, the use of ILs allows for higher temperatures to be maintained than for aqueous systems, thus boosting the maximum power outputs of these devices.

The thermoelectrochemical response for $I^-/[I_3]^-$ has previously been investigated in a range of solvents including many organic solvents and ILs. The current study seeks to expand on this by investigating the Seebeck coefficients and power output data for this redox couple in a range of PILs as well as one AIL. In addition, the performance of this redox couple is studied in water, with the aim of providing an accurate reference point for the other systems. The voltametric response is also investigated for each redox species in each of the ILs used in order to understand the reasoning behind the results that are observed.

The Q/QH₂ and metal acetylacetonate complexes are selected due to the potential addition of chemical steps in their redox reactions, in the hope that this will lead to higher entropies are achieved, and thus higher Seebeck coefficients. The quinone redox couple has also been selected as it is an organic alternative to more commonly employed halide and metal complexes systems, potentially reducing cost and improving sustainability for thermoelectric devices.

Further to this, the electrochemical responses of Q and QH₂ have been studied in in three PILs consisting of different combinations of acid and base in their synthesis. Two different acids and two different bases are used in these PILs. The acids have a significant difference in their, which changes the lability of the transferred proton in the resultant liquid. Since the electrochemical pathways of the reactions of Q and QH₂ are dependent on the concentration of H⁺ ions in solution, the change in lability of the proton should alter the electrochemical pathways. This provides insight into the reactions of these two species in PILs and the current investigation seeks to expand the current knowledge of quinone electrochemistry in these PILs. This also provides an understanding of how these PILs behave, and the nature of the labile proton.

1.6 References

1. T. J. Abraham, et al., *Chem. Commun.*, 2011, **47**, 6260-6262.
2. T. J. Abraham, et al., *Electrochim. Acta*, 2013, **113**, 87-93.
3. P. F. Salazar, et al., *J. Appl. Electrochem.*, 2014, **44**, 325-336.
4. R. Hu, et al., *Nano Lett.*, 2010, **10**, 838-846.
5. H. A. H. Alzahrani, et al., *Electrochem. Commun.*, 2015, **58**, 76-79.
6. M. Bonetti, et al., *J. Chem. Phys.*, 2011, **134**.
7. H. Im, et al., *Nano Research*, 2014, **7**, 443-452.
8. S. Uhl, et al., *J. Electron. Mater.*, 2014, **43**, 3758-3764.
9. N. S. Hudak, G. G. Amatucci, *J. Electrochem. Soc.*, 2011, **158**, A572-A579.
10. R. Koerver, et al., *Electrochim. Acta*, 2015, **184**, 186-192.
11. E. H. B. Anari, et al., *Chem. Commun.*, 2016, **52**, 745-748.
12. B. Burrows, *J. Electrochem. Soc.*, 1976, **123**, 154 - 159.
13. T. Migita, et al., *Electrochemistry*, 2009, **77**, 639-641.
14. A. Gunawan, et al., *Int. J. Heat Mass Transfer*, 2014, **78**, 423-434.
15. B. R. Sundheim, J. Rosenstreich, *J. Phys. Chem.*, 1959, **63**, 419-422.
16. J. D. Kellner, *J. Phys. Chem.*, 1967, **71**, 2434-2438.
17. D. D. Macdonald, et al., *J. Electrochem. Soc.*, 1979, **126**, 1618-1624.
18. Y. V. Kuzminskii, et al., *J. Power Sources*, 1994, **52**, 231-242.
19. K. Cornwell, *J. Phys. D: Appl. Phys.*, 1972, **5**, 1199-1211.
20. R. Haase, *Z. Naturforsch., A: Phys. Sci.*, 1976, **31**, 1731-1732.
21. H. G. Hertz, S. K. Ratkje, *J. Electrochem. Soc.*, 1989, **136**, 1698-1704.

22. A. Grimstvedt, et al., *J. Electrochem. Soc.*, 1994, **141**, 1236-1241.
23. T. Murakami, et al., *J. Electrochem. Soc.*, 2003, **150**, A928-A932.
24. D. K. Nordstrom, *Geochim. Cosmochim. Acta*, 1977, **41**, 1835-1841.
25. Y. Mua, T. I. Quickenden, *J. Electrochem. Soc.*, 1996, **143**, 2558-2564.
26. T. I. Quickenden, Y. Mua, *J. Electrochem. Soc.*, 1995, **142**, 3652-3659.
27. T. Ikeshoji, R. S. Goncalves, *J. Appl. Electrochem.*, 1993, **23**, 516-519.
28. P. F. Salazar, et al., *J. Electrochem. Soc.*, 2012, **159**, B483-B488.
29. T. J. Abraham, et al., *PCCP*, 2014, **16**, 2527-2532.
30. S. W. Hasan, et al., *Scientific Reports*, 2016, **6**.
31. K. Shindo, et al., *J. Power Sources*, 1998, **70**, 228-234.
32. K. Shindo, et al., *J. Power Sources*, 2002, **110**, 46-51.
33. T. J. Abraham, et al., *Energ. Environ. Sci.*, 2013, **6**, 2639-2645.
34. K. Teramoto, et al., *Electrochemistry*, 2014, **82**, 566-572.
35. M. Bonetti, et al., *J. Chem. Phys.*, 2015, **142**.
36. M. A. Lazar, et al., *PCCP*, 2016, **18**, 1404-1410.
37. A. Sosnowska, et al., *Chemphyschem*, 2016, **17**, 1591-1600.
38. T. A. Siddique, et al., *Rsc Advances*, 2016, **6**, 18266-18278.
39. M. Endo, Y. Yamagishi, *Synth. Met.*, 1983, **7**, 203-209.
40. Y. Qiao, et al., *J. Power Sources*, 2008, **183**, 403-405.
41. W. Qian, et al., *Rsc Advances*, 2015, **5**, 97982-97987.
42. F. Haber, R. Russ, *Z. Phys. Chem.*, 1904, **47**, 257-335.
43. J. M. Hale, R. Parsons, *Trans. Faraday Soc.*, 1963, **59**, 1429-1437.

44. E. Laviron, *J. Electroanal. Chem.*, 1983, **146**, 15-36.
45. K. J. Vetter, *Z. Elektrochem.*, 1952, **56**, 797-806.
46. M. P. Soriaga, A. T. Hubbard, *JACS*, 1982, **104**, 2742-2747.
47. E. Laviron, *J. Electroanal. Chem.*, 1984, **164**, 213-227.
48. R. Rosenthal, et al., *JACS*, 1937, **59**, 1795-1804.
49. O. H. Muller, *JACS*, 1940, **62**, 2434-2441.
50. I. M. Kolthoff, E. F. Orlemann, *JACS*, 1941, **63**, 664-667.
51. M. A. Loshkarev, B. I. Tomilov, *Zh. Fiz. Khim.*, 1960, **34**, 1753-1762.
52. J. C. Abbott, J. W. Collat, *Anal. Chem.*, 1963, **35**, 859-863.
53. S. I. Bailey, et al., *J. Chem. Soc., Perkin Trans. 2*, 1983, 645-652.
54. J. H. White, et al., *J. Electroanal. Chem.*, 1985, **185**, 331-338.
55. S. I. Bailey, I. M. Ritchie, *Electrochim. Acta*, 1985, **30**, 3-12.
56. R. T. Robertson, B. D. Pendley, *J. Electroanal. Chem.*, 1994, **374**, 173-177.
57. Y. B. Shim, S. M. Park, *J. Electroanal. Chem.*, 1997, **425**, 201-207.
58. Y. H. Tang, et al., *J. Electrochem. Soc.*, 2001, **148**, E133-E138.
59. R. J. Forster, J. P. O'Kelly, *J. Electroanal. Chem.*, 2001, **498**, 127-135.
60. H. Park, et al., *Electroanalysis*, 2002, **14**, 1501-1507.
61. M. Rafiee, D. Nematollahi, *Electroanalysis*, 2007, **19**, 1382-1386.
62. M. Quan, et al., *JACS*, 2007, **129**, 12847-12856.
63. M. A. Ghanem, *Electrochem. Commun.*, 2007, **9**, 2501-2506.
64. A. Mendez, et al., *Electrochemistry*, 2013, **81**, 853-856.
65. L. Godeffroy, et al., *Electrochem. Commun.*, 2018, **86**, 145-148.

66. R. Gamage, et al., *J. Chem. Soc., Faraday Trans.*, 1991, **87**, 3653-3660.
67. Y. Sato, et al., *J. Electroanal. Chem.*, 1996, **409**, 145-154.
68. G. Jurmann, et al., *Electrochim. Acta*, 2007, **53**, 390-399.
69. A. T. Masheter, et al., *J. Mater. Chem.*, 2007, **17**, 2616-2626.
70. C. Batchelor-McAuley, et al., *J. Phys. Chem. B*, 2010, **114**, 4094-4100.
71. C. Batchelor-McAuley, et al., *J. Phys. Chem. C*, 2011, **115**, 714-718.
72. M. Mooste, et al., *J. Electroanal. Chem.*, 2013, **702**, 8-14.
73. B. Huskinson, et al., *Nature*, 2014, **505**, 195-198.
74. M. Lu, R. G. Compton, *Analyst*, 2014, **139**, 4599-4605.
75. M. Lu, R. G. Compton, *Analyst*, 2014, **139**, 2397-2403.
76. K. X. Lin, et al., *Science*, 2015, **349**, 1529-1532.
77. Z. J. Ayres, et al., *Electrochem. Commun.*, 2016, **72**, 59-63.
78. Z. J. Ayres, et al., *Anal. Chem.*, 2016, **88**, 974-980.
79. K. Wedege, et al., *Scientific Reports*, 2016, **6**.
80. R. Emanuelsson, et al., *Russ. J. Electrochem.*, 2017, **53**, 8-15.
81. D. G. Kwabi, et al., *Joule*, 2018, **2**, 1894-1906.
82. S. Wawzonek, et al., *J. Electrochem. Soc.*, 1956, **103**, 456-459.
83. B. R. Eggins, J. Q. Chambers, *J. Electrochem. Soc.*, 1970, **117**, 186-192.
84. V. D. Parker, *Electrochim. Acta*, 1973, **18**, 519-524.
85. B. R. Eggins, P. K. J. Robertson, *J. Chem. Soc., Faraday Trans.*, 1994, **90**, 2249-2256.
86. G. Pastor-Moreno, D. J. Riley, *Electrochem. Commun.*, 2002, **4**, 218-221.

87. B. Jin, et al., *J. Electroanal. Chem.*, 2010, **650**, 116-126.
88. Z. Yu, et al., *Electrochim. Acta*, 2013, **107**, 695-700.
89. K. Seto, et al., *J. Phys. Chem. B*, 2013, **117**, 10834-10845.
90. S. Groni, et al., *Chem. Commun.*, 2014, **50**, 14616-14619.
91. R. Salazar, et al., *New J. Chem.*, 2015, **39**, 1237-1246.
92. P. D. Astudillo, et al., *J. Electroanal. Chem.*, 2007, **604**, 57-64.
93. J. Medina-Ramos, et al., *J. Phys. Chem. C*, 2012, **116**, 20447-20457.
94. C. Russel, W. Jaenicke, *J. Electroanal. Chem.*, 1986, **199**, 139-151.
95. I. M. Kolthoff, T. B. Reddy, *J. Electrochem. Soc.*, 1961, **108**, 980-985.
96. N. Gupta, H. Linschitz, *JACS*, 1997, **119**, 6384-6391.
97. W. R. Turner, P. J. Elving, *J. Electrochem. Soc.*, 1965, **112**, 1215-1217.
98. Y. Wang, et al., *J. Electroanal. Chem.*, 2010, **648**, 134-142.
99. S. Ernst, et al., *Chem. Phys. Lett.*, 2011, **511**, 461-465.
100. V. A. Nikitina, et al., *J. Phys. Chem. B*, 2011, **115**, 668-677.
101. M. A. Bhat, *Electrochim. Acta*, 2012, **81**, 275-282.
102. H. N. A. Mustafa, et al., *Int. J. Electrochem. Sci.*, 2015, **10**, 9232-9245.
103. A. P. Doherty, et al., *J. Mex. Chem. Soc.*, 2015, **59**, 263-268.
104. P. Navalpotro, et al., *J. Power Sources*, 2016, **306**, 711-717.
105. C. Karlsson, et al., *ACS Appl. Energy Mater.*, 2018, **1**, 6451-6462.
106. E. Zeigerson, E. Gileadi, *J. Electroanal. Chem.*, 1970, **28**, 421-432.
107. M. Bauscher, W. Mantele, *J. Phys. Chem.*, 1992, **96**, 11101-11108.

Chapter 2

Introduction to Electrochemical Techniques and Thermoelectrochemistry

2.1 Electrochemical Theory

When an isolated electrode is placed in a solution, there is an immediate transfer of electrons between the electrode surface and the solution. This transfer occurs due to the energy difference between the metal surface and the solution as shown in the left diagram of Fig. 2.1. If the potential of the metal is negative of the solution, there will be a transfer of electrons to the solution.

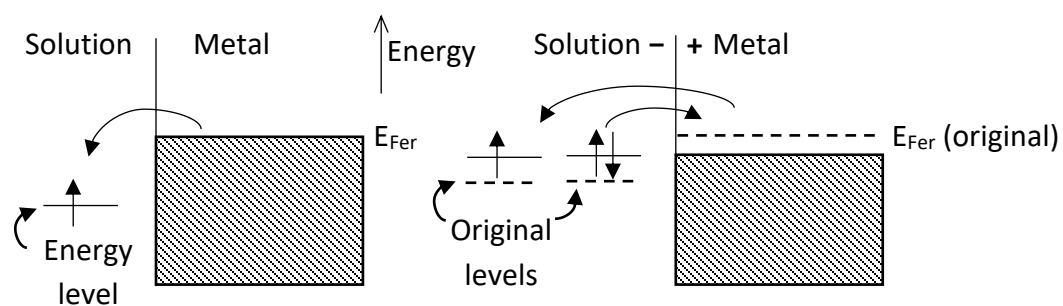


Fig. 2.1 Energy of electrons in solution and on an electrode surface. M denotes a metal solute and E_{Fe} denotes the Fermi-level. Based on fig. 1.8 in Compton and Banks.^{1, p. 11}

As this transfer occurs the metal Fermi-level, E_{Fe} , decreases and the energy levels in the solution slightly increase. Since an isolated electrode is necessarily not connected to an external circuit, this induces a build-up of charge at the

interface which will eventually resist any further net charge transfer and equilibrium is reached. This transfer of electrons will be small relative to the bulk solution.^{1, pp. 9-11} This is shown in the right diagram of Fig. 2.1.

A potential difference builds-up between the electrode and the solution due to the charge difference between them. It is not possible to measure this potential directly, since a current is required, which relies on a completed circuit. In order to measure the potential of an electrode a second electrode must be used and the potential difference between the two measured.

If an external positive potential is applied to the electrode, E_{Fer} will decrease further. As the Fermi-level in the metal approaches and passes one of the filled energy levels of the solution, it will become energetically favourable to transfer an electron from the solution to the metal surface, and the molecules near the surface will thus be oxidised. This consequently creates a current through an external circuit which can be measured. Applying negative potentials will have the opposite effect, with the molecules in solution being reduced and negative current flowing. This forms the basis of the electroanalytical techniques used in this study.

2.2 Electroanalysis

Electroanalysis was carried out using a three-electrode cell. A typical setup is shown in Fig. 2.2. The analysis is carried out by monitoring reactions occurring at the Working Electrode (WE). In order to allow current to flow freely through this electrode a Counter Electrode (CE) is required to complete the electrochemical

circuit. Since passing large currents through an electrode will alter the potential of that electrode, a third electrode, the Reference Electrode (RE), is required that has a fast and stable reaction occurring at the surface. Negligible current flows through this electrode and it is used as a reference against which the potential of the WE can be applied and measured. A Potentiostat is therefore used to control the potential of the WE relative to that of the RE.

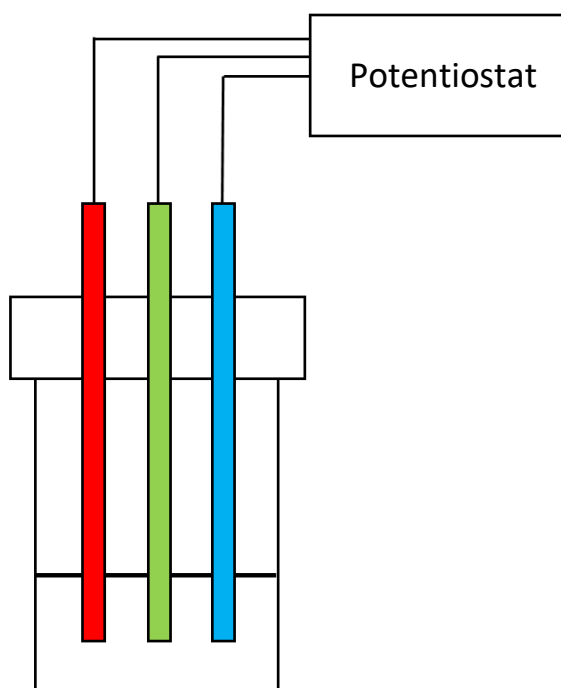


Fig. 2.2: A typical three-electrode setup for isothermal electrochemical measurements containing a WE, CE and RE. The Potentiostat controls the potential of the WE with respect to the RE. the CE takes the bulk of the current from the WE allowing the RE to remain at a constant potential during the experiment.

The WE is typically a planar disc of which there are two main types, macrodisc and microdisc electrodes. The practical difference between these two electrodes is the way in which the analyte diffuses to the electrode surface. Macrodisc

electrodes are large compared to the size of molecules (typically millimetres to centimetres in diameter).^{2, p.169} These can be treated as being infinite relative to the size of the molecule and therefore linear diffusion is the dominant method by which the analyte travels to the electrode surface, with edge effects contributing little to the overall current. This is shown in Fig. 2.3 (left). The result of this is that over the course of an experiment as the analyte is either oxidised or reduced, the analyte concentration at the surface is rapidly depleted and the reaction slows as fresh analyte must travel from further away to reach the electrode surface.

For microdisk electrodes the electrode surface is of the order of micrometres. At this size diffusion cannot be accurately modelled by linear diffusion since the effect of lateral diffusion at the edges is no longer negligible Fig. 2.3 (right). This has a consequence that the analyte concentration at the surface does not get fully depleted and instead reaches a steady rate, with fresh analyte more rapidly reaching the electrode surface. Diffusion to the surface is instead modelled by a hemisphere with analyte travelling to the surface in 3 dimensions. The upper boundary for an electrode to be modelled in this way is a radius of around $25\mu\text{m}$.^{2,}

p.170

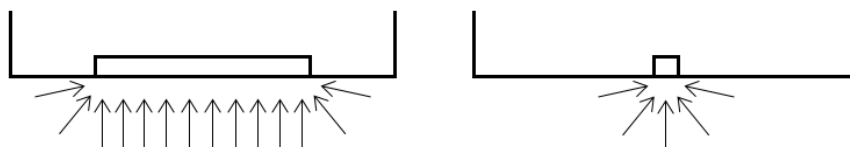
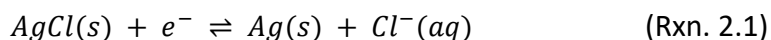


Fig. 2.3: Diffusion at a macrodisc (left) and microdisc (right) electrode. Adapted from Compton and Banks Fig. 5.18.^{1, p.182}

For the RE to be stable, an electrochemical reaction must be occurring at this electrode that is sufficiently fast to counteract the tiny amounts of current entering or leaving the metal. One of the most common reactions for aqueous REs is the reaction:^{3, p.15}



The ideality of this reaction lies in the states of the substances involved as well as the fast kinetics.^{3, pp.11-12} The equilibrium of any reaction will change depending on changes in the activities of the molecules and ions involved in the reaction. The activity of dilute solutions is roughly equal to the concentration of the solute, while the activity of a solid is equal to unity. This means that for the Ag/AgCl electrode the reference at a given temperature and in equilibrium becomes dependent only on the concentration of Cl^{-} . Thus, by having a large excess of Cl^{-} ions and passing minimal current through the electrode the potential of this electrode remains stable.

An alternative is to use a quasi-reference electrode, such as a metal wire. While there is no specific reaction involved, provided the solution composition remains relatively constant these can provide good stability over the course of a series of experiments.^{2, p. 53}

2.2.1 Cyclic Voltammetry

Cyclic voltammetry is one of the key electrochemical techniques that can be used to analyse the behaviour of a redox species in solution.

A typical, well-defined voltammogram for a macrodisk electrode is shown in Fig. 2.4. In cyclic voltammetry a potential is applied to the WE and is gradually increased and decreased, with the current response measured. The rate at which the potential changes is known as the scan rate and remains constant throughout a given voltammogram. The current output is the combination of two different processes. Non-Faradaic current, involves the transfer of electrons to electrode surface, but with no transfer of charge between the electrode and the solution^{2, p.11}. This results in a build-up of a layer of charge on the electrode surface. This also results in a layer of charge opposite to the charge of the electrode building up at the in the solution. These two layers are collectively known as the electric double layer. This is also referred to as capacitive current and emulates the effect observed in supercapacitors. Faradaic current corresponds to the oxidations and reductions of species in solution^{2, pp.18-19}, so involves transfer of electrons between the electrode and solution.

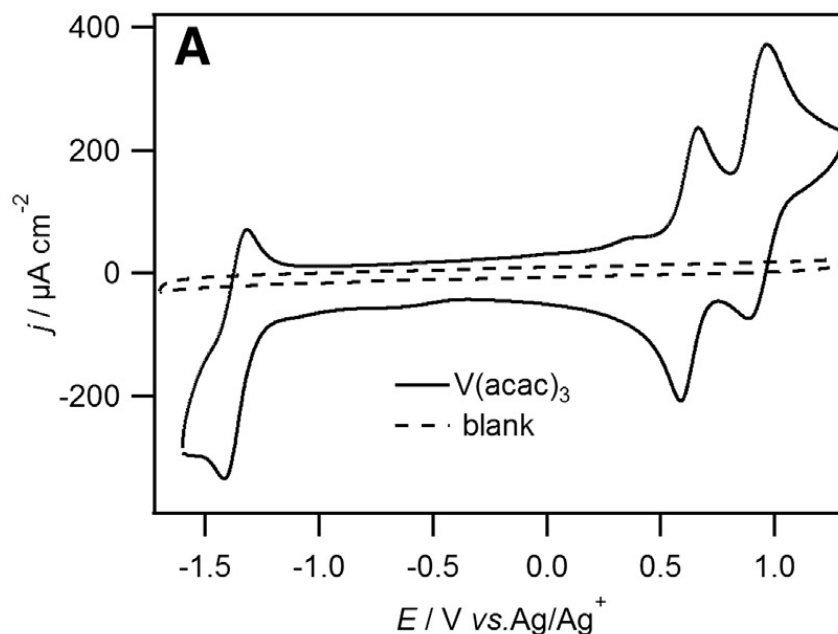


Fig. 2.4: A voltammogram of 10 mM $V(acac)_3$ dissolved in $[EMIm][NTf_2]$ extracted from Ejigu et al.⁴ The current is measured using a 5 mm Glassy-Carbon (GC) WE at a scan rate of 50 mV s^{-1} .

Fig. 2.4 shows an example voltammogram containing 10 mM vanadium acetylacetonate ($V(acac)_3$) in solution at a macrodisc electrode. By IUPAC convention positive current involves electrons travelling from the WE through the external circuit and vice versa for the negative current.

In Fig. 2.4, the relatively flat region between -1.2 V and 0.4 V contains almost entirely Non-Faradaic current and the vanadium at the surface remains in its original oxidation state as V^{3+} . As the applied potential increases beyond 0.5 V , a sharp rise in current occurs due to oxidation of the metal increases to V^{4+} ($[V(acac)_3]^+$). As the voltage increases further, the concentration of V^{3+} at the surface of the electrode begins to diminish and the current reaches a maximum before decreasing. The size of the peak and rate of the drop is related to the rate

at which new V^{3+} diffuses to the electrode surface from the bulk solution. A second oxidation peak is observed in the figure at approximately 1.0 V which corresponds to a further oxidation to V^{5+} ($V[acac]_3^{2+}$).

After the potential has reached 1.3 V the applied potential is then gradually reduced. This leads to two negative peaks in current at 0.9 V and 0.6 V which correspond to reductions from V^{5+} to V^{4+} and V^{4+} to V^{3+} , respectively. A further reduction peak can be seen at -1.4 V which corresponds to the reduction to V^{2+} ($V[acac]_3^-$), with its corresponding oxidation occurring at -1.3 V.

In an electrochemically reversible system, the difference between the oxidation and reduction peaks, ΔE_p , will be 59 mV.^{5, p.31} This value should be independent of the scan rate of the system so by conducting voltammetry at increasing scan rates, the reversibility of the system can be investigated.

For a reversible solution-based process at 298 K, the peak current, i_p , at any given scan rate, ν , should obey the Randles-Sevcik equation:^{2, p. 231}

$$i_p = 2.69 \times 10^5 n^{3/2} AC (D\nu)^{1/2} \quad (\text{Eq. 2.1})$$

Where A is the electrode area and D and C correspond to the diffusion coefficient and concentration respectively of the analyte being reduced or oxidised. However, for an irreversible system the transfer coefficient, α , must also be included and the adjusted equation becomes:^{2, p. 236}

$$i_p = 2.99 \times 10^5 AC (\alpha D\nu)^{1/2} \quad (\text{Eq. 2.2})$$

The transfer coefficient, α , gives a measure of the symmetry of the redox energy barrier.^{2, p.97} This generally falls within in the range of 0.3 to 0.7. However, if this is unknown the approximate value of 0.5 is often used. It is also of note that for the irreversible case there is no 'n' term as the equation applies specifically to the case of having a single electron transfer.

For a surface-based process, whereby the reactant adsorbs onto the electrode surface i_p will vary directly with v , rather than the square root of scan rate as in equations 2.1 and 2.2. In addition the peak to peak separation is no longer limited to 59 mV and for a reversible process the oxidation and reduction peaks will occur at the same potential.^{5, p.44} The voltammograms are also more symmetrical with a bell-shaped curve typically observed.

For a reversible or quasi-reversible system, the half-wave potential, $E_{1/2}$, is approximately the midpoint between the potentials of the oxidation and reduction peak.⁶ This value will be close to, but not the same as the formal potential, E_f , which is the reduction potential of a given redox couple at a given temperature, pressure and concentration. The half-wave deviates from this according to the equation:⁷

$$E_{1/2} = E_f - \frac{RT}{nF} \ln \left(\frac{D_{ox}}{D_{red}} \right) \quad (\text{Eq. 2.3})$$

D_{ox} and D_{red} here refer to the diffusions of the oxidised and reduced form of a redox couple respectively. Thus $E_{1/2} = E_f$ is a good approximation if the diffusion coefficients are similar values.

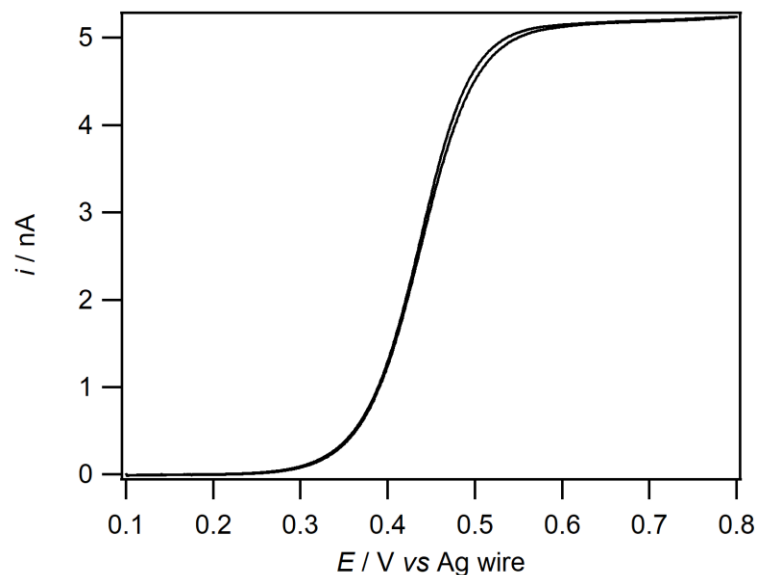


Fig. 2.5: Voltammogram of 10 mM QH₂ dissolved in wet [tea][TfO] at 40 °C. The current is measured using a 25 μm radius Pt microdisk WE at a scan rate of 1 mV s⁻¹.

For microdisc electrodes, at slow enough scan rates, the voltammogram can no longer be treated as a planar electrode, as seen in Fig. 2.3. At these slow scan rates, a peak is not observed in the voltammogram, and instead as the potential is increased and an oxidation occurs the current increases to a maximum and then remains at this steady state value. This is seen in Fig. 2.5 at potentials positive of 0.6 V. The reason for this is that the increased diffusion compared to the current of the electrode means that the concentration of the species at the electrode surface effectively remains the same as that of the bulk. Any product likewise rapidly diffuses away from the electrode surface and is effectively zero at the electrode surface and in the bulk. Therefore, when the potential sweep is reversed, the current output is still only from the oxidation process. The current therefore decreases along almost the same path back to zero with no reduction

peak observed. At faster scan rates the analyte is oxidised more rapidly which results in an oxidation peak appearing with currents above that of the steady state. A corresponding reduction peak also appears and the voltammogram tends towards that of a planar electrode at significantly fast scan rates.^{2, p.232}

2.2.2 Chronoamperometry

Chronoamperometry involves stepping the applied potential between two or more potentials and recording the resultant current decay with time passed. The most common experiment involves initially holding the electrode at a potential where no Faradaic processes occur and therefore the analyte is in its initial oxidation state. The potential is then stepped to a potential where the analyte is readily oxidised or reduced. It is key that the second potential is well beyond the peak current observed in the voltammogram, such that the analyte species at the surface rapidly decreases to zero.

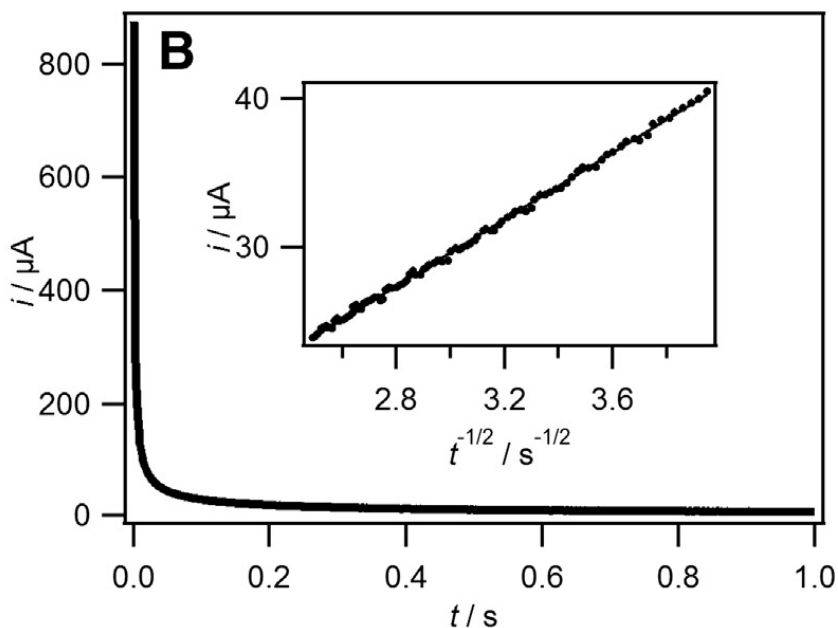


Fig. 2.6: A potential step of ≈ 10 mM $V(acac)_3$ dissolved in $[EMIm][NTf_2]$ for a single electron oxidation. Taken from Ejigu et al.⁴

This results in a sharp increase in the current which then decays over time as the analyte travels from further away to reach the electrode. In the case in Fig. 2.4, this could be initially holding the electrode at 0 V and then stepping to either 0.7 or 1.1 V to record the decay for a single or double-electron oxidation respectively. The decay is described by the Cottrell equation:^{1, p. 90}

$$i = \frac{nFACD^{0.5}}{\pi^{0.5}} t^{-0.5} \quad (\text{Eq. 2.4})$$

By plotting a graph of i against $t^{-1/2}$ a linear relationship should arise, as shown in the smaller graph in Fig. 2.6. The diffusion coefficient can then be calculated from the gradient of the graph. Unlike the Randles-Sevcik equation the Cottrell equation is not dependent on the reversibility of the species and allows for a wider range of diffusion coefficients to be calculated.

There are a few other factors that influence the current such that Eq. 2.4 does not apply over the entire timeframe. At very short times the current is not purely Faradaic but also has a component of capacitive current that increases the current at very short times until the double layer forms.^{1, p.94} In addition, at longer times of beyond a few seconds the accumulation of product and the lack of reactant near the electrode surface creates a concentration gradient that causes convection to occur. This again increases the current and so deviates from that predicted by Eq. 2.4. The consequence of this is that data can only be used in the middle region of time, where the relationship is truly linear, to calculate D .

For microdisc electrodes, the planar approximation only applies at very short timescales,^{1, p.163} and therefore Eq. 2.4 cannot be used to accurately predict the current at these electrodes. A different approach must therefore be used to model the current over the whole timeframe of an experiment. For microdisc electrodes the transient current at any point in time is described by:

$$i = 4nFCDrf(\tau) \quad (\text{Eq. 2.5})$$

Where $f(\tau)$ is a function of the dimensionless time, τ with $\tau = \frac{4Dt}{r^2}$. In order to take the transient current at longer experimental timescales into account, Shoup and Szabo⁸ devised an empirical equation to model the chronoamperometric data:

$$f(\tau) = 0.7854 + 0.8862 \tau^{-0.5} + 0.2146 e^{-7823 \tau^{-0.5}} \quad (\text{Eq. 2.6})$$

This equation has been shown to be accurate to within 0.6%. The advantage of using microdisc electrodes in determining the diffusion coefficient is that the current has a $D^{1/2}$ relationship at shorter times, while at longer times the dependence scales directly with D . On the other hand, the product nC always scales linearly. Provided the concentration is known equations 2.5-2.6 can therefore be used to calculate both D and n simultaneously.

2.3 The Seebeck Effect

The Seebeck effect states that a temperature difference between two electrodes, or even two points in a conducting material, will induce a potential difference between the two sides. For the solution-based effect, involving two electrodes in solution held at different temperatures, the origin this effect can be understood by considering the Nernst equation:

$$E = E^\circ - \frac{RT}{nF} \ln \left(\frac{a_{red}}{a_{ox}} \right) \quad (\text{Eq. 2.7})$$

Expanding this using the two equations:

$$\Delta G^\circ = -nFE^\circ \quad (\text{Eq. 2.8})$$

$$\Delta G^\circ = \Delta H^\circ - T\Delta S^\circ \quad (\text{Eq. 2.9})$$

Yields an expanded form of the Nernst equation:

$$E = \frac{T\Delta S^\circ - \Delta H^\circ}{nF} - \frac{RT}{nF} \ln \left(\frac{a_{red}}{a_{ox}} \right) \quad (\text{Eq. 2.10})$$

By differentiating this with respect to T we can get a relationship between the E and T , and from this define the Seebeck Coefficient as:

$$S_e = \frac{\partial E}{\partial T} = \frac{\Delta S^\circ}{nF} - \frac{R}{nF} \ln\left(\frac{a_{red}}{a_{ox}}\right) \quad (\text{Eq. 2.11})$$

For dilute systems, the activities of the electrolyte can be approximated as equal to the concentration of the respective redox species. By using a 1:1 ratio of the oxidised and reduced species of a specific electroactive solute we then arrive at Eq. 1.1:

$$S_e = \frac{\partial E}{\partial T} = \frac{\Delta S^\circ}{nF}$$

Assuming that ΔS° is approximately constant across a limited temperature range, a graph of temperature difference, ΔT , vs potential difference, ΔE , results in a straight line from which S_e can be calculated.

2.3.1 Thermoelectrochemical measurements

In a non-isothermal, two-electrode set up, the potential difference between the two electrodes is measured by letting a negligible current flow between the two electrodes. This is the open-circuit condition that allows S_e to be calculated.

At a given temperature these two parameters allow the power of the system to be calculated using the equation:

$$P = i \times \Delta E \quad (\text{Eq. 2.12})$$

However, since the current is close to zero P will be very small. If a larger amount of current is permitted to flow the potential difference between the two electrodes will drop. A new equilibrium at a lower potential is then established, however the power output will increase due to the increased current flow. As more current flows, the power will reach a peak before decreasing back to zero at the point when no resistance in the cell occurs and the potential difference between the two electrodes drops to zero. Thus, by plotting the power between these two extremes for a given ΔT , the maximum power output can be established as shown in Fig. 2.7.

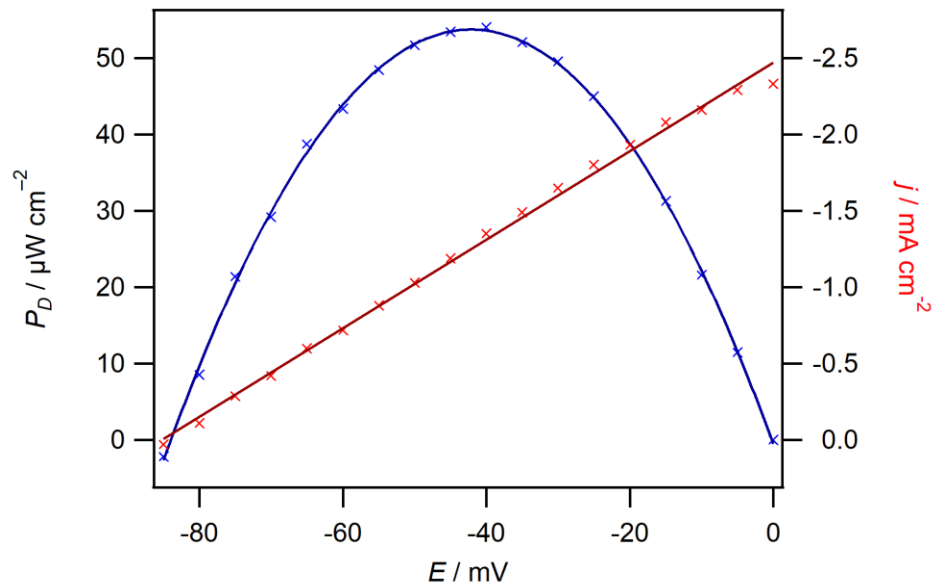


Fig. 2.7: Power (blue) and current (red) measurements are recorded in a non-isothermal cell with a constant ΔT as a function of potential difference. The power curve is parabolic in shape and peaks at a potential with maximum power, P_{max} .

2.4 References

1. R. G. Compton, C. E. Banks, *Understanding Voltammetry*, Imperial College Press, 2011, United Kingdom.
2. A. J. Bard, L. R. Faulkner, *Electrochemical Methods: Fundamentals and Applications*, John Wiley, 2001, United States.
3. R. G. Compton, G. H. W. Sanders, *Electrode Potentials*, Oxford university Press Inc., 2009, United States.
4. A. Ejigu, et al., *Electrochem. Commun.*, 2015, **54**, 55-59.
5. A. C. Fisher, *Electrode Dynamics*, Oxford University Press Inc., 2009, United States.
6. C. L. Bentley, et al., *J. Phys. Chem. C*, 2015, **119**, 22392-22403.
7. R. Koerver, et al., *Electrochim. Acta*, 2015, **184**, 186-192.
8. D. Shoup, A. Szabo, *J. Electroanal. Chem.*, 1982, **140**, 237-245.

Chapter 3

Characterisation and Thermocell Benchmark

3.1 Introduction

In this chapter, the synthesis procedure for the four PILs used in the present study are laid out. Analysis is carried out through proton Nuclear Magnetic Resonance (NMR), Attenuated Total Reflection Fourier Transform Infrared Spectroscopy (ATR-FTIR) and cyclic voltammetry.

In addition to this, the thermoelectrochemical set up is described. Analysis of $[\text{Fe}(\text{CN})_6]^{3-/4-}$ in order to test the reliability of data in this set up, and also in order to act as a benchmark for the other thermoelectrochemical systems investigated in this study.

3.2 Ionic Liquid Synthesis

In the following investigations four PILs have been used as solvents, along with one AIL and water. The PILs were synthesised from their respective acid and base components according to the following procedure, based on procedure C by Goodwin *et al.*⁶ In each case 1 M of the base in Milli-Q water was cooled down to just above 0 °C. The acid, also at a concentration of 1 M, was then slowly added dropwise to the base solution over 60-120 minutes whilst stirring. Since the base

is extremely volatile a 5% molar excess of the base was used to ensure an equimolar product. No noticeable change in the temperature of the reaction vessel was observed over the course of any of the additions. The resultant solutions were then stirred for at least 60 minutes to ensure that the reaction had gone to completion.

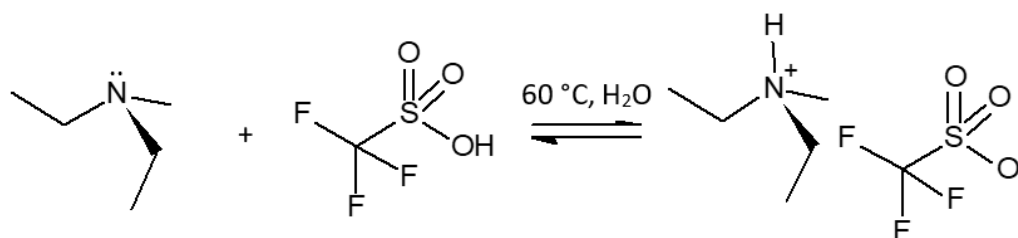


Fig. 3.1 Reaction scheme for the synthesis of [dema][TfO], the same conditions were used for each synthesised PIL.

The resultant solutions were then put on a rotary evaporator at 60 °C to remove the excess base and the bulk of the water. Once the evaporation had sufficiently slowed the solution was then dried further using a Schlenk line at $< 5 \times 10^{-2}$ mbar and a temperature of 60 °C for several days until the water content was at 100 ppm or less, as measured using Karl-Fischer titration (Mitsubishi CA-200 Moisturemeter). The resultant solutions were all colourless, or near colourless with a slight yellow tinge observed especially in liquids involving dema as the base.

The three PILs synthesised using this procedure were diethylmethylammonium triflate ([dema][TfO]), triethylammonium triflate ([tea][TfO]) and triethylammonium trifluoroacetate ([tea][TFAc]). The acids used were trifluoromethanesulfonic acid (99%, Acros Organics) and trifluoroacetic acid

(99%, Aldrich) and bases were diethylmethanamine (98%, Acros Organics) and triethylamine ($\geq 99.5\%$, Aldrich). In addition, dimethylbutylammonium triflate ([dmba][TfO]) was synthesised using a similar method by Sean Goodwin, University of Nottingham Darren Walsh group.

The aprotic IL, 1-(2-methoxyethyl)-3-methylimidazolium bis(trifluoromethanesulfonyl)imide ([C₁₀2C₁Im][NTf₂]), was obtained from Iolitec and was dried on a Schlenk line prior to use.

3.2.1 Proton Nuclear Magnetic Resonance

Nuclear Magnetic Resonance (NMR) spectra were recorded on a Bruker Ascend™ 400 MHz spectrometer at ambient temperature.

Figures 3.2 - 3.5 show typical ¹H NMR data for the four synthesised PILs used in this study. For clarity, only the shifts corresponding to the central peak or peaks for each proton site are displayed. In each case DMSO was used as the solvent, which appears on each spectrum at $\delta = 2.5$ ppm.

Fig. 3.2 Shows a typical ¹H NMR spectrum for [dema][TfO], with assignments numbered above each peak. The broad peak at 8.95 ppm is due to the labile proton on the nitrogen ion. This has been previously observed to rapidly exchange with D atoms in D₂O resulting in a broader less defined peak.⁷ The protons on the alkyl chains are observed between 0.9 and 3.1 ppm and are assigned on the spectra in figures 3.2 - 3.5.

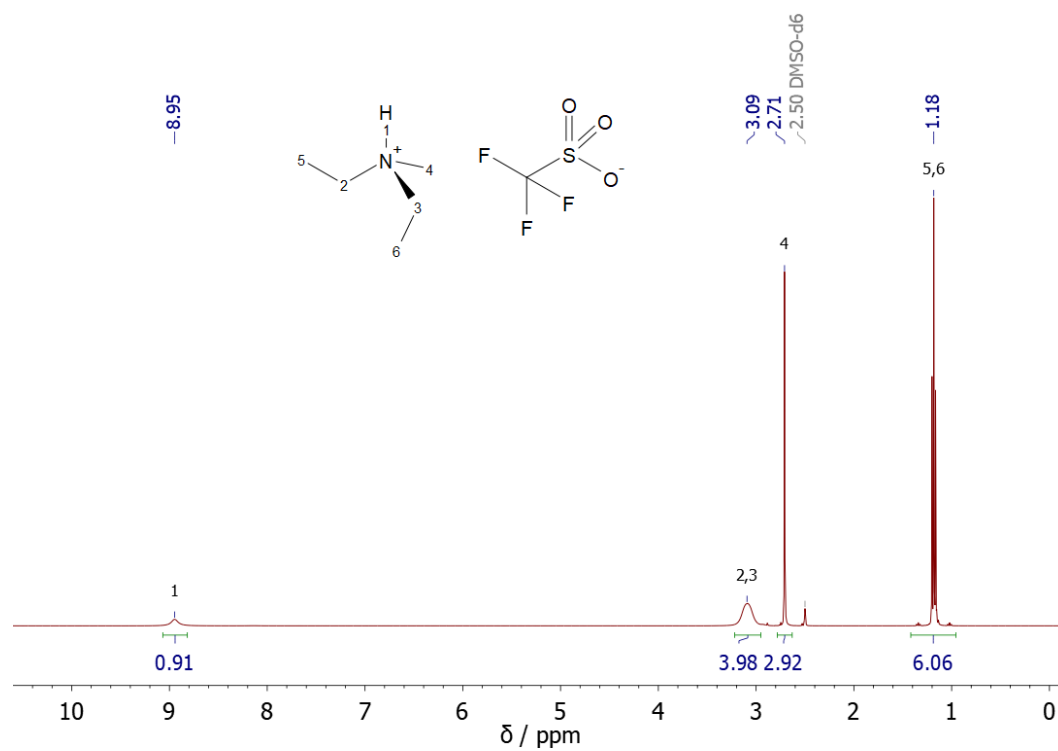


Fig. 3.2: 1H NMR spectrum of $[dema][TfO]$ dissolved in DMSO.

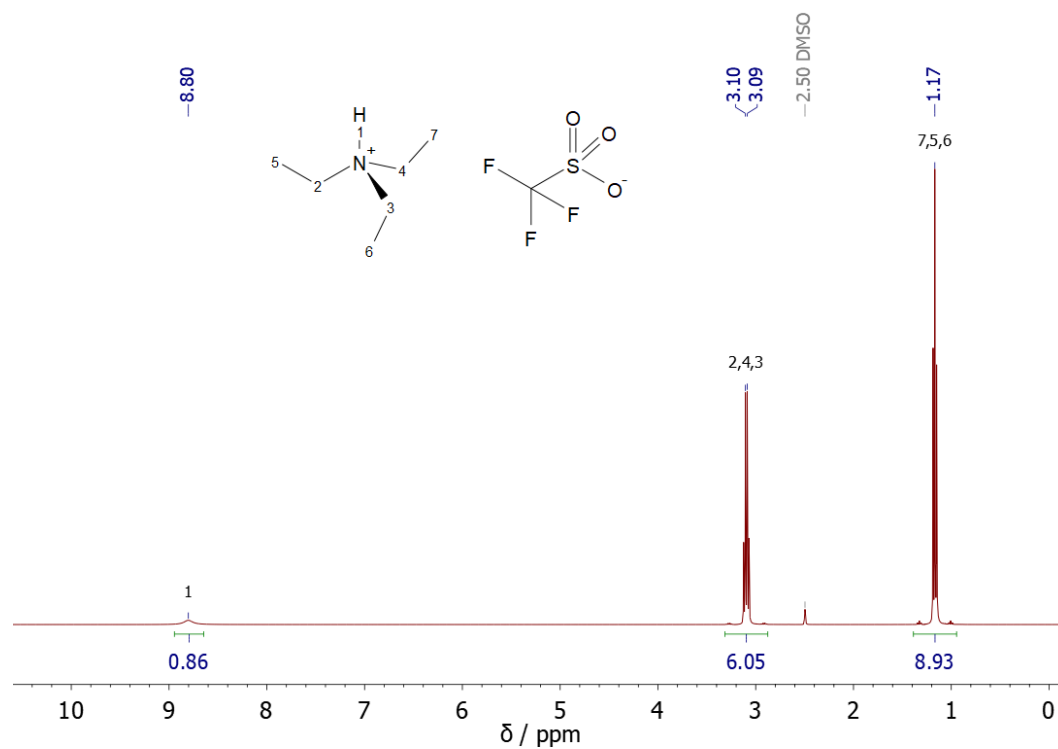


Fig. 3.3: 1H NMR spectrum of $[tea][TfO]$ dissolved in DMSO.

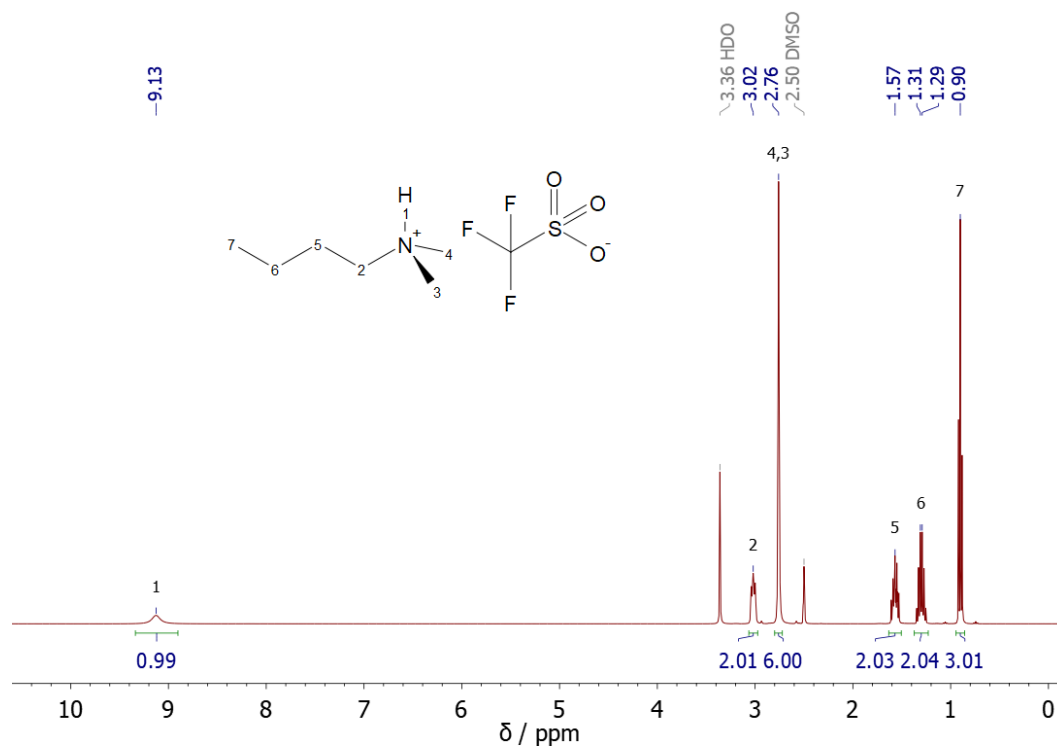


Fig. 3.4: ^1H NMR spectrum of [dmba][TfO] dissolved in DMSO. Liquid was synthesised by Sean Goodwin, University of Nottingham Darren Walsh group.

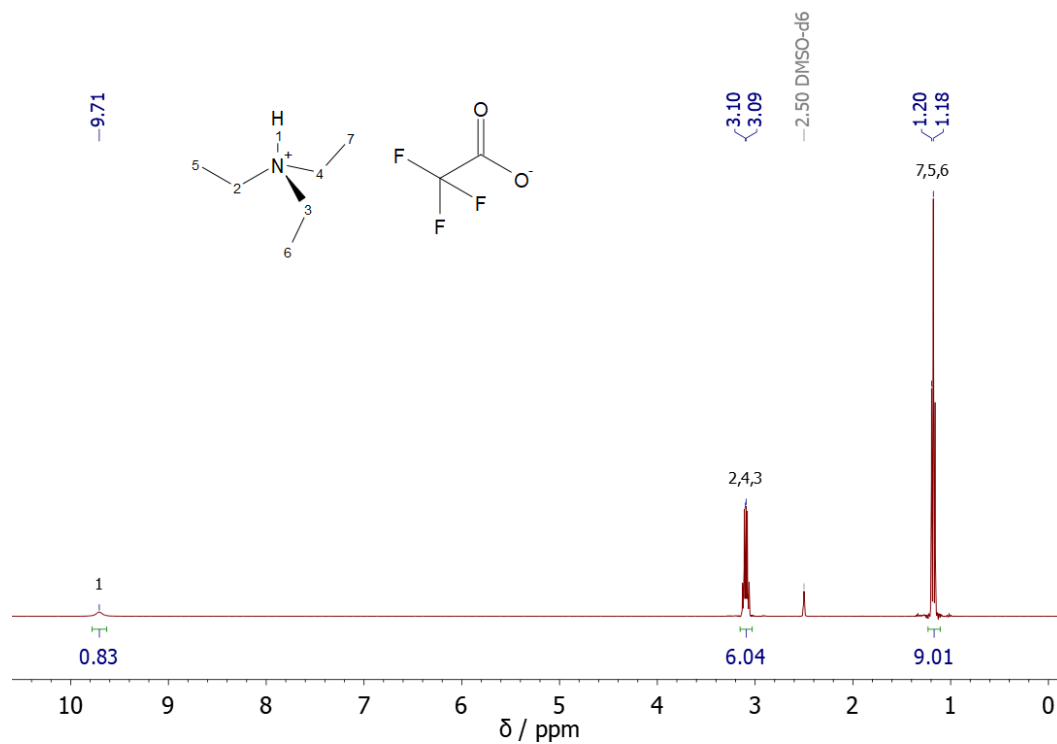


Fig. 3.5: ^1H NMR spectrum of [tea][TFAc] dissolved in DMSO.

3.2.2 Fourier-Transform Infrared Spectroscopy

Attenuated Total Reflection Fourier-Transform Infrared Spectroscopy (ATR FTIR) was carried out using a Bruker Alpha Platinum ATR FTIR spectrometer at ambient temperature. Fig. 3.6 shows typical ATR FTIR spectra for the four PILs. The spectrum for [dema][TfO] is shown in Fig. 3.6 A. This shows peaks corresponding to N-H stretches at 3058 and 2821 cm^{-1} , C-F stretches around 1250-1200 cm^{-1} , C-N stretch at 1024 cm^{-1} and an O-S-O bend at 635 cm^{-1} , in line with what is observed in the literature.⁷ [tea][TfO] and [dmba][TfO] also show similar characteristics consistent with their structures. Additional peaks at around 3500 and 1630 cm^{-1} are particularly present in the [dmba][TfO] sample. These are due to O-H stretching and bending respectively because of the higher water content in this liquid. The spectrum for [tea][TFAc] is likewise consistent with the literature.⁸

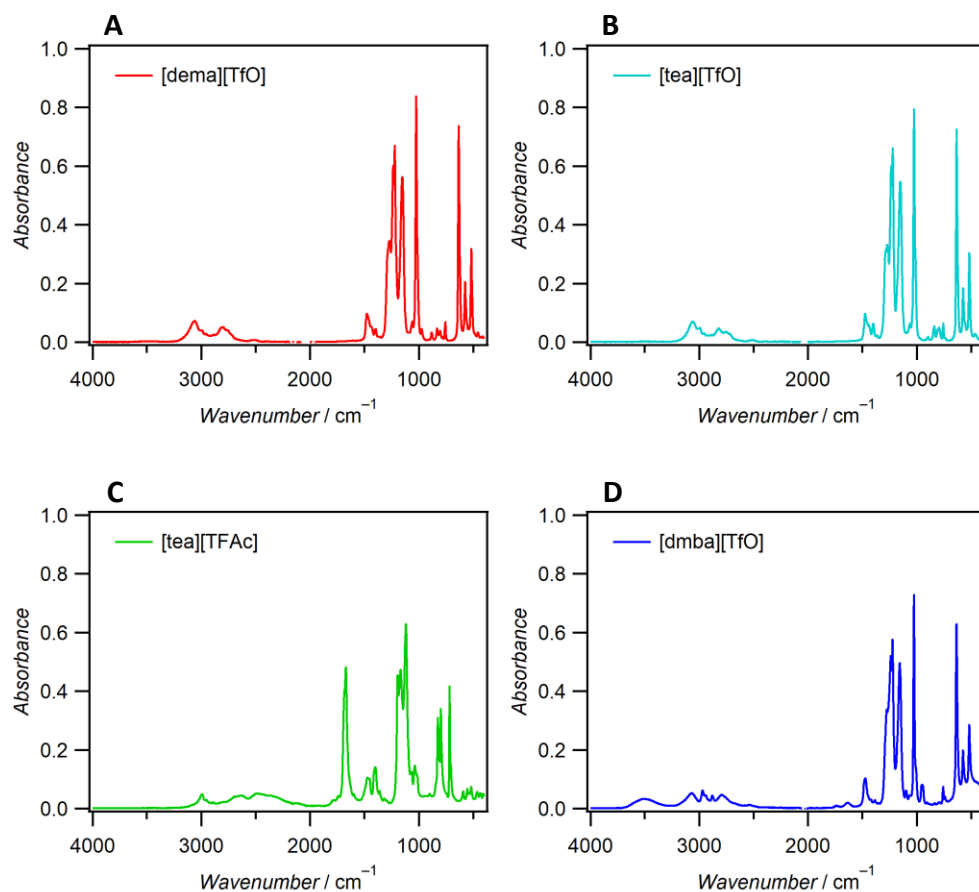


Fig. 3.6: ATR-FTIR spectra of A) [dema][TfO] B) [tea][TfO], C) [tea][TFAc] and D) [dmba][TfO] recorded at ambient temperature. All had a low water concentration (<100 ppm), except for [dmba][TfO], which had a water concentration around 9000 ppm.

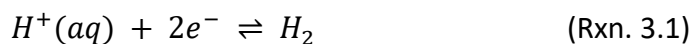
3.2.3 Cyclic Voltammetry of the Protic Ionic Liquids

For voltammetry and when determining diffusion coefficients, a three-electrode isothermal set up was used. This contained either a 3 mm GC, 2 mm Pt macrodisc or 50 μm Pt microdisc WE, Pt wire CE and either Ag/AgCl, Ag wire or SCE RE. Prior to each use, the WE was polished with 0.05 μm alumina suspended in deionised water before being rinsed thoroughly with further deionised water. The solutions used were then purged under N_2 or Ar for a minimum of 15 minutes

prior to initial measurements. A constant output of inert gas was then used to maintain an inert atmosphere during experimentation.

The synthesis of PILs is very sensitive to the synthesis procedure, particularly where the solution is allowed to heat up significantly. In the current syntheses, diluted acid is added slowly to a cooled, dilute base solution in order to avoid localised heating of the base, which can result in evaporation and breakdown of the base.⁹ The pure PILs are generally clear colourless, but colouration of these liquids can occur due to the breakdown of the base. The use of dema is particularly sensitive, where significant temperature increases during syntheses can lead to an opaque, dark brown solution. The colour of these liquids can therefore be used as an initial indicator of the purity of the synthesised liquids.

These poorly synthesised liquids result in an excess of acid being present in the product, even if a significant excess of the base is used at the start. Due to the small proportion of affected ions, these differences can be difficult to distinguish using spectroscopic techniques like NMR and ATR FTIR. However, cyclic voltammetry can be used to detect even small concentrations of excess acid in the solution. When acid is present, a reduction peak is observed in the voltammograms at potentials just positive of the bulk solvent reduction.⁶ This corresponds to the evolution of hydrogen according to the reaction:



Figures 3.7 and 3.8 show typical voltammograms for the two main PILs used in this study. The voltammograms are relatively flat over the middle region between the solvent breakdown potentials. There is no clear reduction peak observed positive of the solvent breakdown potential indicating that little excess acid is present in the PILs.

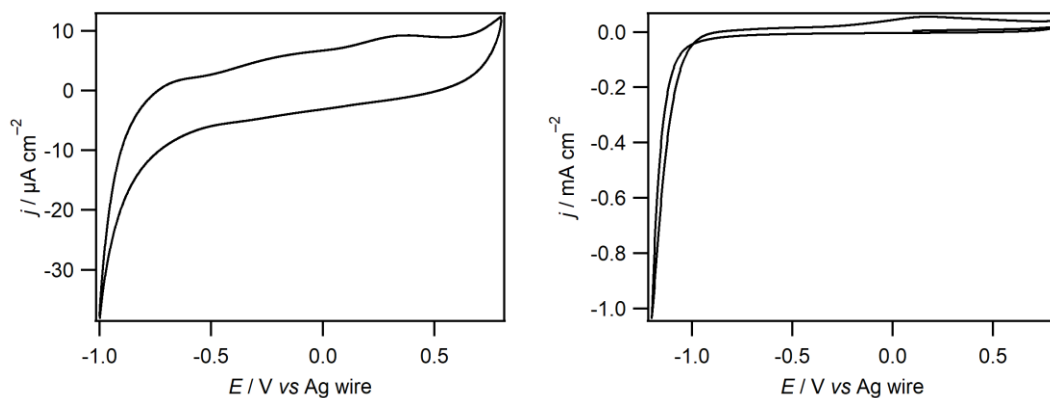


Fig. 3.7: Cyclic voltammograms of synthesised [dema][TfO] at a 1 mm diameter Pt working electrode. The scans were taken at 50 mV s^{-1} (left) and 100 mV s^{-1} (right).

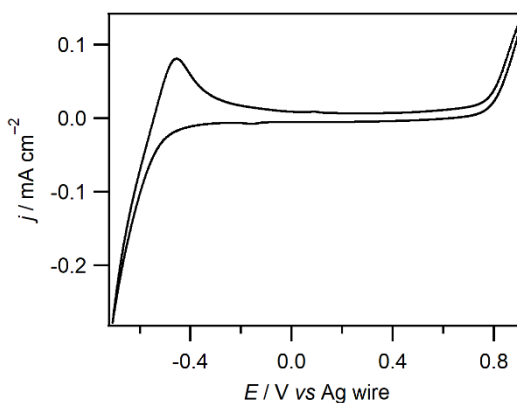


Fig. 3.8: Cyclic voltammogram of synthesised [tea]TfAc at a 1 mm diameter Pt working electrode. The scan was taken at 50 mV s^{-1} .

3.2.4 Viscosity and Density Measurements

The viscosities and densities of the dried ILs used in this study were measured at temperatures between 20 and 40 °C. The exception was [tea][TfO], which was prone to crystallisation at room temperature. Therefore, viscosity measurements could not be carried out on this liquid. The results of these measurements are shown in Fig. 3.9.

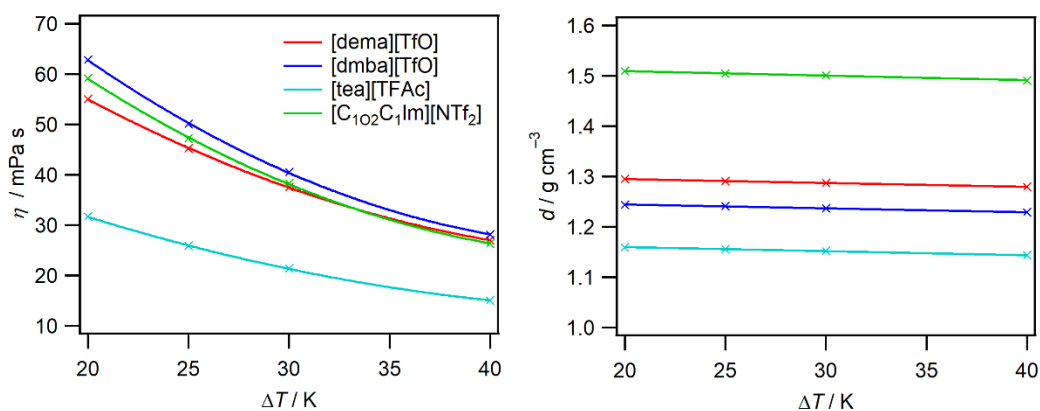


Fig. 3.9: Dynamic viscosities (left) and densities (right) of four of the ILs at temperatures of 20 to 40 °C.

The results show that the aprotic IL, along with the HTfO based liquids have similar viscosities across the range with values of around 50 mPa s at 25 °C. The viscosity of [tea][TFAc] is significantly less than the others with a viscosity of 25.9 mPa s at 25 °C. The density of [tea][TFAc] is also lower than the other ILs with a value of 1.156 g cm⁻³ at 25 °C. The aprotic liquid has the highest density of 1.504 g cm⁻³ at 25 °C.

3.3 Thermoelectrochemical Setup

Non-isothermal measurements were collected in a U-shaped glass cell with a Pt electrode in either side. A schematic and picture of this cell is shown in Fig. 3.10. The electrodes were 0.5 mm diameter Pt disks which were sealed in glass. The depth of the two electrodes was set so that they were equal height and the shortest path between the two was 10 cm for consistency between different experiments. Prior to each experiment, each electrode was polished with 0.05 μm alumina and then washed in concentrated nitric acid to ensure a smooth, clean surface.

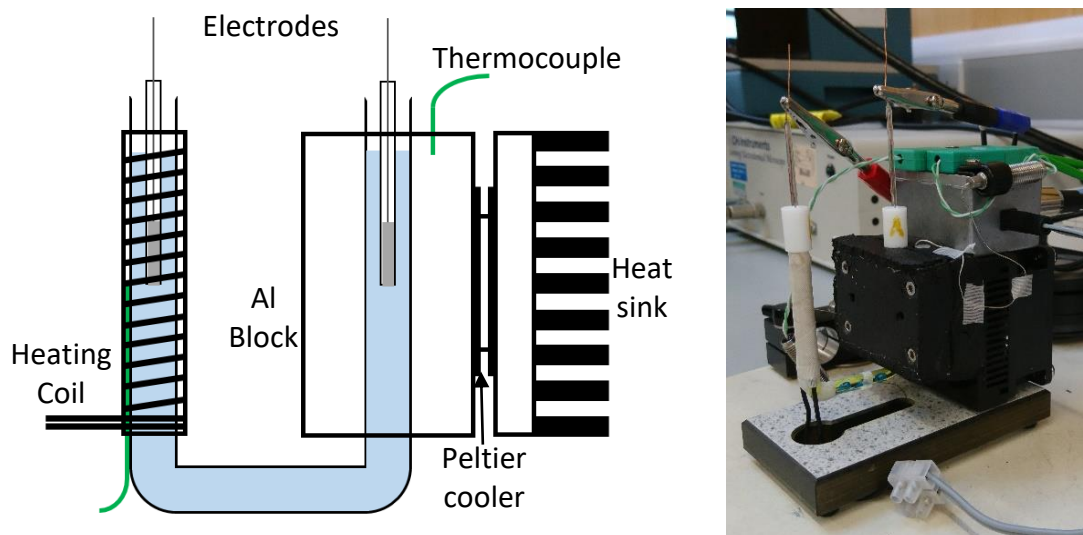


Fig. 3.10: Left: Schematic diagram of the U-shaped cell used for non-isothermal measurements, with the hot side on the left and cool side on the right. Right: Photograph of the TEC setup.

The hot side of the cell was heated by passing a current through an insulated, resistance wire. The wire was coiled up the tube, then down again along the same

path to negate any induced magnetic field within the tube that may disrupt measurements. The cold side of the cell was kept at a constant temperature of 20 °C for all measurements at $\Delta T > 10$ °C. For $\Delta T < 10$ °C the cold temperature was generally slightly warmer in order to get the required temperature difference. The cold temperature was maintained by enclosing the tube in an Al block, which was cooled using a Peltier cooler. A very thin layer of padding between the block and the glass to avoid excessive pressure being applied directly to the glass tube. The one exception was for the acetylacetonate measurements in Chapter 7 where the cold temperature was kept at ambient temperature, which was between 21.8-24.1 °C for these experiments.

Due to the potential interference of the thermocouple in some measurements, especially those involving iodine, the thermocouples were not submerged in the solution. Instead, the thermocouples were outside the glass and the thermocouple temperature was calibrated with water to the internal temperature to account for the temperature difference between the thermocouple and the electrode surface.

In this two-electrode set up the counter electrode also acts as a reference and the potential of the hot electrode is measured relative to the potential of the cold electrode. The temperature of both sides was controlled and measured using a thermostat.

Measurements of the Open Circuit Potential (OCP) of the system were recorded whilst increasing ΔT stepwise by intervals of 5 or 10 °C. The potential was then left to stabilise at each temperature for a minimum of 5 mins prior to measurements being recorded. For the measurements where the potential remained stable up to either 50 or 100 °C, measurements were then recorded whilst decreasing the temperature by the same intervals.

Power measurements were also conducted in this 2-electrode U-shaped cell. For each set of measurements ΔT was kept constant at either 30, 50 or 100 °C. Further details are outlined in section 2.3.1.

3.4 Potassium Ferri/ferrocyanide

Aqueous $[\text{Fe}(\text{CN})_6]^{3-/4-}$ at a concentration of 0.4 M (0.2:0.2 M each species) is widely considered as the benchmark system for TECs.^{10, 11} This therefore can be used as a test of the reliability of the experimental set up and as a comparison for investigating other thermoelectrochemical systems. The high charge on the anions results in a large entropy change for the redox reaction, leading to a high S_e of -1.4 mV K^{-1} . The species also show fast reversible electrochemistry in aqueous systems maximising the power output. In addition to measurements of S_e , power measurements have been conducted for this species to act as a reference for all other solutions studied.

3.4.1 Electrochemical studies

The voltammetry of $[\text{Fe}(\text{CN})_6]^{4-}$ is shown in Fig. 3.11, it shows a single oxidation to $[\text{Fe}(\text{CN})_6]^{3-}$ with its corresponding reduction. There is a slight shift in the peak potential as a function of the scan rate, indicating quasi-reversibility in the system. This relatively high reversibility means that the equilibrium state is rapidly established, meaning that the system will respond quickly to changes at the electrode-solution interface. This means that the equilibrium potential at any temperature will be rapidly established and will maximise the power outputs from the system.

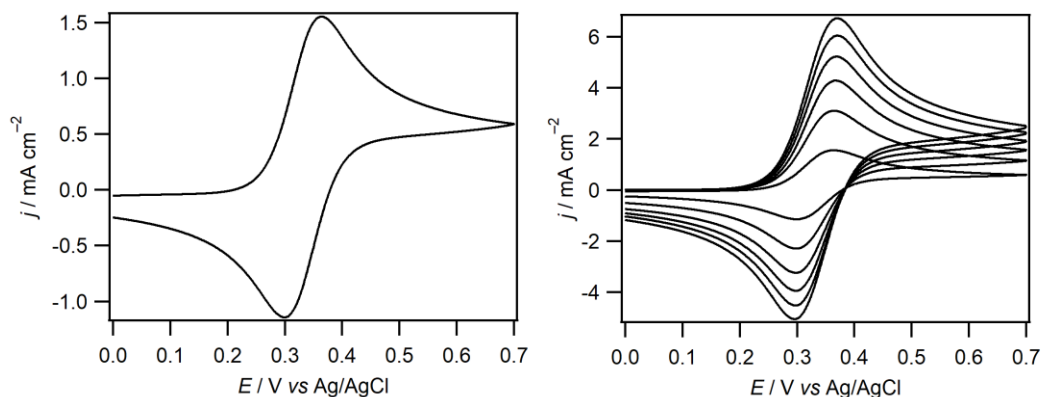


Fig. 3.11: Cyclic voltammogram of a 10 mM solution of $[\text{Fe}(\text{CN})_6]^{4-}$ dissolved in a 1 M aqueous KCl solution. Left: voltammogram at 50 mV s^{-1} . Right: Voltammograms if increasing scan rates from 50 to 1000 mV s^{-1} . All CVs were recorded at ambient temperature using a 1 mm radius Pt WE.

3.4.2 Thermoelectrochemical studies

Fig. 3.12 shows potential vs temperature graphs for $[\text{Fe}(\text{CN})_6]^{3-/4-}$ solutions at concentrations of 0.4, 0.1 and 0.02 M. The Seebeck coefficients measured for

these three solutions are -1.44 , -1.55 and -1.65 mV K^{-1} respectively and show good stability over the whole temperature range. The Seebeck coefficient for the 0.4 M solution is consistent with the value of -1.4 mV K^{-1} generally quoted for 0.4 M of this species. The values at 0.1 and 0.02 M are also consistent with other observations that decreasing the concentration of analyte increases S_e . The high reversibility of the system means there is a very good correlation in the data points.

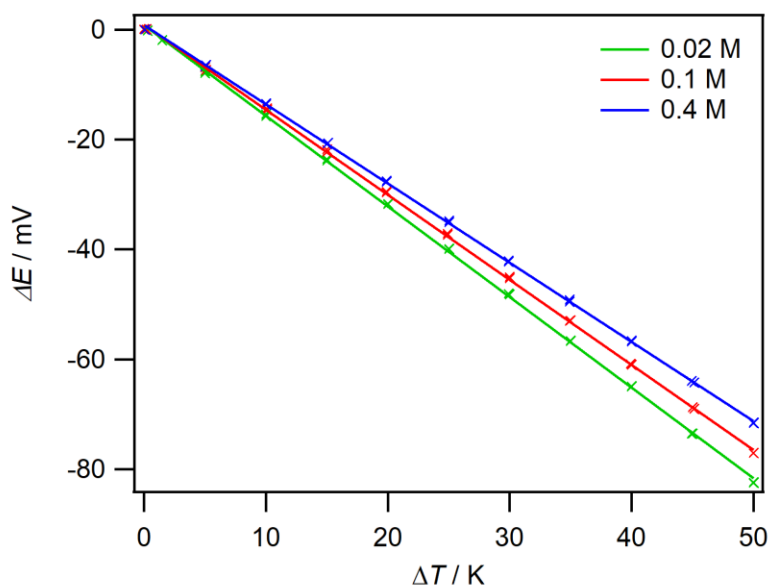


Fig. 3.12: Graph of potential difference vs temperature difference for 0.4 M (red), 0.1 M (blue) and 0.02 M (green) aqueous $[\text{Fe}(\text{CN})_6]^{3-/4-}$ solutions. Data is recorded in 5-degree intervals with ΔT being increased to $50 \text{ }^\circ\text{C}$ then cooled back to $5 \text{ }^\circ\text{C}$ or less.

3.4.3 Power measurements

Fig. 3.13 shows graphs of the power output against applied potential for the three different $[\text{Fe}(\text{CN})_6]^{3-/4-}$ concentrations. The power data is recorded at $\Delta T =$

30 and 50 °C for each solution. In all cases there is a very strong correlation in the recorded data.

At $\Delta T = 30\text{ }^{\circ}\text{C}$ the maximum power outputs, P_{max} , were 2.6, 12 and $40\text{ }\mu\text{W cm}^{-2}$ for the 0.02, 0.1 and 0.4 M solutions respectively. These increased to 8.6, 44 and $150\text{ }\mu\text{W cm}^{-2}$ respectively at $\Delta T = 50\text{ }^{\circ}\text{C}$.

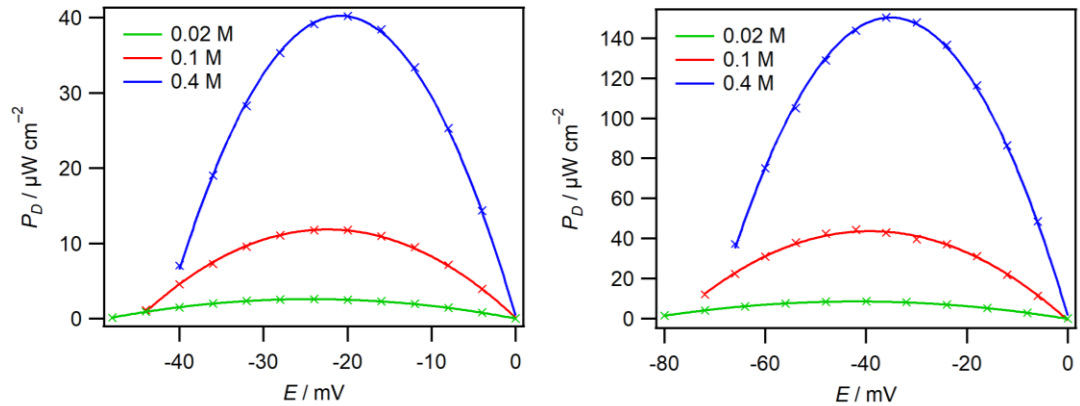


Fig. 3.13: Graph of power densities vs applied voltage for aqueous $[\text{Fe}(\text{CN})_6]^{3-/4-}$ at $\Delta T = 30\text{ }^{\circ}\text{C}$ (Left) and at $\Delta T = 50\text{ }^{\circ}\text{C}$ (Right).

A similar setup was used by Burrows.¹² For that setup values of 29 and $93\text{ }\mu\text{W cm}^{-1}$ were calculated for analyte concentrations of 0.1 and 0.4 M solutions at $\Delta T = 50\text{ }^{\circ}\text{C}$. This is comparable, but slightly lower than observed in the present study. However, Burrow's measurements were recorded with the electrodes at a separation of 25 cm, which would reduce the overall power outputs. This power drop would be partially counteracted by the warmer cold temperature of $30\text{ }^{\circ}\text{C}$, but the larger separation appears to be the dominant factor in this case.

The cold electrode will be the electrode at which the current is limited due to the higher viscosity and lower diffusion coefficients. The actual temperature of

the cold electrode will therefore play a role in the maximum power output as well as the overall temperature difference.

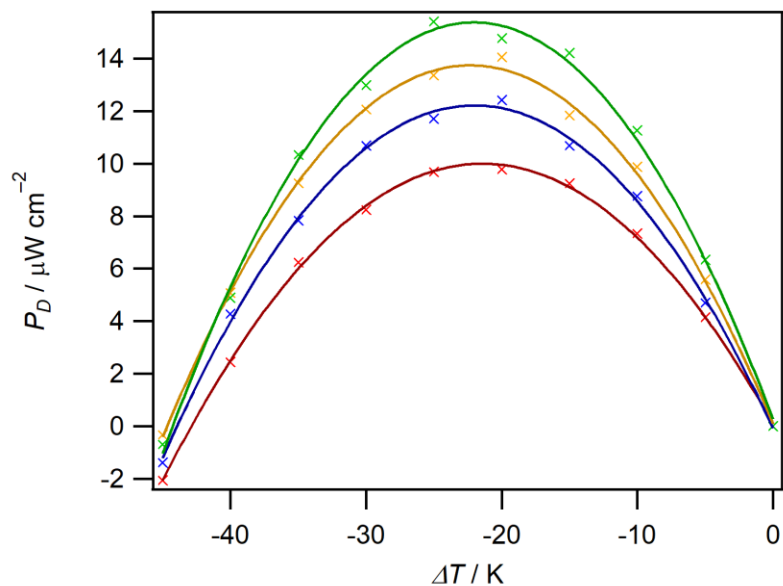


Fig. 3.14: Graph of power density vs applied voltage at $\Delta T = 30^\circ\text{C}$ for a 0.1 M aqueous $[\text{Fe}(\text{CN})_6]^{3-/4-}$ solutions. The data is recorded at $T_C = 10^\circ\text{C}$ (red), 15°C (blue), 20°C (yellow) and 25°C (green).

To quantify the influence of the cold temperature on the overall power output, experiments were conducted at cold temperatures of between 10 and 25 °C for 0.1 M of analyte with a constant ΔT of 30 °C. The results of this are shown in Fig. 3.14.

The maximum power output for the four systems increases from 10 to 15 $\mu\text{W cm}^{-1}$ as the cold temperature increases from 10 to 25 °C (T_H increased from 40 to 55 °C). This represents a significant increase in P_{max} of 12.5% between 20 and 25 °C and a difference of 50 % for the full 15 °C increase. This shows the importance

of controlling the colder temperature in order to accurately compare power data between different systems.

3.5 Conclusions

The PILs synthesised have been characterised by NMR and ATR FTIR spectroscopy as well as investigations of minor impurities through cyclic voltammetry. Measurements of the viscosity, density of these liquids has also been carried out. Each one has been shown to have a good purity with minimal residual acid present in each synthesised PIL. As expected, the viscosities of the ILs are significantly higher than that of water. The lowest is [tea][TFAc] with a viscosity approximately half of that for the other three ILs and also has the lowest density of 1.156 g cm^{-3} .

The thermoelectrochemical studies show the reliability of data recorded by the cell. The Seebeck Coefficients for $[\text{Fe}(\text{CN})]^{3-/4-}$ are consistent with values established elsewhere in the literature. The power outputs are also comparable to measurements obtained by Burrows¹² after accounting for differences in the instrument set up. This therefore provides a good benchmark for comparison with the other systems used in the present study.

A further study focusing on the shifting of the absolute temperatures of the two electrodes shows the significant differences that can occur with even small changes to the temperatures of these electrodes. At $\Delta T = 30 \text{ }^\circ\text{C}$ an increase in the temperature of both electrodes by $15 \text{ }^\circ\text{C}$ revealed an increase in P_{max} of 50%.

Maintaining a constant cold temperature is therefore necessary to maximise the accuracy in comparisons of data for the different systems.

3.6 References

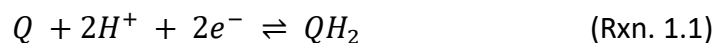
1. T. J. Abraham, et al., *Chem. Commun.*, 2011, **47**, 6260-6262.
2. T. L. Greaves, C. J. Drummond, *Chem. Rev.*, 2008, **108**, 206-237.
3. J. Stoimenovski, et al., *PCCP*, 2010, **12**, 10341-10347.
4. M. Yoshizawa, et al., *JACS*, 2003, **125**, 15411-15419.
5. M. S. Miran, et al., *PCCP*, 2012, **14**, 5178-5186.
6. S. E. Goodwin, et al., *Langmuir*, 2017, **33**, 8436-8446.
7. K. Mori, et al., *Bull. Chem. Soc. Jpn.*, 2010, **83**, 328-334.
8. Bio-Rad Laboratories, Inc. SpectraBase:
<https://spectrabase.com/spectrum/EnNpaKjTmAi>
9. D. E. Smith, D. A. Walsh, *Advanced Energy Materials*, 2019, **9**.
10. H. A. H. Alzahrani, et al., *Electrochem. Commun.*, 2015, **58**, 76-79.
11. T. J. Abraham, et al., *PCCP*, 2014, **16**, 2527-2532.
12. B. Burrows, *J. Electrochem. Soc.*, 1976, **123**, 154 - 159.

Chapter 4

Electrochemical Studies of Hydroquinone/p-benzoquinone in Ionic Liquids

4.1 Background

As outlined in Chapter 1, the electrochemistry of QH₂ and Q has been widely analysed in a variety of solvents. It is well known that the reaction pathways and products of these reactions depend largely on the nature of the solvent it is in. In a well buffered aqueous solution Q is reduced in a 2-electron single-wave to form QH₂:¹



In unbuffered aqueous systems this reduction only occurs when there is sufficient acid to fully protonate Q. If the pH is sufficiently high the lack of protons results in deprotonated forms of QH₂ becoming the major product:



In aprotic media, where there is a lack of proton availability and the radical Q^{•-} is stabilised the reduction proceeds via two single-electron waves to form a double anion species:²



While quinones have been studied in a range of AILs,²⁻⁸ investigations of quinones in PILs is far more limited. As stated in Chapter 1.4, PILs contain a labile proton, which can therefore influence proton dependent reactions, such as for quinone. However, the exact nature of this interaction between the PIL and quinone species will be influenced the nature of the acids and bases involved in the PIL synthesis. Stronger acids and bases will result in a more strongly bound proton and therefore it is less likely to influence the quinone electrochemistry. For processes such as PIL fuel cells and proton accepting batteries, nonstoichiometric PILs using an excess of the parent acid are required for sufficient protonation to occur.^{9, 10}

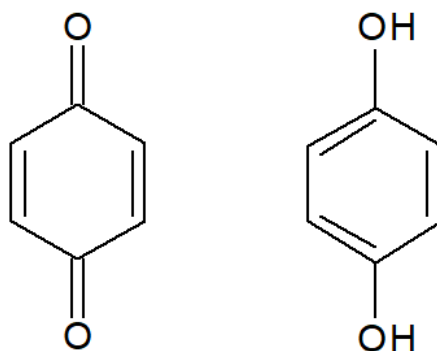


Fig. 4.1: The chemical structures of p-benzoquinone (left) and hydroquinone (right).

Here, cyclic voltammetry and chronoamperometry have been used to probe the oxidations and reduction reactions of Q and QH₂ in three PILs, triethylammonium trifluoroacetate ([tea][TFAc]) and diethylmethylammonium

trifluoromethanesulfonate ([dema][TfO]) and triethylammonium trifluoromethanesulfonate ([tea][TfO]). For the first two PILs the electrochemical response was investigated in the presence of additional acid and base. For the [tea][TfO] solutions higher temperatures were required for electrochemical experiments to ensure the IL remained liquid. Measurements using excess base were therefore not conducted in this liquid due to the increased volatility of the base. Investigations of both analytes in the presence of excess water were also conducted in [dema][TfO]. For all measurements involving adding excess acid or base the reference electrode was placed behind a fritted tube which contained only the pure PIL.

The aim of this chapter is to provide a detailed analysis of the electrochemistry of Q and QH₂ in PILs. In doing this, a better understanding can be gained of these systems and of the influence of different acid and base combinations on the nature of the synthesised PIL.

In the context of TECs, it is desirable that a single redox couple is present, with the simplest choice for quinones being Q and QH₂. It is therefore necessary to understand the reactions present in these PILs in order to ensure that no complicating side reactions are occurring.

4.2 Experimental

4.2.1 Chemicals

Analytical grade hydroquinone (99%, Acros Organics) and p-benzoquinone (98%, Aldrich) were used as obtained for all electrochemical measurements. The ionic liquids used were all synthesised from their respective acids and bases. The acids used were trifluoromethanesulfonic acid (99%, Acros Organics) and trifluoroacetic acid (99%, Aldrich) and bases were diethylmethylamine (98%, Acros Organics) and triethylamine ($\geq 99.5\%$, Aldrich).

The PILs were synthesised as outlined in section 3.2, by the addition 1 M acid solution dropwise to 1 M base with a 5% molar excess of the base. All solutions were stored in a glove box under a N_2 atmosphere to maintain dryness. The water content was measured to be <100 ppm by Karl-Fischer titration for each liquid prior to experiments being carried out. Tests conducted after experiments using excess acid suggest the water content remained below 1000 ppm (72 mM), however, in the presence of excess base the ppm was sometimes slightly higher than this value.

4.2.2 Electrochemical measurements

For all experiments, except those involving the addition of base, measurements were conducted in a glove box under a nitrogen atmosphere. For experiments involving the addition of base, measurements were taken in a sealed glass vessel with a constant positive pressure of dried Ar within the cell to ensure minimal amounts of water entered the system. All measurements taken use either

a Glassy Carbon (3 mm diameter) or Pt microdisk (25 μm radius) WE. An Ag wire quasi RE and Pt wire CE were also used.

For all measurements involving the addition of acid or base the reference electrode was kept behind a glass frit to minimise any shift in the potential over the course of each set of experiments. Using this method, the reference was observed to remain relatively stable. No noticeable changes were observed across the course of an experiment and minimal shift was observed over several months of use.

For measurements involving the addition of acid and water, specific volumes of the species were added and the change in mass of the solutions were measured to get a more accurate calculation of the concentrations. Since the acid solution was not dried prior to the addition there may be errors in the exact concentration of acid due to absorbed water from the atmosphere. Carl-Fischer titrations were conducted after some of the experiments and suggested that the water content remained below 1000 ppm (72 mM). For experiments where water was intentionally added, the concentration of water at the start and end the experiment was determined by Carl-Fischer titration. This was found to be in good agreement with calculations based on the increase of mass between each measurement.

Due to the volatility of the base, it was necessary to add this drop wise via a syringe. Since a single drop is too small to be accurately measured by the 1 mL

syringes, calibration runs were taken by measuring the volume and mass of 20 drops several times and taking an average over the runs to get an average volume per drop. Errors for these experiments are therefore higher than those involving the addition of acid or water.

All electrochemical measurements were recorded using a CHI700D Potentiostat with IR correction used to compensate for the internal resistance of the cells. Each experiment consisted of between 1 and 10 mM of analyte dissolved in the various ILs. Additional amounts of either acid, base or water were then added to these solutions. The solutions were then mixed and left for at least 15 minutes to let the solution equilibrate. For each set of experiments two voltametric scans were recorded approximately 15-20 minutes apart. This was used to check for consistency and that the solution was sufficiently well mixed.

For voltametric measurements involving Q, the potential sweep usually began around 0.1-0.2 V and initially scanned negatively. Similarly, for QH₂ the sweep began around 0.1-0.2 V and was initially scanned positively. The starting point was chosen to be before the Q oxidation or QH₂ reduction reactions had taken place where the current was around 0.

4.3 Results and Discussion

4.3.1 Electrochemistry of Q and QH₂ in [dema][TfO]

Typical electrochemical responses for 10 mM Q (red) and QH₂ (blue) are shown in Fig. 4.2. The trace for Q shows a large reduction peak at -0.32 V, along with a smaller reduction wave at approximately -0.1 V. Two oxidation peaks are observed at 0.10 V and 0.68 V with a further small shoulder observed around 0.55 V. The most positive oxidation at 0.1 V is symmetric in shape, suggesting there is adsorption of the reactants onto to the electrode surface. Peak clipping experiments reveal that the major reduction at -0.32 V is coupled with the oxidation at 0.1 V. Shoup-Szabo fitting at a micro electrode reveals that the Q reduction is a 2-electron process.

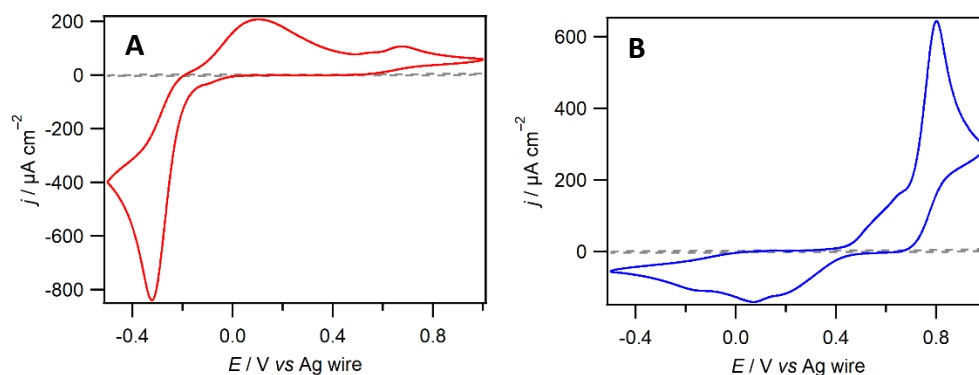


Fig. 4.2: Cyclic voltammogram of 10 mM Q (A) and 10 mM QH₂ (B) dissolved in [dema][TfO]. In both cases a scan of pure [dema][TfO] is shown as a grey dotted line. The voltammograms were taken at a 3 mm GC working electrode at a scan rate of 50 mV s⁻¹.

For QH₂ in blue, there is a large oxidation peak at 0.80 V, with smaller waves around 0.45-0.7 V. There are also three reduction waves at 0.16, 0.07 and -0.12 V. Shoup-Szabo fitting at a micro electrode reveals that the QH₂ oxidation is a 2-electron process.

Due to the sensitivity in the synthesis of the IL, it is difficult to get perfect consistency between different batches of the IL. This was particularly noticeable in [dema][TfO], where slightly different voltammetry was observed in each case. Overall, three different batches of [dema][TfO] were used in the present study. The voltammograms for 10 mM solutions of Q or QH₂ in each of these liquids are shown in Fig. 4.3, labelled IL 1.1, 1.2 and 1.3.

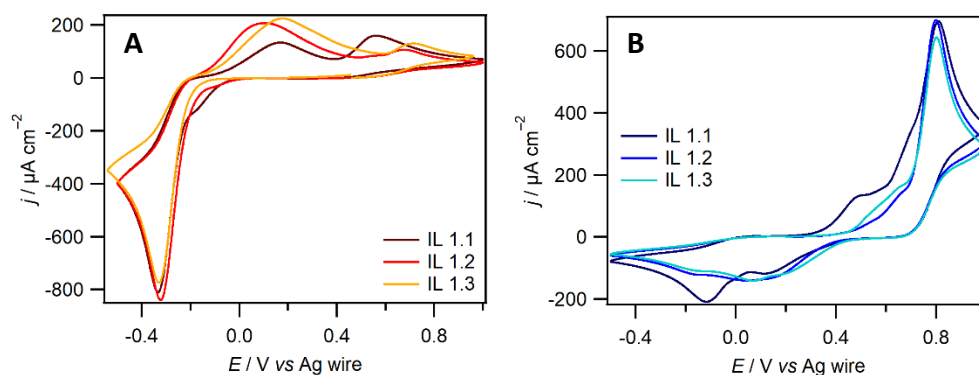


Fig. 4.3: Cyclic voltammogram of 10 mM Q (A) and QH₂ (B) dissolved in [dema][TfO]. Taken with IL samples 1.1 to 1.3. The voltammograms were taken at a 3 mm GC working electrode at a scan rate of 50 mV s⁻¹.

While the voltammograms for IL 1.2 and 1.3 are relatively similar, the voltammetry of IL 1.1 has a few differences. The major Q reduction and QH₂ oxidation reactions remain consistent between the three liquids. The most distinct difference for Q in Fig. 4.3 A is that in IL 1.1, the first oxidation reaction at 0.17 V is smaller than for the other two liquids, while there is a more prominent peak observed at 0.58 V. For the QH₂ in Fig. 4.3 B, there is a more prominent oxidation reaction at 0.50 V in IL 1.1 than the other two liquids. There is also a larger reduction reaction at -0.12 V.

The differences observed in Fig. 4.3 are likely to be the result of differences in composition of the liquid, which possibly a result of some decomposition of the base. To produce the most reliable and consistent analysis of these solutions, most measurements in the present study were conducted in IL 1.2 or 1.3, where IL 1.1 has been used it is specified in the figure caption.

Fig. 4.4 shows a cyclic voltammetry of a 50:50 mix (black) of Q and QH₂ at 5 mM each dissolved in [dema][TfO]. In addition, voltammograms of 10 mM Q (red) and 10 mM QH₂ (blue) are also shown. Each analyte is dissolved in IL 1.1. The trace of the 50:50 solution shows two reductions at -0.31 and -0.19 V and three oxidation peaks at 0.01, 0.47 and 0.71 V. The most negative reduction at -0.33 V in the Q trace lines up well with the reduction at -0.31 V in the 50:50 solution, suggesting that the same reaction is occurring.

The more positive reduction wave around -0.2 V also appears to be the same reaction occurring at -0.19 V in the 50:50 solution. The increase in the size of this reduction peak when QH₂ is present shows that this reaction becomes more favourable as the acid content increases and is therefore likely to involve a protonation reaction. A comparison of these two reductions with those observed in the pure QH₂ solution is difficult due to the large differences in peak potential of the reactions.

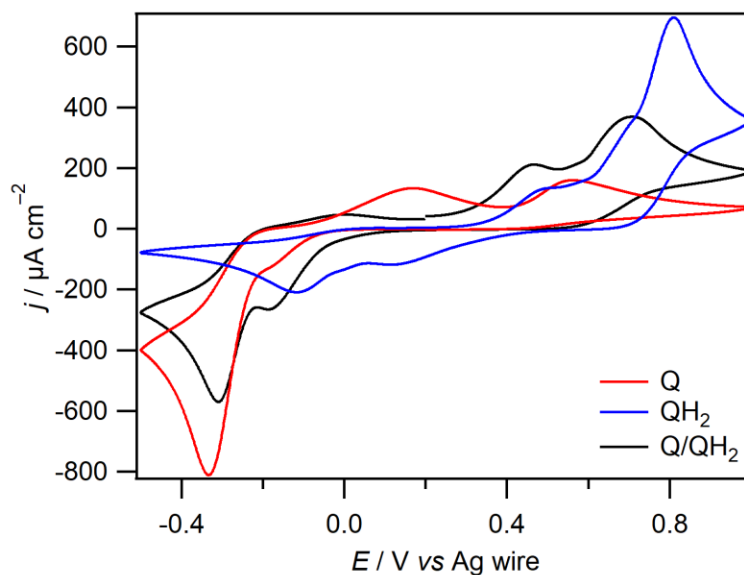


Fig. 4.4: Cyclic voltammogram of 10 mM QH_2 (blue), Q (red) and 5 mM each Q and QH_2 dissolved in $[\text{dema}][\text{TfO}]$ (IL 1.1). The 50:50 mixture was first scanned negatively with the above trace starting at 0.2 V on the subsequent positive going scan. The voltammograms were taken at a 3 mm GC working electrode at a scan rate of 50 mV s^{-1} .

The two oxidations observed at 0.47 and 0.71 V in the 50:50 solution follow a similar form to the oxidation peaks at 0.5 and 0.81 V for the pure QH_2 solution, which suggests these involve the same oxidation reactions. The smaller broad peak at 0.01 V in the 50:50 mixture has a similar broad shape to the Q oxidation wave that peaks at 0.17 V, again suggesting the same reaction is occurring. However, for the 50:50 solution this wave is much smaller and shrinks more rapidly than the corresponding reduction at -0.31 V . Such a significant decrease in the size of the oxidation reaction suggests that the product of the reduction is reacting after the initial reduction occurs. This is likely to be a protonation reaction. The oxidation wave in the pure Q solution at 0.56 V is not easily comparable to the oxidations in the other two liquids.

To gain a better understanding of these reactions further analysis is required of these systems. By lowering the analyte concentrations, the electrochemical reactions become more sensitive to the acid concentration in the PIL, since the ratio of protons to analyte is increased. To investigate these differences the electrochemical response was measured with analyte concentrations ranging from 1 to 10 mM. The results of this are shown in figures 4.5 and 4.6.

Fig. 4.5 shows the electrochemical response for different concentrations of Q in [dema][TfO]. As the concentration of Q is decreased, the major reduction peak at -0.32 V decreases. Fig. 4.5 B shows that this decrease is slightly more than the drop in concentration. The corresponding oxidation wave around 0.1 V decreases more rapidly than the corresponding reduction and at a Q concentration of 2 mM is barely visible in the voltammetry. This suggests that the product of the reduction at -0.32 V becomes unstable at higher relative proton concentrations, which may be due to further protonation of the product after the reduction reaction has occurred.

The smaller reduction wave around -0.1 V becomes proportionally larger as the Q concentration decreases to 2 mM. The oxidation waves at 0.68 and 0.55 V merge at lower electrolyte concentrations with a single peak observed at 0.55 V in the 2 mM Q solution. These become the dominant oxidation reactions at the lower Q concentrations. Fig. 4.5 B shows that the shape of the 2 mM and 1 mM voltammograms are almost identical, with the reactions only dependent on the Q

concentration. This shows that there is little significant change in the reactions between these two concentrations.

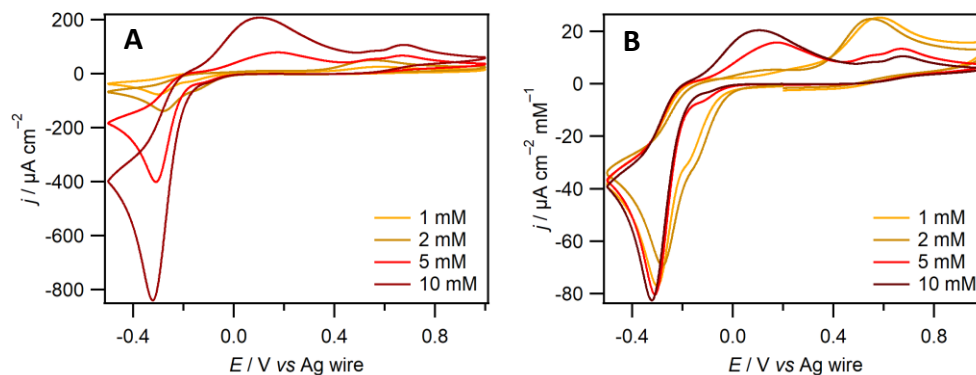


Fig. 4.5: Cyclic voltammograms of Q dissolved in [dema][TfO] at concentrations of 1-10 mM. Measurements were taken at a 3 mm GC working electrode at a scan rate is 50 mV s⁻¹. A) Current density. B) Current density per mM of analyte.

Crude measurements taken of the acidity of well synthesised [dema][TfO] estimate the pH to be around 3, thus putting the proton concentration of the liquid in the mM range. A mechanistic change in the Q reaction would be expected as the Q concentration is decreased and becomes similar to the proton concentration. From Fig. 4.5 this suggests that the natural proton concentration for [dema][TfO] is in the low mM range, which would put the pH slightly below 3.

The major reduction is therefore likely to form a deprotonated form of QH₂ such as in reactions 1.4 and 1.5. As further acid is added this then favours the formation of more protonated products as in reactions 1.1 and 1.4. This would also account for the irreversibility of the corresponding oxidation at 0.1 V. Any deprotonated product that does form according to reactions 1.4 and 1.5 will then

subsequently become protonated, resulting in the disappearance of this corresponding oxidation wave.

The electrochemical response for different QH₂ concentrations in [dema][TfO] is shown in Fig. 4.6. As the concentration of QH₂ drops, the oxidation peak at 0.81 V drops at a rate slightly more quickly than the drop in QH₂ concentration. There is also a broadening of this oxidation wave. A larger drop is observed in the height of the corresponding reduction wave at -0.02 V, with this wave being barely visible at a QH₂ concentration of 2 mM.

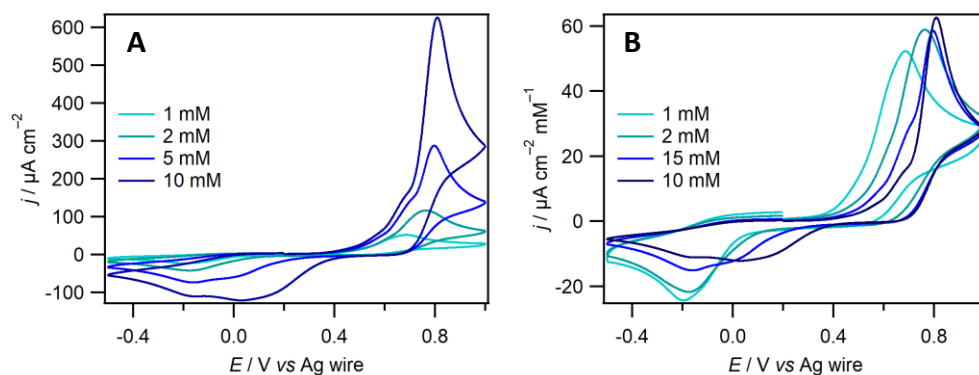


Fig. 4.6: Cyclic voltammograms of QH₂ dissolved in [dema][TfO] at concentrations of 1-10 mM. Measurements were taken at a 3 mm GC working electrode at a scan rate is 50 mV s⁻¹. A) Current density. B) Current density per mM of analyte.

This is likely to be due to the reduced concentration of protons in the liquid as a result of the lower QH₂ concentration. There is also a negative shift in potential for both the oxidation and reduction reactions by -0.12 V. For a 2-proton, 2-electron process as in Rxn. 1.1, a shift of this size would correspond to a pH change of 2 in accordance with Eq. 1.3. This is higher than would be expected if the pure

IL has a pH of 3 or lower. This shift is therefore likely to be a combination of a pH change and other factors, such as changes in the reversibility of the reaction.

The smaller oxidation wave around 0.7 V remains approximately a constant height as the QH₂ concentration is decreased from 10 to 5 mM. This suggests that this is limited by the solution, rather than the concentration of the QH₂ itself at these concentrations. At lower concentrations this then merges with the main peak. The corresponding reduction wave around -0.15 V becomes larger with respect to the QH₂ concentration.

4.3.2 Effect of Excess Acid on the [dema][TfO] solutions

By altering the proton concentration of the solution, the Q and QH₂ reactions can be studied more closely. This enables a better understanding to be gained of the system. In order to increase the proton concentration excess HTfO was added to the 10 mM and 1 mM solutions of both quinone species, with the results shown in figures 4.7 and 4.8.

The electrochemical responses for the Q solutions as increments of additional HTfO is added are shown in Fig. 4.7. Both the 10 mM and 1 mM Q solutions show significant changes when even a small excess of acid is added, as expected for proton dependent reactions. The major reduction peak at -0.3 V decreases in size for both solutions when a small amount of acid is added. The corresponding oxidation cannot be observed when small quantities of acid are added to the 1 mM Q solution and can only just be observed at 0.15 V when closely inspecting

the 10 mM voltammogram. This is similar to that observed at lower Q concentrations in Fig. 4.5.

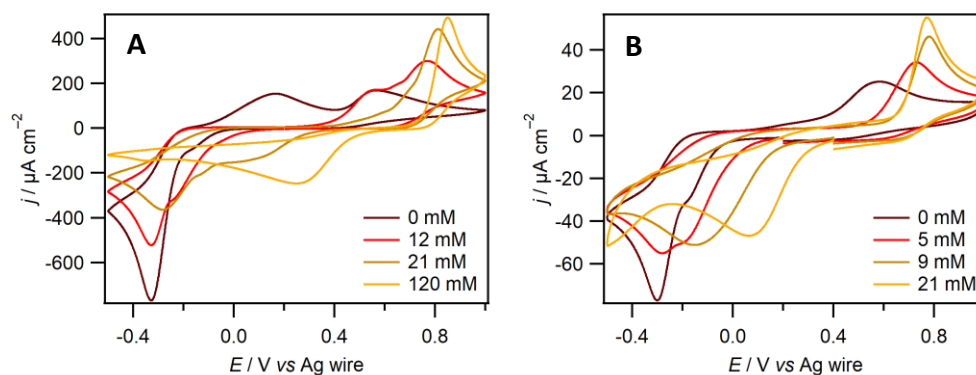


Fig. 4.7: Cyclic voltammogram of 10 mM (A) and 1 mM (B) Q dissolved in [dema][TfO] with varying HTfO concentrations. The voltammograms were taken at a 3 mm GC working electrode at a scan rate is 50 mV s^{-1} . The solution in A uses IL 1.1.

The reduction wave around -0.2 V in Fig. 4.7 increases as acid is added to the solution in both cases, this is therefore likely to be the result of further protonation of Q to QH_2 . A similar effect was also observed when the Q concentration was decreased in Fig. 4.5. At an acid concentration of 21 mM the 10 mM Q solution shows a further reduction wave at -0.1 V . This reduction wave becomes the only observable reduction wave at the highest concentration. For the 1 mM solution in Fig. 4.7 B there are only two observable reduction reactions.

When 12 mM excess acid is added to the 10 mM Q solution in Fig. 4.7 A, two oxidation waves are observed at 0.57 and 0.77 V, along with the small oxidation wave at 0.15 V. However, when no additional acid is present only the oxidation at 0.17 V and one further oxidation at 0.56 V are observed. It is notable that the 10 mM solution uses IL 1.1, and a comparison with Fig. 4.3 and Fig. 4.5 shows that

two oxidations are observed around these potentials when Q is dissolved in IL 1.2. This suggests that both waves initially increase in size when 12 mM of acid is added. As further acid is added the oxidation at 0.68 V continues to increase in size, while the oxidation at 0.56 V decreases in size. At the highest concentration only the oxidation at the highest potential is still visible. There is also an increase in the reversibility of the most positive redox reaction, which is most evident in the 1 mM solution in Fig. 4.7 B.

At the highest concentration an additional reduction reaction occurs due to the reduction of protons due to the excess acid. This is observed at 0.35 V in the 10 mM Q solution, and at lower potentials in the 1 mM solution.

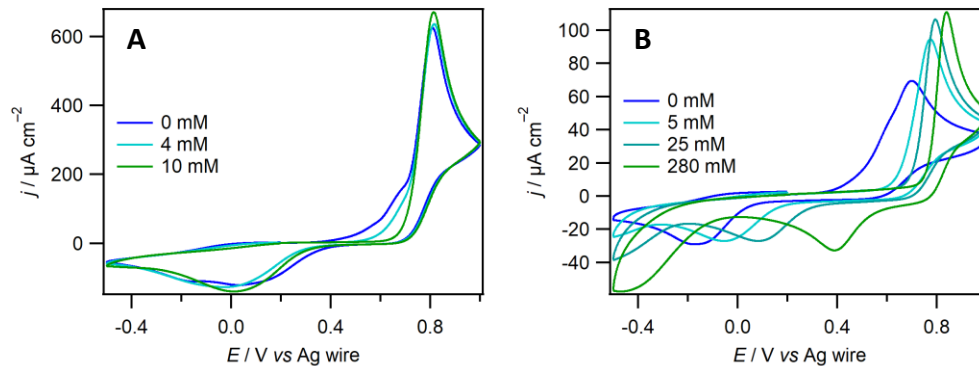


Fig. 4.8: Cyclic voltammogram of 10 mM (A) and 1 mM (B) QH_2 dissolved in $[\text{dema}][\text{TfO}]$ with varying acid concentrations. The voltammograms were taken at a 3 mm GC working electrode at a scan rate is 50 mV s^{-1} .

Fig. 4.8 shows the electrochemical response of 10 and 1 mM QH_2 dissolved in $[\text{dema}][\text{TfO}]$ as increments of additional HTfO are added to the solution. The results for the 10 mM QH_2 solution in Fig. 4.8 A show that when small amounts of acid are added the smaller oxidation waves around 0.45-0.7 V disappear, leaving

only the major oxidation wave at 0.8 V. The reduction waves also merge leaving only a single reduction reaction when 10 mM acid is added.

The 1 mM solution in Fig. 4.8 B also only shows a single peak at higher acid concentrations. The reaction also becomes more reversible and both waves becoming sharper with the peak-to-peak separation narrowing from 0.87 V down to 0.45 V at the highest acid concentration. The reactions also shift to more positive potentials as acid is added. At the highest acid concentrations, the acid reaction is again observed at negative potentials.

A comparison of QH_2 in the absence of acid against Q presence of 21 mM acid is shown in Fig. 4.9 A. At these concentrations there will be similar quantities of protons in each solution, since QH_2 will generate 20 mM of protons upon oxidation. The oxidation reactions are broadly similar with each oxidation wave overlapping indicating that the same oxidation reactions are occurring. In both cases the main oxidation reaction occurs at 0.81 V. Since this oxidation at 0.81 V was shown to be the same as the oxidation at 0.68 V in the 10 mM Q solution in Fig. 4.5, it shows that some QH_2 is being generated in the absence of additional acid.

There is a larger difference between the reduction reactions, with the reductions in the Q solution being negative of those found in the QH_2 solution. This therefore shows that the reduction observed at -0.12 V in the QH_2 voltammogram is the same reduction observed at -0.33 V in the Q voltammogram

in Fig. 4.7 A. Similarly, the oxidation observed at -0.2 V in the Q solution in the absence of acid is observed around 0 V in the QH₂.

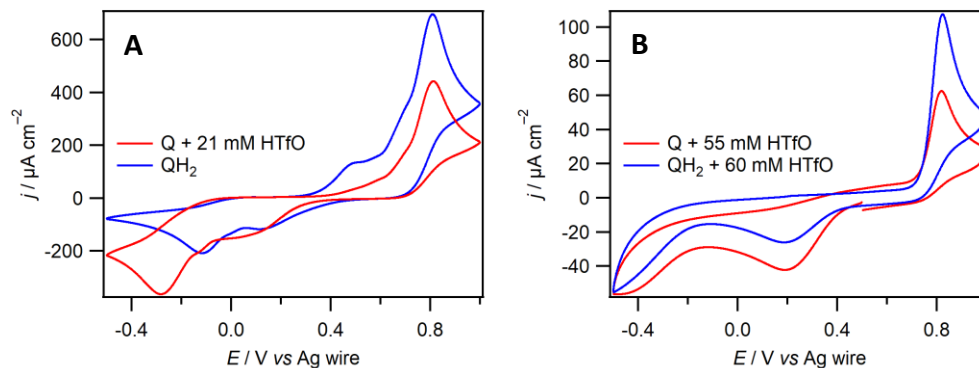


Fig. 4.9: Cyclic voltammograms of QH₂ (blue) and Q (red) dissolved in [dema][TfO] in the presence of similar proton concentrations. A) 10 mM Q with 21 mM excess acid against 10 mM QH₂ in the absence of acid (both use IL 1.1). B) 1 mM Q with 55 mM HTfO against 1 mM QH₂ with 60 mM acid. The voltammograms were taken at a 3 mm GC working electrode at a scan rate is 50 mV s^{-1} .

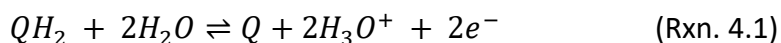
A further comparison is observed in Fig. 4.9 B showing the 1 mM solutions of Q and QH₂ in the presence of a significant excess of acid. Both the oxidation and reduction reactions occur at the same potential showing the same reactions are occurring in each case.

From this it can be concluded that a total of three main reduction reactions and three main oxidation reactions are present in the two solutions. All three reduction reactions appear to shift to higher potentials as acid is added, which suggests protonation is occurring.

The oxidation at the highest potential is observed at 0.81 V in the QH₂ solution in Fig. 4.8 when acid is absent. This wave is also observed in the 10 mM Q solution

in Fig. 4.5 at 0.68 V. As acid is added this becomes the only visible oxidation reaction. This is therefore likely to proceed according to Rxn. 1.1, with the protons coming from the HTfO. The corresponding reduction reaction is most clearly observed in the QH₂ solution in Fig. 4.9 A at 0.12 V and is not visible in the Q solutions when acid is not present.

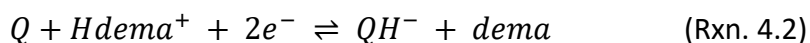
The oxidation wave observed at 0.5 V in the 10 mM QH₂ solution in Fig. 4.9 A is again observed in the 10 mM Q solution in Fig. 4.5. The corresponding reduction is observed around 0 V for the QH₂ solution in Fig. 4.9 A and just positive of the main Q reduction at -0.2 V in the Fig. 4.7. Since this reaction is at a lower potential it shows that deprotonation requires less energy. Since this reaction is still present when small quantities of acid are present it suggests that the product of this reaction is reasonably acidic. Since water is present in small quantities in all the PILs it is likely that this is the proton acceptor with the oxidation proceeding according to the reaction:



This reaction will then continue to occur as long as there is enough neutral water, which will require that the water content is higher than the acid content.

The major reduction reaction observed at -0.33 V in the Q solution in Fig. 4.7 A is also observed in the QH₂ solution in Fig. 4.8 A around -0.15 V. This quickly disappears as acid is added to the solution indicating that this only occurs when

there is insufficient acid to fully protonate Q. The most viable proton source for this reduction reaction is therefore the protonated base. The aqueous pKa of QH⁻ is 11.4 while that of the protonated dema is 10.35, indicating that Q²⁻ is a stronger base in water than dema. Although the pKa values will be altered in the pure IL it is viable that the reaction produces QH⁻ by the reaction:



The aqueous pKa of QH₂ is 8.85, meaning it is unlikely the product would be double protonated. The corresponding oxidation is observed at 0.17 V in the 10 mM Q solution in Fig. 4.7. This oxidation is absent when sufficient protons are present to further protonate QH⁻ to QH₂. The symmetric shape of this oxidation reaction indicates that a surface reaction is occurring, which is likely a result of the neutral dema sticking to the electrode surface.

4.3.3 Effect of excess base on the [dema][TfO] solutions

To substantiate these findings the reactions for Q and QH₂ were investigated in the presence of additional amounts of the base. The results for this are shown in Fig. 4.10.

The voltammetric response for Q in Fig. 4.10 A shows that as base is added the reduction at -0.33 V shifts negatively, supporting the conclusion that this reaction involves protonation. However, there is also a large decrease in the height of the reduction peak as base is added. It is possible that this change is due to a dilution

of the base resulting in less Hdema⁺ being present. This may also be a result of passivation of the electrode surface by the dema.

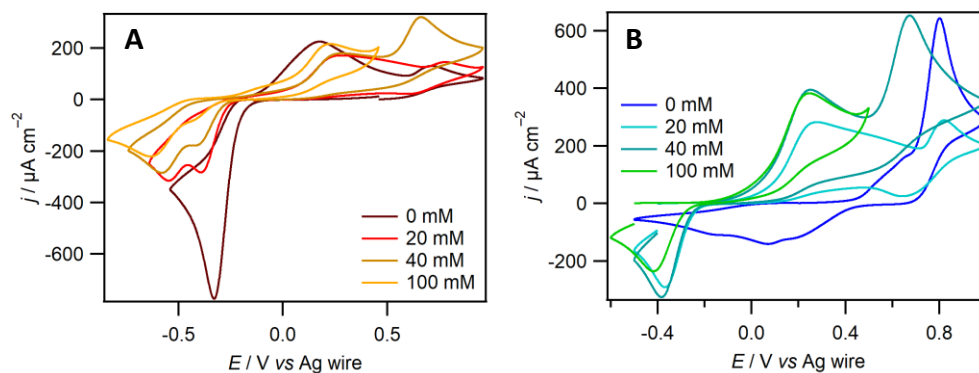


Fig. 4.10: Cyclic voltammogram of 10 mM Q (A) and 10 mM QH₂ (B) dissolved in [dema][TfO] with increasing concentrations of added base. The voltammograms were taken at a 3 mm GC working electrode at a scan rate is 50 mV s⁻¹.

An additional reduction peak also appears at -0.51 V in the solution with 20 mM base. The peak of this reaction is observed to shift negatively, however this may be due to a decrease in reversibility of this reaction at higher base concentrations. It is possible that this reaction occurs due to a depletion of protonated base at the electrode surface, leading to a change in the reduction reaction. The quinone could be taking protons from neutral H₂O, although given that the aqueous pK_a of H₂O is 14 this is unlikely. An alternative is that this involves an unprotonated reduction production Q⁻ or Q²⁻, although further investigation is required to determine this.

The leftmost Q oxidation wave at 0.22 V in the absence of base remains as further base is added, as expected from Rxn. 4.2. However, this becomes slightly less reversible in the presence of base, which might be related to passivation of

the electrode surface. The oxidation at the highest potential remains when the excess base concentration is 20 mM, indicating that small quantities of QH₂ remain. At higher concentrations this becomes engulfed by the base oxidation which is observed at 0.70 V in the solution with 40 mM base.

The response for QH₂ in Fig. 4.10 B shows that as base is added the reaction becomes similar to that observed for Q. These comparisons are seen more clearly in Fig. 4.11 A, where the reduction at -0.33 V in the Q solution is also present in QH₂ when 10 mM of base is added. The corresponding oxidation reaction is also present in both cases, while it was absent when no base was added to QH₂. The further oxidation at higher potentials is also present in both with the oxidation being larger in the QH₂ solution due to the higher proton concentration. In the presence of more base as in Fig. 4.11 B it shows that the additional reduction reaction is not observed in the QH₂ solution when 100 mM of base is present.

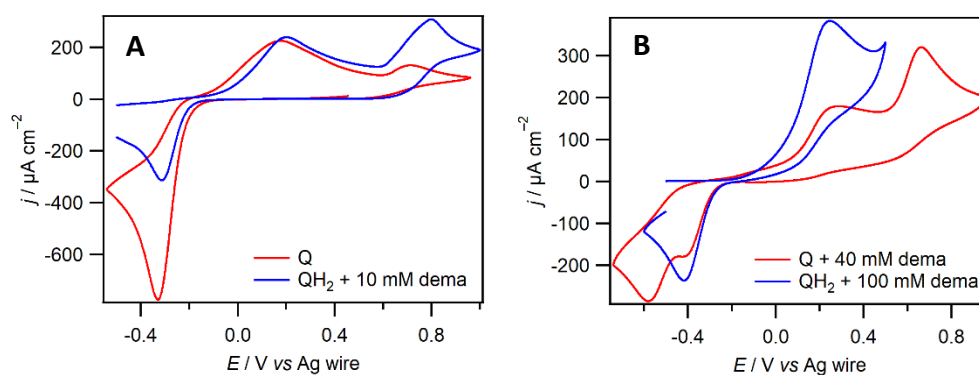


Fig. 4.11: Cyclic voltammogram of 10 mM Q (red) and 10mM QH₂ (blue) dissolved in [dema][TfO] in the presence of base. A) Comparison of Q in the absence of excess dema against QH₂ in the presence of 10 mM dema. B) Comparison of Q in the presence of 40

mM dema against QH₂ in the presence of 100 mM dema. All voltammograms were taken at a 3 mm GC working electrode at a scan rate is 50 mV s⁻¹.

4.3.4 Effect of additional water on the [dema][TfO] solutions

Further substantiation of the findings laid out in section 4.3.2 can be gained by investigating the effects of additional water of the quinone electrochemistry. The results of adding water to 10 mM solutions of Q and QH₂ are shown in Fig. 4.12.

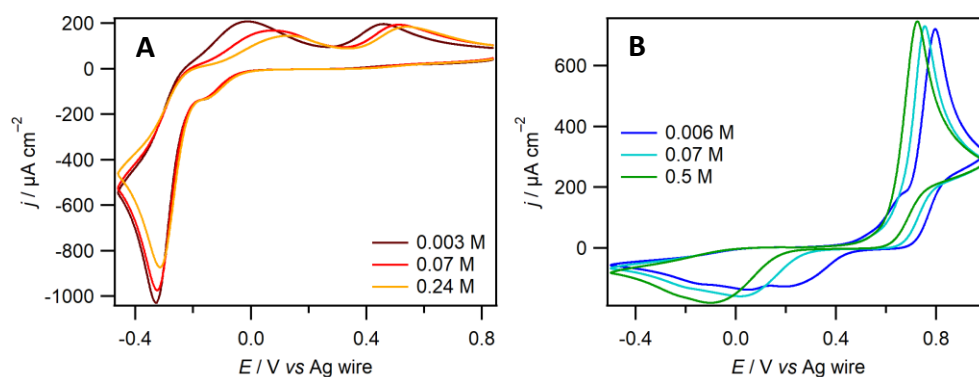


Fig. 4.12: Cyclic voltammogram of 10 mM Q (A) and 10mM QH₂ (B) dissolved in [dema][TfO] with increasing concentrations of added water. The voltammograms were taken at a 3 mm GC working electrode at a scan rate is 50 mV s⁻¹.

The results for Q in Fig. 4.12 A show very little change as the concentration of water is increased from the driest state at 3 mM up to 0.4 M. There is a small drop in the reduction reaction at -0.33 V and also the corresponding oxidation. This may be due to dilution of the solution. There is no change in the reduction reaction at -0.2 V. This is most likely due to the fact that although the water content has increased, the H₃O⁺ concentration will not have changed as the acidity of the solution is constant.

For QH₂ in Fig. 4.12 B, as the water content is increased the main oxidation peak shifts more positively, which is expected due to the higher concentration of neutral H₂O making the deprotonation of QH₂ easier. In addition, only one oxidation reaction is observed indicating that Rxn. 4.1 becomes the major pathway for the deprotonation of QH₂ in this solution. In the absence of additional water, three reduction reactions are observed. However, as water is added the reduction at the highest potential disappears, while the second reduction reaction increases in size. This supports the conclusion that this second reduction involves Rxn. 4.1, since the extra water is picking up the excess protons leading to an increase in the concentration of H₃O⁺ and a drop in other protons from the acid.

4.3.5 Electrochemistry of Q and QH₂ in [tea][TFAc]

Whilst still being classed as a strong acid, Trifluoroacetic acid (HTFAc) is far weaker than HTfO with a pK_a of 0.52 compared to -14.7 for the latter. This will result in a change in the resulting PIL, with this liquid having a larger availability of protons since the ratio of ionised to neutral acid and base will be increased. This will in turn affect the quinone electrochemistry.

The electrochemical response of 10 mM QH₂ (blue) and Q (red) and a 1:1 mix of the two species totalling 10 mM dissolved in [tea][TFAc] are shown in Fig. 4.13. The potential is initially held at 0.2 V then first swept positively for QH₂ or negatively for Q. For the mixture, the data is taken from 0.2 V on the second cycle to ensure maximum height for both peaks.

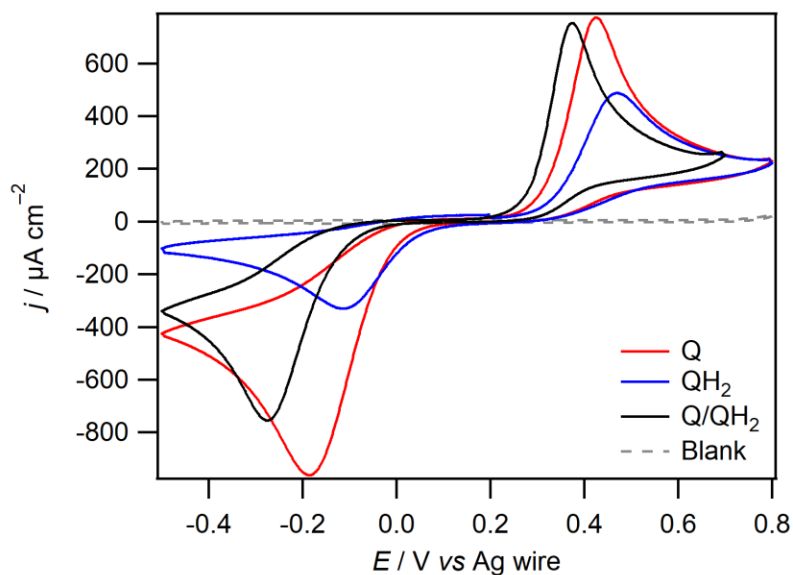


Fig. 4.13: Cyclic voltammogram of 10 mM QH₂ (blue), Q (red), 5 mM each QH₂ and Q (black) dissolved in [tea][TFAc]. The scans were taken at a 3 mm GC electrode at a scan rate is 50 mV s⁻¹.

For both Q (red) and QH₂ (blue), only one reduction and oxidation reaction is observed in each case, and all these reactions are centred at a similar potential indicating that the same process is occurring in each case. Shoup-Szabo fitting of chronoamperometric measurements at a microelectrode were conducted for the Q reduction and QH₂ oxidation. In both cases it was revealed that a 2-electron redox process is occurring. This therefore suggests that these reactions involve the direct conversion of Q to QH₂ as in Rxn. 1.1.

Using a 50:50 mix, as shown in black, similarly reveals a single redox reaction is present indicating the same reaction occurring for Q and QH₂. This reveals that there are adequate free protons available to protonate Q and adequate base sites to deprotonate QH₂. The voltammograms reveal very irreversible voltammetry

with a peak-to-peak separation of approximately 0.6 V for each solution. This is probably due to the slowness of proton transfer in the solutions.

Further investigations on these solutions were carried out by investigating the influence of acid and base on these reactions. The results of these are shown in figures 4.14 and 4.15.

Fig. 4.14 shows the voltammograms of Q (red) and QH₂ (blue) dissolved in [tea][TFAc] when 0.3M HTFAc is added to the solution. The results show very little change occurs, showing that adequate acid is already present in the solution. The reversibility of the reaction does not change significantly in either case, indicating that the main proton source remains the same in each case.

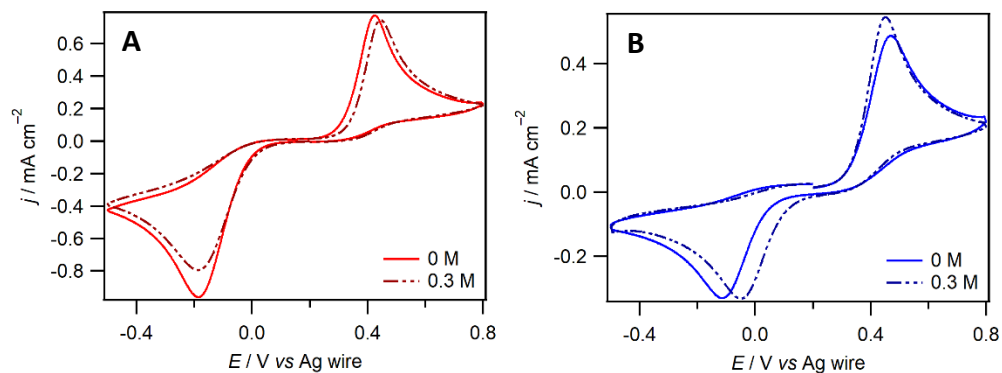


Fig. 4.14: Cyclic voltammogram of 10 mM Q (A) and QH₂ (B) dissolved in [tea][TFAc] before and after an excess of 0.3 M HTFAc. The CVs were taken at a 3 mm GC electrode at a scan rate of 50 mV s⁻¹.

Fig. 4.15 shows the electrochemical response for Q and QH₂ in the presence of an excess of tea against the original solutions. No new reactions are observed indicating that there is still sufficient proton availability on the solution. In both

cases the oxidation shifts to positive potentials, indicating that deprotonation of QH₂ is becoming easier. The reduction peak is observed to increase in size and become sharper. This shows that the reduction is becoming more reversible.

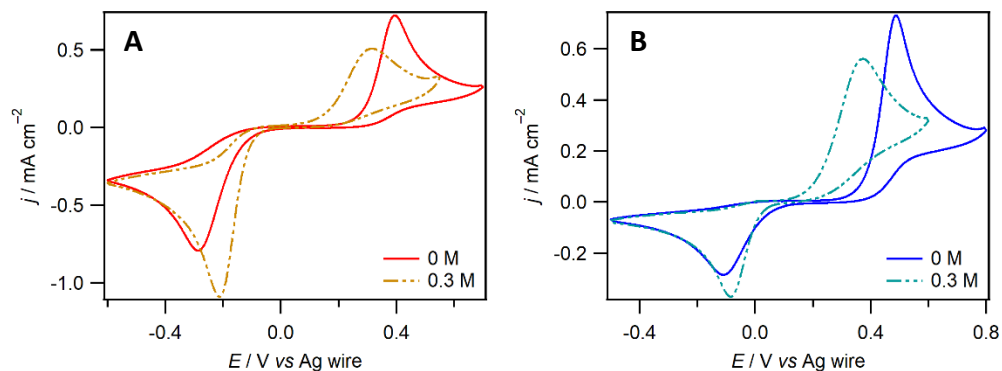


Fig. 4.15: Cyclic voltammogram of 10 mM Q (A) and QH₂ (B) dissolved in [tea][TfAc] before and after an excess of 0.3 M tea is added to the solution. The CVs were taken at a 3 mm GC electrode at a scan rate of 50 mV s⁻¹.

These results show that the original PIL is reasonably well buffered with no significant changes when 0.3M of acid is added to the solution. As base is added a larger difference is observed with the base becoming more reversible.

4.3.6 Electrochemistry of Q and QH₂ in [tea][TfO]

The quinone electrochemical interactions have been studied in both [dema][TfO] and [tea][TfAc], with the differences concluded to be the result of a change in the acid strength. However, the base was also changed. In order to confirm the origin of these differences the electrochemical response of Q and QH₂ was investigated in [tea][TfO]. Since IL was found to crystallise at room temperature when given an appropriate nucleation point, it was therefore

required that the solution was heated to 40°C to ensure the solution remained liquid throughout the experiment. The results of this are shown in Fig. 4.16.

The electrochemical response of 10 mM QH₂ (blue) and Q (red) dissolved in [tea][TfO] are shown in Fig. 4.16. The initial potential is 0.2 V for each solution with the first sweep being positive for QH₂ and negative for Q. Both solutions show similar behaviour to that of [dema][TfO], as expected since the aqueous pKa of dema and tea are similar.

The electrochemical response of Q in Fig. 4.16 shows the same two reductions observed [dema][TfO], as in Fig. 4.3. The first oxidation corresponding to the oxidation of QH⁻, is larger than for the [dema][TfO], although this may be a result of the higher temperature. There is only one other oxidation observed, this may be due to the QH⁻ oxidation peak being larger.

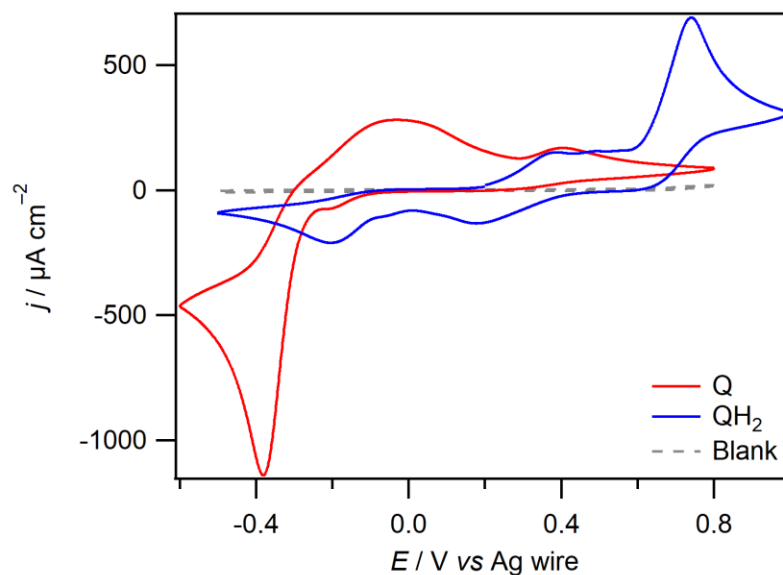


Fig. 4.16: Cyclic voltammogram of 10 mM QH₂ (blue) and Q (red) dissolved in [tea][TfO]. The voltammograms were recorded using a 3 mm GC working electrode at a scan rate is 50 mV s⁻¹. The measurements were taken at 40 °C.

A comparison of the QH₂ voltammetry in Fig. 4.16 with that observed in [dema][TfO] in Fig. 4.3 shows that the voltammetry looks closest to that observed in the [dema][TfO] solution labelled IL 1.1. The major oxidation and its corresponding reduction are similar in both [tea][TfO] and [dema][TfO]. The reduction corresponding to the reduction via the base to QH⁻ is the largest reduction, in line with what is observed in QH₂ in [dema][TfO] 1.1. The oxidation of QH₂ via water is also more similar to that observed in [dema][TfO] 1.1.

While there are small differences between the quinone electrochemistry in [tea][TfO] and [dema][TfO], this is expected due to the change of base and higher temperature. However, the results show that the acid is the main cause for the differences observed between [tea][TFAc] and [dema][TfO].

4.4 Conclusions

The electrochemical responses of Q and QH₂ have been investigated in three PILs. Two of these are synthesised with the very strong acid HTfO, and one with the slightly weaker acid HTFAc.

A comparison of these solutions reveals that when HTfO is used as the acid, the electrochemical responses for Q and QH₂ are different and are very sensitive to even small changes in the acid concentration present in the solution. From the current work it is proposed that three distinct redox reactions occur in both [dema][TfO] and [tea][TfO]. The redox reaction at the lowest potential corresponds to the reduction of Q to QH⁻, with the protons coming from the protonated base in either case as in Rxn. 4.2. The next process involves the protonation of Q to QH₂, with the protons coming from H₃O⁺ as in Rxn. 4.1. The redox reaction at the highest potential also corresponds to the oxidation of Q to QH₂, but with the protons coming more directly from the HTfO.

When acid is added only the oxidation at the highest potential is present indicating that Q is readily protonated to QH₂ upon reduction. When an excess of base is added the reduction of Q to QH⁻ via the base is then favoured due to the decreased proton concentration. An additional reduction is observed at a lower potential when the proton concentration is sufficiently low, possibly indicating the reduction of Q to Q²⁻.

While the electrochemical response of Q and QH₂ in HTfO, based PILs shows significant differences, the response for HTFAC based PILs is similar. Only one oxidation and reduction reaction are observed in the synthesised PIL indicating the conversion of Q to QH₂. This redox reaction was observed to be significantly irreversible with a peak-to-peak separation of above 0.6 V. The addition of acid does not significantly alter the voltammograms, showing that the solution is reasonably well buffered at this point. A larger change is observed in the presence of excess base; however, the same two redox reactions are still observed to occur in both cases.

The results of this study reveal the sensitivity of the Q/QH₂ redox couple to small changes in the proton concentration in the PILs formed from strong acid and base combinations. For TECs a single redox couple is generally preferred to allow for a stable system to be created. To this end Q and QH₂ dissolved in [tea][TFAC] shows this characteristic without further modification. For this couple dissolved in [dema][TfO], non-stoichiometry is required with a large excess of acid added in order to readily generate Q from QH₂.

4.5 References

1. Y. B. Shim, S. M. Park, *J. Electroanal. Chem.*, 1997, **425**, 201-207.
2. M. A. Bhat, *Electrochim. Acta*, 2012, **81**, 275-282.
3. Y. Wang, et al., *J. Electroanal. Chem.*, 2010, **648**, 134-142.
4. S. Ernst, et al., *Chem. Phys. Lett.*, 2011, **511**, 461-465.

5. V. A. Nikitina, et al., *J. Phys. Chem. B*, 2011, **115**, 668-677.
6. H. N. A. Mustafa, et al., *Int. J. Electrochem. Sci.*, 2015, **10**, 9232-9245.
7. A. P. Doherty, et al., *J. Mex. Chem. Soc.*, 2015, **59**, 263-268.
8. P. Navalpotro, et al., *J. Power Sources*, 2016, **306**, 711-717.
9. C. Karlsson, et al., *ACS Appl. Energy Mater.*, 2018, **1**, 6451-6462.
10. D. E. Smith, D. A. Walsh, *Adv. Energy Mater.*, 2019, **9**.

Chapter 5

Thermoelectrochemical studies of Iodide/triiodide in Ionic liquids

5.1 Background

The redox couple has been of particular interest for TECs due to its stability in a wide variety of solvents.¹⁻⁸ This is due to the high solubility and high reversibility of the redox couple in many solvents. In the simplest case, the iodide redox reaction occurs in a single wave according to the reaction:⁹



This results in a single oxidation wave, as observed in water. Since I^- is a Lewis base and I_2 is a Lewis acid, the two will then react chemically according to the reaction:



However, in solvents where the stability constant of $[I_3]^-$ is high, such as is the case for many ILs, the redox reaction changes. Instead of a single redox reaction, two redox waves are observed, which proceed according to the reactions:



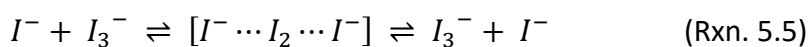
However in both cases the oxidation of I^- will lead to the production of $[I_3]^-$. This redox couple therefore can be used to investigate thermoelectrochemical responses across a range of solvents.

Investigations of 0.7 M $I^-/[I_3]^-$ in water was carried out by Hasan et al.,⁵ with the system producing a $S_e = 0.4 \text{ mV K}^{-1}$. The maximum power output obtained for the system was 245 nW cm^{-2} , although it should be noted the temperature difference here was just $10 \text{ }^\circ\text{C}$.

Abraham et al.¹ carried out investigations of 0.4 M $I^-/[I_3]^-$ in a wide range of solvents. The aqueous system produced $S_e = 0.53 \text{ mV K}^{-1}$. The higher S_e observed compared to that of the investigation by Hassan et al. is due to the lower concentration, with the two generally being inversely related. Abraham et al. also investigated this redox couple in several AILs. They found $[C_2C_1Im][BF_4]$ gave the highest S_e of 0.26 mV K^{-1} out of the ones tested.

Laux et al.⁸ also investigated the thermoelectrochemistry of $I^-/[I_3]^-$ in several ILs, with the highest S_e being 0.97 mV K^{-1} in ethylammonium nitrate. However, this value was for 10 mM of solute, and at when the concentration was increased 0.1 M, the value of S_e dropped to around 0.75 mV K^{-1} . For the 0.1 M solution at $\Delta T = 25 \text{ }^\circ\text{C}$ they achieved a power output of $0.5 \text{ } \mu\text{W cm}^{-1}$. At a concentration of 0.4 M and the same temperature this value increased to almost $1.4 \text{ } \mu\text{W cm}^{-1}$, however at higher temperatures the value began to fall.

ILs can often tolerate high temperatures and have low vapour pressures, which makes them attractive for use in devices requiring high temperatures. However, they also suffer from high viscosities, with observed diffusion coefficients for solutes often several orders of magnitude below that of aqueous systems. This can limit the performance of such devices. However in the case of $I^-/[I_3]^-$, Grothuss-like mechanisms have been identified through the reactions:^{10, 11}



This mechanism is more prevalent when the stability of $[I_3]^-$ is high. The result of this is higher diffusion coefficients can be achieved for the two species provided both are present in the liquid. This system may therefore help to counteract the high viscosities of the liquids, potentially improving the performance of devices employing this system.

The stability of $[I_3]^-$ can be calculated from the difference in the half-wave potentials, $E_{1/2}$, between the two reactions. The value of $E_{1/2}$ is approximately equal to the the mid-point between the two peaks of the redox couple, E_{mid} .⁹ Thus a comparison of E_{mid} for the two redox couples allows comparative analysis on the stability of the $[I_3]^-$ molecule involved in the reactions.

In the present study, the thermoelectrochemistry of $I^-/[I_3]^-$ has been investigated in three PILs and one AIL. The performance in water has also been investigated for comparison. In addition, the voltametric response has been investigated in these liquids at a range of temperatures. The aim is to provide a

full electrochemical study of this redox couple in these liquids and evaluate their performance for use in TECs. By utilising the higher achievable temperatures for such devices it enables higher potential differences to be generated, allowing for further enhancement of the systems.

5.2 Experimental

5.2.1 Chemicals

Reagent grade LiI (99.9%, Aldrich) and I₂ (99.8 % Aldrich) were used as obtained for all measurements. 50:50 mixtures were obtained by dissolving both species at a ratio of 2:1 LiI to I₂. For [I₃]⁻ voltammetry this ratio was 1:1. The reaction was assumed to be heavily in favour of forming [I₃]⁻, although in reality the limit to which this is achieved will depend on the exact stability of [I₃]⁻ in solution.

The acids used were trifluoromethanesulfonic acid (99%, Acros Organics) and trifluoroacetic acid (99%, Aldrich) and bases were diethylmethylamine (98%, Acros Organics) and triethylamine (≥99.5%, Aldrich). The protic ionic liquids were synthesised as outlined in section 3.1, by the addition 1 M acid solution dropwise to 1 M base with a ratio of 1:1.05 acid:base. All solutions were stored in a glove box under a N₂ atmosphere to maintain dryness. The water content for the stock solutions of IL were established to be <100 ppm by Karl-Fischer titration.

5.2.2 Electrochemical measurements

Electrochemical and thermoelectrochemical measurements have been conducted for the redox couple $I^-/[I_3]^-$ in the ionic liquids diethylmethylammonium triflate ([dema][TfO]), dimethylbutylammonium triflate ([dmba][TfO]), triethylammonium trifluoroacetate ([tea][TFAc]), and 1-(2-methoxyethyl)-3-methylimidazolium bis(trifluoromethylsulfonyl)imide ([C₁₀2C₁Im][NTf₂]). For each experiment the results have been plotted with respect to the potential of the $I^-/[I_3]^-$ redox couple.

For all electrochemical measurements an Iviumstat, CHI700D or CHI760B Potentiostat was used for measurements. For voltammetry and when determining diffusion coefficients, a three-electrode isothermal set up was used. This contained a Pt macroelectrode WE, Pt CE and either Ag/AgCl or Ag wire RE. Since the potential of the Ag wire shifted during the experiments the potential was adjusted to be centred on the first redox reaction corresponding to Rxn. 5.1 in water, or Rxn. 5.3 in the non-aqueous systems. Prior to each use, the WE was polished with 0.05 μm alumina suspended in deionised water before being rinsed thoroughly with further deionised water. The solutions used were then purged under N₂ or Ar for a minimum of 15 minutes prior to initial measurements. A constant output of inert gas was then used to maintain an inert atmosphere during experimentation. For experiments involving an increased temperature of up to 120 °C a further measurement was taken as the temperature cooled to 60 °C in

order to observe any permanent changes to the system as a result of the higher temperature.

Diffusion coefficients were calculated using chronoamperometry at a macro electrode as outlined in chapter 3.

5.3 Electrochemical studies

Cyclic voltammograms for LiI and $[I_3]^-$ (as 1:1 LiI:I₂) have been conducted in the four different ILs at temperatures up to 120 °C. Fig. 5.1 shows the voltammetric responses for LiI in the four different ILs at ambient temperature. For each system there are two redox processes due to the presence of reactions 5.3 and 5.4. The difference in amplitude of the two redox waves arises from the 2:1 ratio of electrons passed in the first and second process.

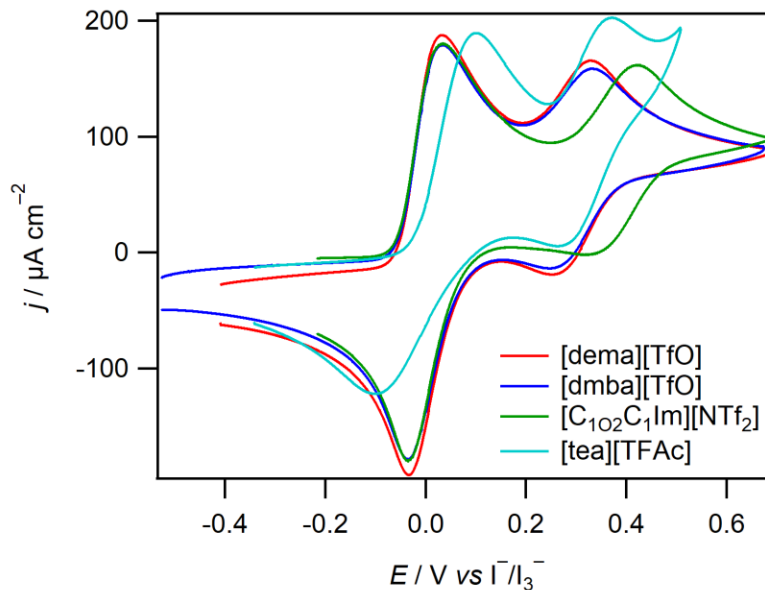


Fig. 5.1: Cyclic voltammograms of 10 mM I_3^- in each of the different ILs at ambient temperature. Each voltammogram was measured using a 0.5 mm Pt WE at a scan rate of 50 mV s^{-1} .

In both [dema][TfO] and [dmba][TfO], the $I^-/[I_3]^-$ voltammograms are very similar, with the redox reactions overlaying well. In these two voltammograms, the first redox reaction corresponding to Rxn. 5.3 has a reasonably good reversibility with peak-to-peak separations of under 70 mV. The second redox reaction is slightly more irreversible with ΔE_p of 78 and 85 mV for in [dema][TfO] and [dmba][TfO] respectively. The difference in E_{mid} is 0.29 V in both systems, suggesting that $[I_3]^-$ is equally stable in each liquid. Calculated diffusion coefficients are also similar, with I^- and $[I_3]^-$ values of 3.3 and $2.9 \times 10^{-7} \text{ cm}^2 \text{ s}^{-1}$ respectively for [dema][TfO] and 2.4 and $2.8 \times 10^{-7} \text{ cm}^2 \text{ s}^{-1}$ respectively for [dmba][TfO].

In [tea][TFAc], the $I^-/[I_3]^-$ redox couple is significantly less reversible with a ΔE_p of 200 mV. Showing that kinetics are significantly limiting the rate of this reaction. The second redox wave, likewise, is less reversible than for the other two IL systems with a ΔE_p of 110 mV. The difference in E_{mid} between the two redox couples is slightly larger than for the other two ILs, with a value of 0.32 V. This suggests a greater stability of the $[I_3]^-$ ion at ambient temperature, however the irreversibility of the two redox couples increases the error in calculations of E_{mid} . The mass transport is slightly higher with diffusion coefficients of $3.5 \times 10^{-7} \text{ cm}^2 \text{ s}^{-1}$ for both I^- and $[I_3]^-$ reflecting the decreased viscosity of this liquid compared to [dema][TfO] and [dmba][TfO].

The reversibility of the $I^-/[I_3]^-$ redox couple in [C₁₀2C₁Im][NTf₂] is very similar to [dema][TfO] and [dmba][TfO] with a ΔE_p of 70 mV for this first redox reaction. However, the second redox couple is less reversible with a ΔE_p of 100 mV. The most significant difference is the difference in E_{mid} , which is 0.37 V, suggesting a significantly higher stability for $[I_3]^-$ in this liquid. Diffusion coefficients were lower in this case at 2.0 and $2.6 \times 10^{-7} \text{ cm}^2 \text{ s}^{-1}$ reflective of this liquid having the highest viscosity of the four.

Figures 5.2-5.5 outline the effect increasing the temperature has on the voltammetry for each of the solutions. In each case the larger current for the $[I_3]^-$ arises from 10 mM of the species being used, and thus three times the equivalent concentration of I^- .

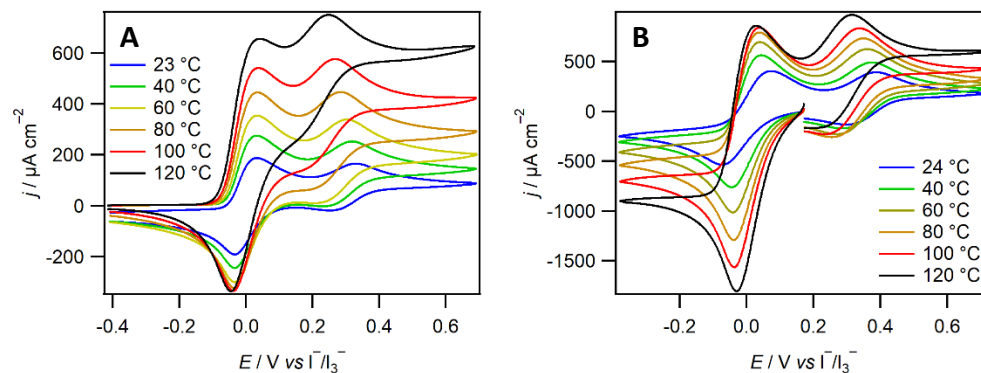


Fig. 5.2: Cyclic voltammogram of 10 mM LiI (A) and $[I_3]^-$ (B) in [dema][TfO] as a function of temperature. Each voltammogram is measured using a 0.5 mm Pt WE at a scan rate of 50 mV s^{-1} .

Figures 5.2 and 5.3 shows the results for the [dema][TfO] and [dmba][TfO] solutions. As the temperature of the solutions increase the most notable change is the decrease in ΔE_{mid} between the two redox couples. In Fig. 5.2 A the value decreases from 0.29 V at ambient temperature to 0.2 V at 120 °C indicating a significant decrease in the stability of $[I_3]^-$ at higher temperatures. Similar changes are observed in the other three sets of voltammograms in these two figures.

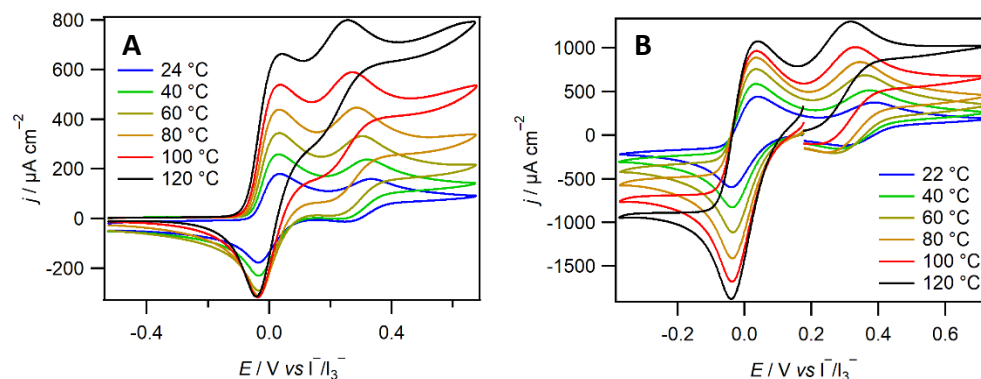


Fig. 5.3 Cyclic voltammogram of 10 mM LiI (A) and $[I_3]^-$ (B) in $[dmba][TfO]$ as a function of temperature. Each voltammogram is measured using a 0.5 mm Pt WE at a scan rate of 50 $mV s^{-1}$.

In each case the waves remained defined showing that there was a high stability of the analyte at these temperatures. In each case after being increased to 120 °C the temperature was reduced back down to 60 °C and a further data set recorded. Both voltammetry and diffusion measurements were found to be in reasonable agreement. This shows that no irreversible side reactions occurred at these elevated temperatures and the electrodes remained clean during the experiments.

Fig. 5.4 shows the voltammetry of LiI in $[tea][TfAc]$ at temperatures up to 60 °C along with voltammetry of $[I_3]^-$ at 24 °C. As the temperature increases, the difference in E_{mid} decreases again indicating a decrease in the stability of the $[I_3]^-$ species. At 60 °C a large increase in the current at potentials above 0.4 V. This is due to the oxidation of the base. At higher temperatures this continued to shift negatively interfering with the second redox process. At a temperature of 120 °C this then began to also interfere with the first redox couple. As the temperature

was reduced back to 60 °C the voltammetry returned to that previously observed at this temperature, indicating no permanent change to the analyte or electrode occurred at high temperatures.

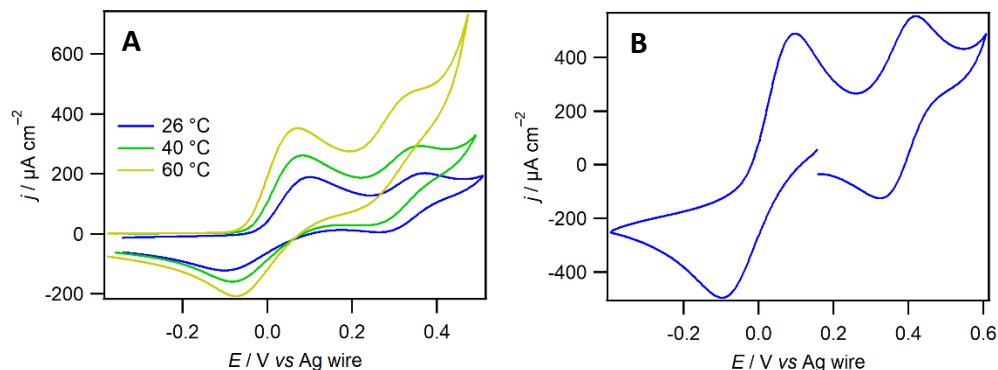


Fig. 5.4: Cyclic voltammogram of 10 mM LiI (A) and $[I_3]^-$ (B) in [tea][TFAc] as a function of temperature. Each voltammogram is measured using a 0.5 mm Pt WE at a scan rate of 50 $mV s^{-1}$.

Fig. 5.5 shows the voltammetric response of I^- and $[I_3]^-$ in $[C_{10}C_1Im][NTf_2]$ as a function of temperature. As with the other systems, ΔE_{mid} is observed to decrease in this liquid as the temperature increases. However, the two redox reactions remained separate and distinct at the highest temperature. Measurements taken after the temperature was reduced back down to 60 °C showed that no additional reactions happened at higher temperatures with the electrodes remaining clean.

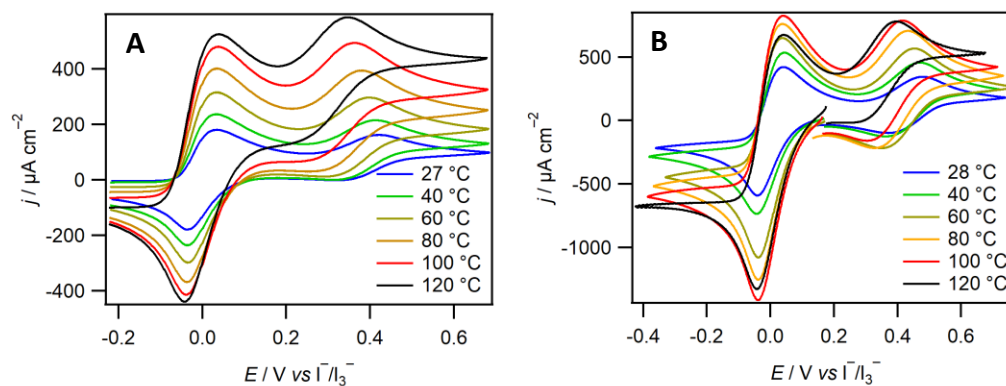


Fig. 5.5: Cyclic voltammogram of 10 mM LiI (A) and $[I_3]^-$ (B) in $[C_{10}O_2C_1Im][NTf_2]$ as a function of temperature. Each voltammogram is measured at 50 mV s^{-1} using a Pt wire reference electrode.

5.4 Thermoelectrochemical studies

Measurements of OCP against ΔT have been measured for $I^-/[I_3]^-$ in the four ILs above. In addition, measurements have been conducted in aqueous $I^-/[I_3]^-$ solution for comparison. The results of this are shown in Fig. 5.6. Water measurements were limited to $\Delta T = 50 \text{ }^\circ\text{C}$ (upper temperature of $70 \text{ }^\circ\text{C}$), due to significant evaporative losses beyond this point. For the rest of the solutions measurements were either recorded up to $\Delta T = 100 \text{ }^\circ\text{C}$ (upper temperature of $120 \text{ }^\circ\text{C}$), or to the point at which the potential became unstable.

For $I^-/[I_3]^-$ in both $[tea][TfAc]$ and $[dema][TfO]$, the potential at the electrodes became unstable before an upper temperature of $120 \text{ }^\circ\text{C}$ was reached.

For $I^-/[I_3]^-$ in $[tea][TfAc]$, this instability was noticed at $\Delta T = 30 \text{ }^\circ\text{C}$. This corresponds to an upper temperature of $50 \text{ }^\circ\text{C}$, which is reflective of the negative potential shift observed in the base oxidation in Fig. 5.4. This then influences the

ability of the hot electrode to establish a stable equilibrium potential resulting in unstable OCP measurements.

For the redox couple in [dema][TfO] the instabilities were noticed above $\Delta T = 50$ °C, which corresponds to an upper temperature of 70 °C. However, the voltammetry for this system in Fig. 5.2 shows that the redox reactions were stable up to the highest temperature of 120 °C. Since the electrochemical response to this solution was so similar to that of the [dmba][TfO] solution, similar thermoelectric stabilities would be expected. However, [dmba][TfO] was observed to be stable up to the highest temperature difference of $\Delta T = 100$ °C. The origin of this instability is therefore difficult to pinpoint from the data.

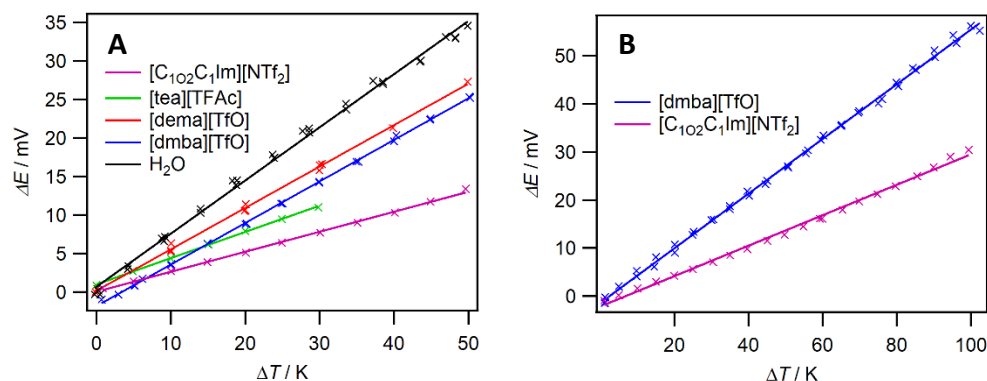


Fig. 5.6: Open circuit potential measurements vs time for 0.1 M $I^-/[I_3]^-$ in [C₁₀₂C₁Im][NTf₂] (purple), [tea][TFAc] (green), [dema][TfO] (red), [dmba][TfO] (blue) and water (black). With the exception of measurements below $\Delta T = 10$ °C, all measurements were taken with a constant lower temperature of 20 °C.

The comparison of all solutions in Fig. 5.6 A shows that the highest S_e was obtained in water, with a value of 0.69 mV K⁻¹. Of the IL solutions, the [dema][TfO] and [dmba][TfO] solutions have the highest S_e of 0.54 mV K⁻¹. The aprotic IL,

[C₁₀₂C₁Im][NTf₂], gave the lowest S_e of just 0.26 mV K⁻¹. The slope of [dmba][TfO] meets a little way below the origin. However, there is a strong trend in this data with deviation from the best fit line being small, suggesting some systematic error such as an offset in the potential measurement in this case.

The highest potential difference observed in these systems is 54.9 mV for the redox couple dissolved in [dmba][TfO]. This was measured at $\Delta T = 100$ °C and is higher than the maximum for the aqueous system, with the highest being 34.5 mV. This difference is due to the lower ΔT of 50 °C for the aqueous system and shows the advantage of being able to obtain higher temperature differences, even if the value of S_e is lower. The [C₁₀₂C₁Im][NTf₂] system was also able to reach $\Delta T = 100$ °C, however the maximum potential was lower than for the aqueous system at 30.4 mV, reflective of the significantly lower S_e .

To attempt to improve the stability of the [tea][TFAc] solution at higher temperatures, the influence of additional water or acid on the system was investigated. The addition of 5% acid, equivalent to approximately 0.7 M may result in the base oxidation shifting to higher potentials, thus stabilising the higher temperature reaction. Although it should be noted the buffered nature of this liquid observed chapter 4.3.5 may limit the extent to which this occurs. The presence of water in the system may increase the reversibility of the system, with the reversibility of I⁻/[I₃]⁻ being far better in water than [tea][TFAc]. This would again reduce the influence of the base oxidation on this reaction.

The results of these experiments are shown in Fig. 5.7. The addition of either water or acid results in a slight increase in the stability of the upper potential, with the solutions becoming stable up to 40 °C in each case. This is in line with what was anticipated when these extra solutes were added to the system. However, the highest obtainable potential is still lower than that obtained for $I^-/[I_3]^-$ in the other liquids.

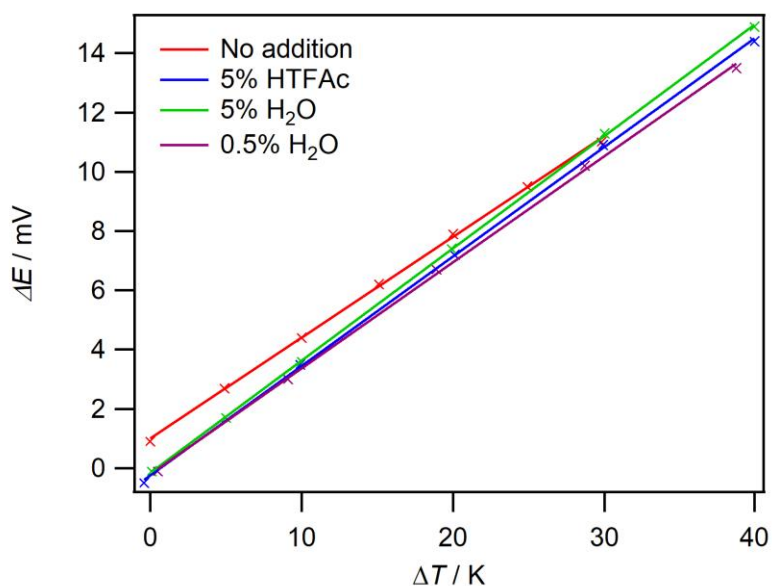


Fig. 5.7: Open circuit potential measurements vs time for 0.1 M $I^-/[I_3]^-$ in [tea][TFAc] with no additive (red), 5% excess HTFAC (blue), 5% excess water (green) and 0.5% excess water (purple). With the exception of measurements below $\Delta T = 10$ °C, all measurements are taken with a cold temperature of 20 °C. All percentages are v/v.

The slope for the system in the absence of additional acid, or water lies further than the origin than the other two systems. However, there is a strong trend in the data which again suggests a systematic error. There is also an increase in S_e when either water or acid are added, although this is relatively small.

Fig. 5.8 A and B show the effect of altering the $I^-/[I_3]^-$ concentration on the aqueous and [tea][TFAc] solutions respectively. In both cases S_e decreases as the concentration is increased as is generally observed for TECs. The stability of the solutions at higher temperatures also increases with increasing concentration. This is seen for the 6 mM aqueous solution in Fig. 5.8 A, where the equilibrium potential could not be established above $\Delta T = 30$ °C. For the [tea][TFAc] solution in Fig. 5.8 B, the potential becomes stable up to $\Delta T = 40$ °C when the $I^-/[I_3]^-$ concentration is increased from 0.1 M to 0.4 M. This difference may be due to the higher current generated from these redox waves, which will further dominate over any small redox waves observed in the solutions, such as the base oxidation in [tea][TFAc].

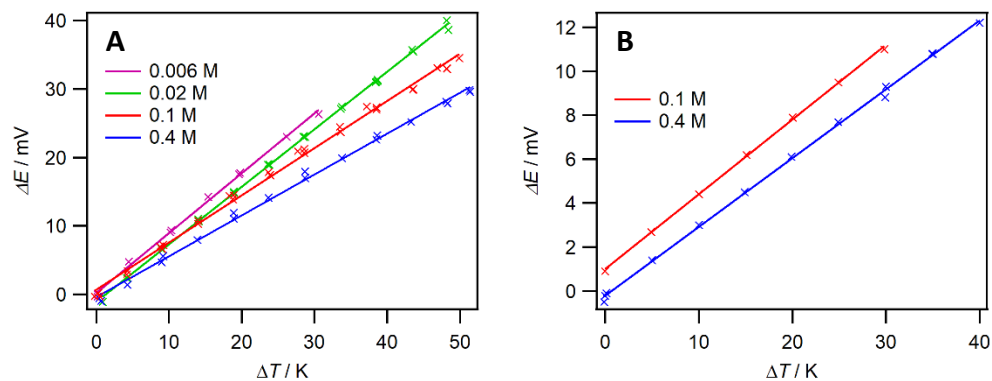


Fig. 5.8: Open circuit potential measurements vs time for $I^-/[I_3]^-$ in water (A) and [tea][TFAc] (B) at analyte concentrations of 6 mM (purple), 20 mM (green), 0.1 M (red) and 0.4 M (blue). Except for measurements below $\Delta T = 10$ °C, all measurements are taken with a cold temperature of 20 °C.

5.4.1 Power measurements

Further to OCP measurements, power outputs were investigated for the solutions at various temperatures. This is to test the performance of the difference systems for TEC applications. Since 0.1 M $I^-/[I_3]^-$ in [tea][TFAc] began to be unstable at these temperatures the power outputs were not obtained for this concentration of analyte in this liquid.

A comparison of the power outputs for the various solutions at 0.1 M at $\Delta T = 30$ °C is shown in Fig. 5.9. The best performance is observed in water with the maximum power, $P_{max} = 2.9 \mu W cm^{-2}$. This is two orders of magnitude higher than the highest for the IL systems of 71 nW cm^{-2} in [dema][TfO], which shows that the viscosity is still having a significant impact of these systems. Despite the same Seebeck coefficient, P_{max} for the [dmba][TfO] system is lower than that in [dema][TfO], with a value of 57 nW cm^{-2} observed in the former. This difference can largely be accounted for by the lower potential difference observed in Fig. 5.6, which is due to the negative offset. Since the power is the product of current and potential, small changes in the potential can have a significant impact on the maximum power calculations, and may suggest some error is present in these calculations. The [C₁₀2C₁Im][NTf₂] system has a far lower power output at 12 nW cm^{-2} , reflective of the much smaller S_e and the high viscosity of this system.

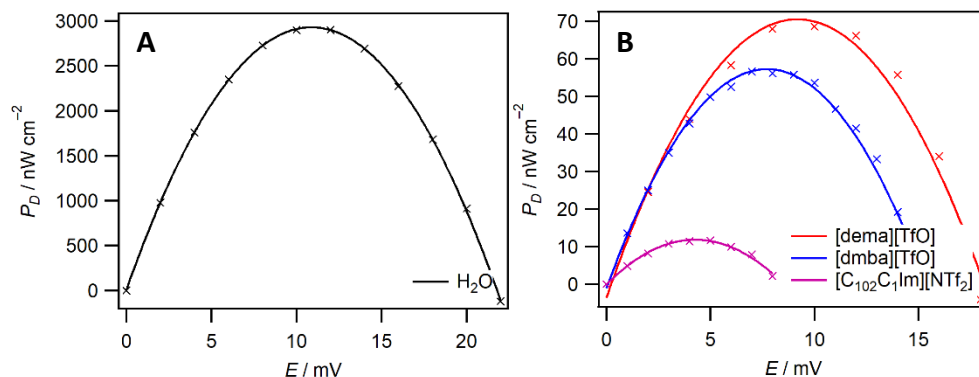


Fig. 5.9: Power density measurements of 0.1 M $I^-/[I_3]^-$ at $\Delta T = 30\text{ }^\circ\text{C}$ in H_2O (black), $[dema][TfO]$ (red), $[dmba][TfO]$ (blue) and $[C_{102}C_1Im][NTf_2]$ (purple).

Fig. 5.10 shows a comparison of 0.1 M $I^-/[I_3]^-$ in the water against the two ILs that reached the maximum temperature difference of $\Delta T = 100\text{ }^\circ\text{C}$. These upper temperatures were used to maximise the power output of each system.

The results show that the aqueous system still provides the highest P_{max} of $8.2\text{ }\mu\text{W cm}^{-2}$ at $\Delta T = 50\text{ }^\circ\text{C}$, which is more than double the value at $30\text{ }^\circ\text{C}$. The highest value obtained for the two ILs is in $[dmba][TfO]$, with a value of 680 nW cm^{-2} . Although this is an order of magnitude improvement on P_{max} at $\Delta T = 30\text{ }^\circ\text{C}$, this is still far below that of the aqueous system. This shows the impact the higher viscosities of the ILs has on the overall power outputs, in spite of the higher potential difference obtained for the $[dmba][TfO]$ system at these temperatures.

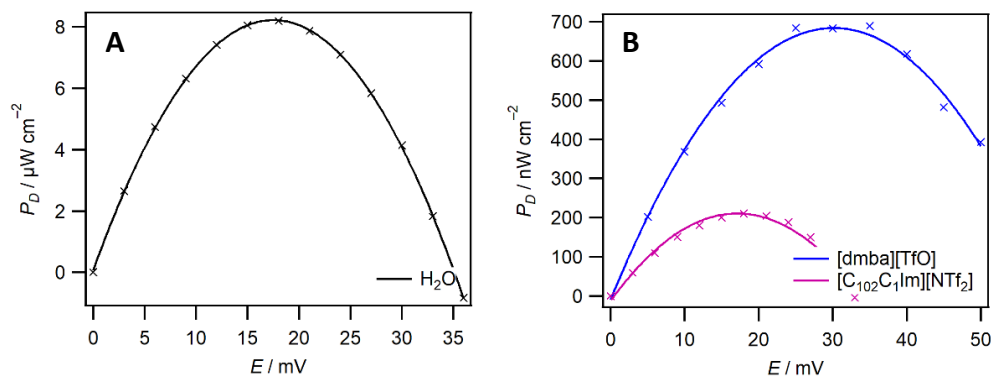


Fig. 5.10: Power density measurements of 0.1 M I^-/I_3^- at $\Delta T = 50^\circ\text{C}$ in H_2O (black), and 100°C in [dmba][TfO] (blue) and [C₁₀₂C₁Im][NTf₂] (purple).

By increasing the amount of solute in the solutions, the power can be further maximised for the systems. Since 0.1 M aqueous I^-/I_3^- produced a significantly higher P_{max} than the [dmba][TfO] and [C₁₀₂C₁Im][NTf₂] systems, this difference would also be expected at an increased concentration. However, this concentration increase allows a comparison to be made with the [tea][TfAc] system, which becomes more stable at this higher concentration.

Fig. 5.11 A shows the results of the aqueous systems at 0.4 M, close to the solubility limit of the analyte in this solvent, at $\Delta T = 30$ and 50°C . Fig. 5.11 B shows power output for 0.4 M I^-/I_3^- in [tea][TfAc]. Due to the instability of this system at higher temperatures the power output could only be recorded at $\Delta T = 30^\circ\text{C}$.

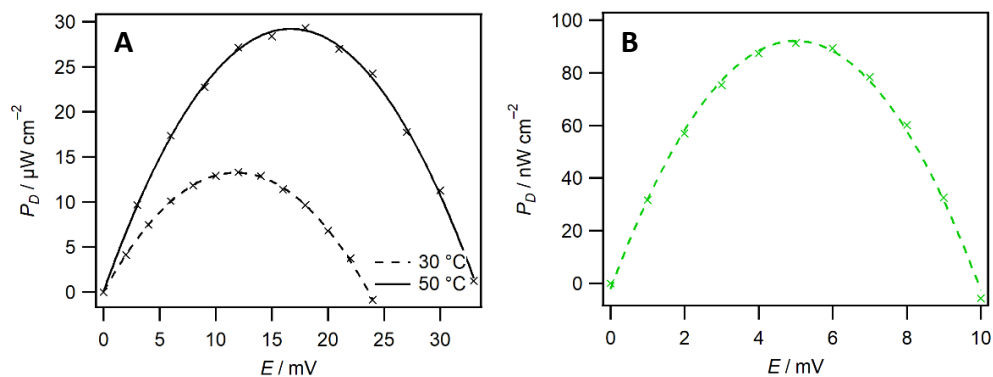


Fig. 5.11: Power density measurements of $0.4 \text{ M I}^- / [\text{I}_3]^-$. A) In H_2O at $\Delta T = 50 \text{ }^\circ\text{C}$ (solid) and $30 \text{ }^\circ\text{C}$ (dotted). B) In $[\text{tea}][\text{TFAc}]$ at $30 \text{ }^\circ\text{C}$.

The aqueous system shows a maximum power output of $13 \mu\text{W cm}^{-2}$ at $\Delta T = 30 \text{ }^\circ\text{C}$ and $29 \mu\text{W cm}^{-2}$ at $\Delta T = 50 \text{ }^\circ\text{C}$. Both represent approximately a 4-fold increase in P_{max} for the 0.1 M solutions reflecting a 4-fold increase in the concentration. The small decrease from this 4-fold increase is likely to be due to the lower potential difference for this higher concentration of the analyte. The highest P_{max} is still far below the value of $150 \mu\text{W cm}^{-2}$ obtained for $0.4 \text{ M } [\text{Fe}(\text{CN})_{3/4}]^{3-/4-}$ in chapter 3, which reflects the lower S_e obtained in the $\text{I}^- / [\text{I}_3]^-$ system.

The maximum power for $0.4 \text{ M I}^- / [\text{I}_3]^-$ in $[\text{tea}][\text{TFAc}]$ is 92 nW cm^{-2} , which is significantly lower than the aqueous system at the same concentration. Since measurements at $30 \text{ }^\circ\text{C}$ for 0.1 M of $\text{I}^- / [\text{I}_3]^-$ in $[\text{tea}][\text{TFAc}]$ could not be obtained, a direct comparison is not possible with these systems. However, assuming a 4-fold decrease would also be present for 0.1 M solutions of $\text{I}^- / [\text{I}_3]^-$ in $[\text{tea}][\text{TFAc}]$ this suggests that this maximum far below the maximum for the other IL systems, reflective of the lower S_e .

5.5 Conclusions

Thermoelectrochemical measurements have been carried out for the $I^-/[I_3]^-$ redox couple in a variety of ILs. The results show that the redox couple is stable in many of the ILs. Instabilities were observed in [tea][TfAc] voltammetry at higher temperatures, which lead to instabilities in the OCP and power measurements of this system when elevated temperatures were used.

The results reveal that the aqueous system provides the highest Seebeck Coefficient for concentrations of 0.1 M with a value of 0.69 mV K^{-1} . This compares to a value of 0.54 in [dema][TfO] and [dmba][TfO], the highest for ILs. These values are still far below -1.55 mV K^{-1} found for the 0.1 M aqueous $[Fe(CN)_6]^{3-/4-}$.

The maximum power outputs were also higher in the aqueous solutions. The 0.1 M aqueous solution produced a power output of $8.2 \text{ } \mu\text{W cm}^{-2}$ at $\Delta T = 50 \text{ }^\circ\text{C}$. However this is far lower than the value of $44 \text{ } \mu\text{W cm}^{-2}$ for 0.1 M $[Fe(CN)_6]^{3-/4-}$ in water. The highest IL system at this concentration was for [dmba][TfO], which had a maximum power output of $0.68 \text{ } \mu\text{W cm}^{-2}$ at $\Delta T = 100 \text{ }^\circ\text{C}$. This value is nearly 10 times smaller than the value for the aqueous system at this concentration.

Power outputs improve with increased concentration for the aqueous system, with a value of $29.2 \text{ } \mu\text{W cm}^{-2}$ obtained at $\Delta T = 50 \text{ }^\circ\text{C}$ for the highest concentration of 0.4 M. This is again far below that of 0.4 M $[Fe(CN)_6]^{3-/4-}$, which was found to be $150 \text{ } \mu\text{W cm}^{-2}$. In both cases, these concentrations are close to the maximum solubility in water. Since the maximum solubility limit for [dmba][TfO] was not

studied, higher values for P_{max} are likely to be obtainable. However given large difference in values and the linear relationship generally observed between the solubility and power output, this system is unlikely to match that of the aqueous $I^-/[I_3]^-$ system, and would still be far less than for 0.4 M aqueous $[Fe(CN)_6]^{3-/4-}$.

5.6 References

1. T. J. Abraham, et al., Chem. Commun., 2011, **47**, 6260-6262.
2. T. J. Abraham, et al., Electrochim. Acta, 2013, **113**, 87-93.
3. H. A. H. Alzahrani, et al., Electrochem. Commun., 2015, **58**, 76-79.
4. E. H. B. Anari, et al., Chem. Commun., 2016, **52**, 745-748.
5. S. W. Hasan, et al., Scientific Reports, 2016, **6**.
6. T. A. Siddique, et al., Rsc Advances, 2016, **6**, 18266-18278.
7. A. Sosnowska, et al., Chemphyschem, 2016, **17**, 1591-1600.
8. E. Laux, et al., J. Electron. Mater., 2016, **45**, 3383-3389.
9. C. L. Bentley, et al., J. Phys. Chem. C, 2015, **119**, 22392-22403.
10. R. Kawano, M. Watanabe, Chem. Commun., 2003, 330-331.
11. C. L. Bentley, et al., J. Phys. Chem. C, 2014, **118**, 22439-22449.

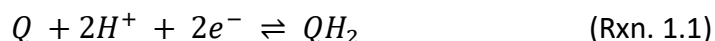
Chapter 6

Thermoelectrochemical studies of hydroquinone and p-benzoquinone

6.1 Background

As outlined in Chapters 1 and 4, the electrochemistry of Q and QH₂ has been studied extensively in both aqueous and non-aqueous systems. However, to the best of our knowledge investigations of these species for use in thermoelectrochemical cells has not been carried out.

As outlined in chapters 1 and 4, the species have shown a good reversibility in buffered aqueous solution, with a single two electron two proton reduction of Q to QH₂¹ as shown in Rxn. 1.1:



In unbuffered, neutral water this reaction only occurs when the pH is lower. At higher pH the Q reduction then forms the deprotonated Q²⁻. The ratio of sizes of these two reactions depends heavily on the pH at the surface of the electrode.

Recently, research has been conducted on the reactions of Q and QH₂ in ILs. In ALLs Q undergoes two single-electron reductions to form Q²⁻ as in reactions 1.8 and 1.9. In order to form QH₂ in these solutions extra acid is required. Research in PILs is more limited, however one recent paper has investigated the use of non-

stoichiometric PILs for protonation of Q.² In this case the non-stoichiometry leads to the presence of both proton donor and acceptor sites.

For a stable TEC to be produced, the electrolyte requires both species of a redox couple to be present in the solution. In general, this requires an equal amount of both the oxidised and reduced form of an electrochemical reaction. For quinones the simplest solution is for the reaction to involve the direct conversion of Q readily to QH₂ as in Rxn. 1.1. This means a protic system is required, which therefore needs to be either sufficiently buffered, or contain an excess of acid or another proton source.

PILs offer an interesting alternative due to the labile proton naturally present in the PIL. If a very strong acid and base are used, such as is the case in [dema][TfO] an excess of acid is required, however this produces a more corrosive solution. The alternative is to use a weaker acid such as HTFAC to form liquids like [tea][TFAC], where there is a wider availability of protons and can act as a buffer.

In this chapter the thermoelectrochemistry of the Q/QH₂ redox couple has been investigated in both buffered and unbuffered water, along with [tea][TFAC] and acidified and as synthesised [dema][TfO]. The aim is to investigate if this redox couple can act as an organic alternative to the commonly used [Fe(CN)₆]^{3-/4-} systems. It is hoped that the protonation will enable a larger entropy change to be observed in this reaction, thus increasing the Seebeck coefficient and maximum power output.

6.2 Experimental

6.2.1 Chemicals

Analytical grade hydroquinone (99%, Acros Organics) and p-benzoquinone (98%, Aldrich) were used as obtained for all electrochemical measurements. Both reagents were stored in a glove box under a N₂ atmosphere to maintain dryness and prevent oxidation.

The ionic liquids were all synthesised from their respective acids and bases. The reagents used were triflic acid (99%, Acros Organics), trifluoroacetic acid (99%, Aldrich), diethylmethanamine (98%, Acros Organics) and triethylamine (≥99.5%, Aldrich). The procedure for this synthesis is as outlined in section 3.1, by the addition of a 1 M acid solution dropwise to a cooled 1 M base solution with an acid-base ratio of 1:1.05. All IL solutions were stored in a glove box under a N₂ atmosphere to maintain dryness.

6.2.2 Electrochemical measurements

Electrochemical and thermoelectrochemical measurements have been conducted for the redox couple QH₂/Q in the ionic liquids triethylammonium trifluoroacetate ([tea][TFAc]), acidified diethylmethanammonium triflate ([dema][TfO]) as well as in buffered and unbuffered aqueous solution.

Electrochemical measurements were conducted in a standard three-electrode cell. For the IL solutions, measurements were carried out under inert conditions in a glove box as outlined in chapter 4. Aqueous measurements were carried out in an Ar atmosphere with a Saturated Calomel Electrode (SCE) as the reference. Each solution was purged for at least 15 minutes prior to the first measurements being carried out. All measurements were conducted using a CHI700D Potentiostat. For IL measurements IR correction was used to account for the solution resistance.

Thermoelectrochemical measurements were conducted in a two-electrode U-shaped cell as outlined in Chapter 3. This consisted of two Pt disk electrodes separated by a distance of 10 cm and kept at different temperatures. Thermoelectric measurements were carried out on either an Iviumstat or CHI700D Potentiostat.

6.3 Results and discussion

6.3.1 Electrochemical Studies

Cyclic voltammograms for 10 mM mix of QH₂ and Q (as 5 mM each) have been carried out in both acidified [dema][TfO] and [tea][TFAc] with the results shown in Fig. 6.1.

For the [tea][TFAc] solution, the electrochemical response shows a single redox peak corresponding to Rxn. 1.1. However, the reversibility of this system is

poor with a ΔE_p exceeding 0.6 V. For the [dema][TfO] solution, acid was required to ensure that QH₂ was produced, since in the absence of acid the deprotonated QH⁻ can also form as in Rxn. 4.7. The reversibility of this acidified solution is slightly better than for [tea][TfAc] with $\Delta E_p = 0.57$ V. However, this is still much higher than for a reversible 2-electron process.

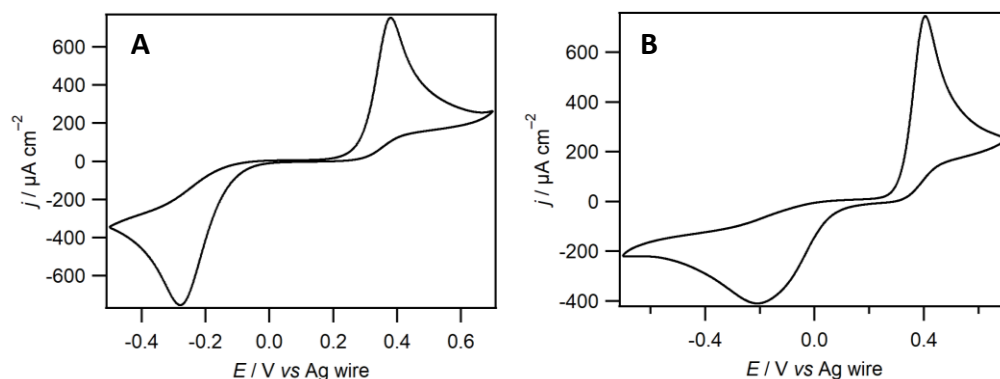


Fig. 6.1: Cyclic voltammetry of a 10 mM mixture of QH₂ and Q (as 5:5 mM) in [tea][TfAc] (left) and acidified [dema][TfO] (right). Each voltammogram is measured using a 3 mm GC WE at a scan rate of 50 mV s⁻¹.

The electrochemical response of both Q and QH₂ were also carried out in aqueous solution in order to compare to literature results, and to ensure a sufficiently buffered solution was produced. The results of this are shown in Fig. 6.2.

Fig. 6.2 A shows the electrochemical response for 5 mM QH₂ and Q in water in the absence of buffer. For Q one major quasi-reversible redox pair is observed corresponding to the two-electron reduction of Q to Q²⁻. For QH₂ the main oxidation corresponds to the oxidation to Q via Rxn. 1.1, with a corresponding

reduction observed at 0.2 V. This reduction is smaller than the oxidation due to the lowering of the pH at the surface. A second reduction is also observed corresponding to the reduction of Q to Q^{2-} as observed for Q. Although there is some crossover between the two reactions the processes are largely separated between the two reactions. These are largely identical to voltammograms observed in the literature outlined in section 1.3.3.

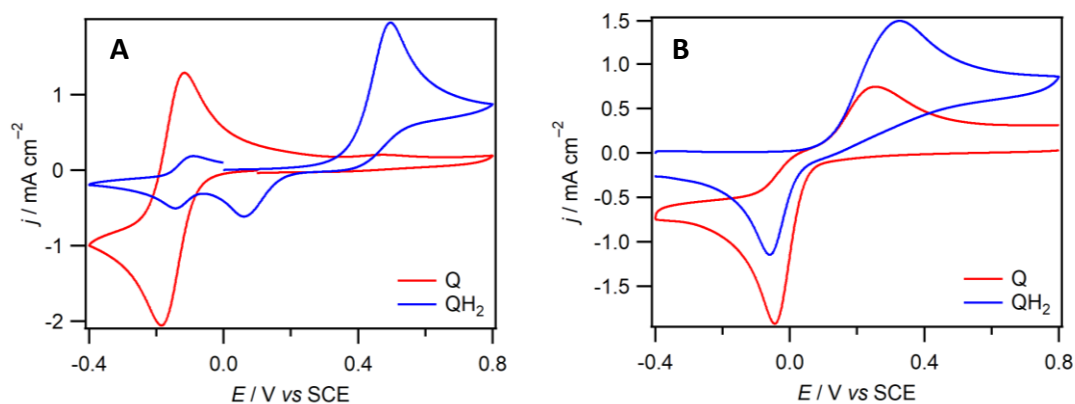


Fig. 6.2: Cyclic voltammogram of 5 mM QH_2 (blue) and Q (red) dissolved in water. A: Solution containing 1 M KCl. B: Solution containing 0.2 M pH 7 NaH_2PO_4/Na_2HPO_4 buffer solution and 1 M KCl. Each voltammogram is measured using a 2 mm Pt WE at a scan rate of 50 mV s^{-1} .

For the buffered solution on the right, only one redox pair is observed in each case corresponding to the conversion of Q to QH_2 as in Rxn. 1.1. However, the processes are not reversible with peak-to-peak separations above 0.3 V. The differences between these and more reversible voltammograms observed in the literature is possibly down to the electrode choice, since the species are known to stick to electrode surfaces such as Pt. However, this electrode was used since the electrodes in the TEC were also Pt.

6.3.2 Thermoelectrochemical studies

OCP measurements have been measured as a function of temperature difference in acidified and non-acidified [dema][TfO], [tea][TFAc] and buffered and unbuffered water. The [dema][TfO] system showed significant instability both with and without excess acid present and thus reliable data could not be obtained. The results for the other three systems are shown in Fig. 6.3. Due to the solubility limits of Q in water, measurements could not be carried out at concentrations of 0.1 M and instead measurements were carried out at 25 mM.

Of the three systems in Fig. 6.3, only the [tea][TFAc] system was found to be stable up to $\Delta T = 50$ °C. The highest Seebeck coefficient was found to be for the buffered aqueous system where the value was -1.08 mV K⁻¹. This then dropped to -0.91 mV K⁻¹ in the unbuffered system. S_e for the redox couple in [tea][TFAc] was lower at -0.51 mV K⁻¹, however this is in part due to the increase in the concentration with 4 times the analyte concentration. The Seebeck coefficient for this redox couple in [tea][TFAc] is therefore higher than that observed for I⁻/[I₃⁻] in the same liquid. The aqueous systems similarly show an improvement with 20 mM I⁻/[I₃⁻] in water showing a lower value of $S_e = 0.84$ mV K⁻¹ despite the lower concentration.

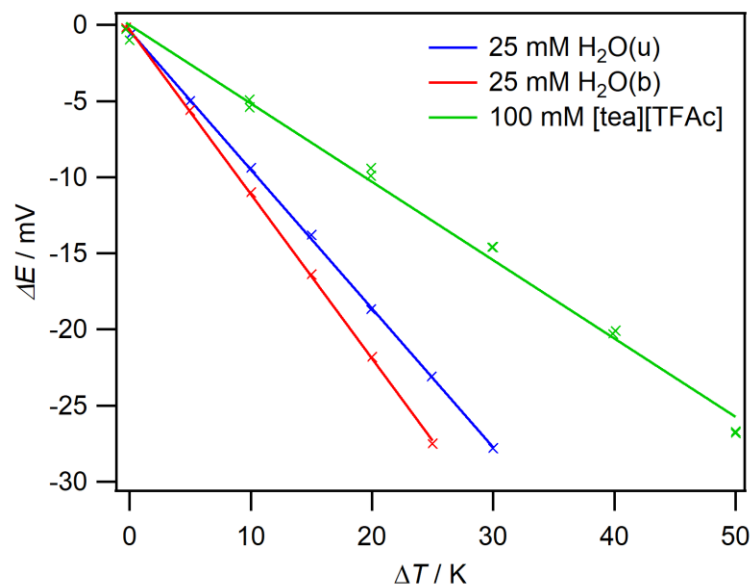


Fig. 6.3: Open circuit potential measurements vs time for 0.1 M QH₂/Q in [tea][TFAc] (green) and 25 mM QH₂/Q in unbuffered water (blue) and buffered water (red). Except for measurements below $\Delta T = 10$ °C, all measurements are taken with a cold temperature of 20 °C.

For the [tea][TFAc] system the OCP was found to be stable up to the maximum temperature used in this case of 50 °C. However, neither of the two aqueous systems were found to be stable above 30 °C, with the buffered system only reaching 25 °C. This resulted in the highest maximum OCP for each system being similar at between -26 to -28 mV.

Further to this, measurements were taken in 50 mM Q/QH₂ in unbuffered water. This was not possible in the unbuffered system, potentially due to the buffer reducing the solubility of Q. The results of this are shown in Fig. 6.4. The increase in concentration of the analyte from 25 to 50 mM in the unbuffered system resulted in a decrease in S_e from -0.91 to -0.79 mV K⁻¹, which is the

expected trend when the concentration is increased. However, the stability of the system increased slightly at the lower concentration, contrary to what was found at low concentrations if I^-/I_3^- in Chapter 5. This difference may be due to 50 mM of analyte being close to the maximum solubility of Q in water.

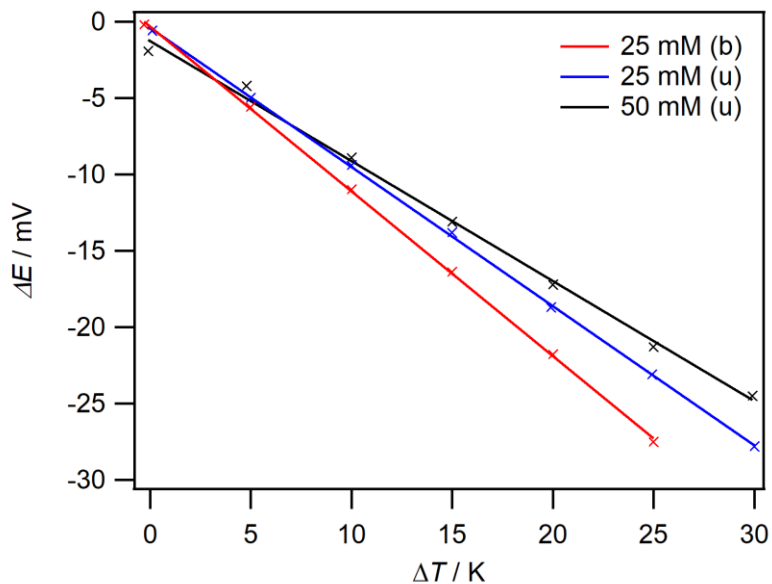


Fig. 6.4: Open circuit potential measurements vs time for 50 mM (black) and 25 mM (blue) QH_2/Q in unbuffered water and 25 mM QH_2/Q in buffered water (red). Except for measurements below $\Delta T = 10^\circ C$, all measurements are taken with a cold temperature of $20^\circ C$.

6.3.3 Power Measurements

Due to the instabilities of the potentials in most of the systems, power measurements at $\Delta T = 30^\circ C$ were only conducted for 25 mM Q/QH_2 in unbuffered water and 0.1 M Q/QH_2 in [tea][TFAC]. Measurements at $\Delta T = 50^\circ C$ were only carried out in the latter. The results for these are shown in Fig. 6.5.

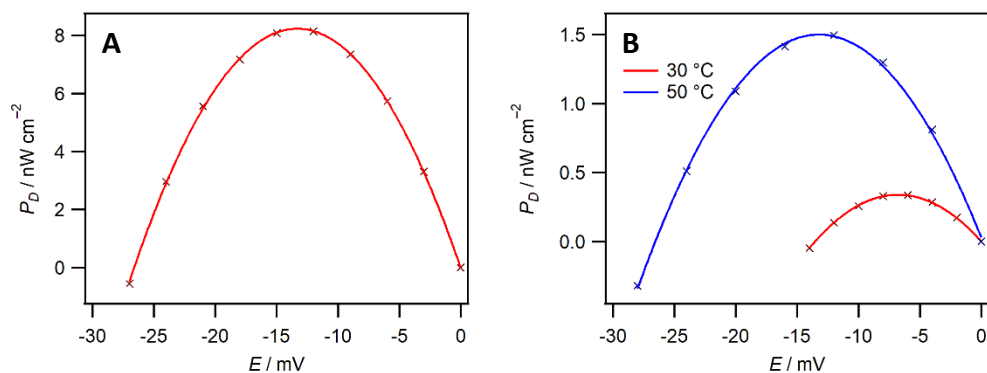


Fig. 6.5: A) Power density measurements at 30 °C for 25 mM QH_2/Q in unbuffered water. B) Power density measurements at 30 °C (red) and 50 °C (blue) for 0.1 M QH_2/Q in [tea][TFAc].

For the aqueous unbuffered system (A), the maximum power density is 8.3 nW cm^{-2} . This is 10 times smaller than the 0.82 $\mu\text{W cm}^{-2}$ for 20 mM of I^-/I_3^- , despite the higher S_e for the Q/QH_2 system. This difference is likely down to the lack of buffer in the system resulting in slower reactions occurring. Since there is a lack of supporting electrolyte in this case it will cause resistances for any Q^{2-} formed, which will further limit the current, and therefore power output. Since higher concentrations cannot be obtained this figure cannot be improved in any significance.

For the [tea][TFAc] system in Fig. 6.5 B, the maximum power for the system at $\Delta T = 30\text{ °C}$ is just 0.4 nW cm^{-2} , rising to 1.5 nW cm^{-2} at $\Delta T = 50\text{ °C}$. Despite the higher concentration and ΔT , the latter power output at is over 5 times smaller than the aqueous system, which is attributed to the high viscosity of the PIL and low reversibility of the redox couple.

6.4 Conclusions

Thermoelectrochemical measurements have been carried out for Q/QH₂ in water and in the PIL [tea][TFAc]. Due to the solubility of the Q in water concentrations were limited to either 25 or 50 mM of the species.

The aqueous Seebeck coefficients were all higher than the values obtained for the IL system. The buffered solution showed an improved S_e with a value of -1.08 mV K⁻¹ compared to -0.91 mV K⁻¹ for the unbuffered system. These are higher than the value of 0.84 mV K⁻¹ obtained for aqueous I⁻/I₃⁻ at a similar concentration (20 mM). However this is still below the value of -1.65 obtained for aqueous [Fe(CN)₆]^{3-/4-} also at 20 mM.

For Q/QH₂ species in [tea][TFAc], the Seebeck coefficient was again higher than that for I⁻/I₃⁻ in the same liquid, with the former having a value of -0.51 mV K⁻¹ compared to 0.34 mV K⁻¹ for the latter.

The stability of the species in [tea][TFAc] was also better than that for the aqueous system with a stable OCP able to be established up to $\Delta T = 50$ °C, while for the aqueous systems the OCP became unstable at temperature differences of between 25 and 40 °C.

Despite the lower maximum concentration and maximum temperature, the unbuffered aqueous system also showed the highest maximum power output of

8.2 nW cm⁻² at $\Delta T = 30$ °C. This compared to 1.5 nW cm⁻² for the [tea][TFAc] solution at $\Delta T = 50$ °C.

A comparison of Q/QH₂ and I⁻/[I₃]⁻ dissolved in [tea][TFAc] shows that the latter provides a higher maximum power output, even at $\Delta T = 50$ °C with a value of 0.17 μW cm⁻² compared to 1.5 nW cm⁻² as already stated for Q/QH₂. This is in spite of the higher S_e for the Q/QH₂ solution. The 2 orders of magnitude difference may be related to the irreversibility of the Q/QH₂ reaction in this liquid compared to the I⁻/[I₃]⁻. If Grothuss-like processes are present, as outlined in section 5.1, these would also play a significant role in increasing P_{max} for the I⁻/[I₃]⁻ solution.

6.5 References

1. J. C. Abbott, J. W. Collat, Anal. Chem., 1963, **35**, 859-863.
2. C. Karlsson, et al., ACS Appl. Energy Mater., 2018, **1**, 6451-6462.

Chapter 7

Thermoelectrochemical studies of metal acetylacetonate complexes

7.1 Background

The electrochemical behaviour of acetylacetonate (acac) complexes have been widely studied in the literature in a variety of organic solvents and ILs.¹⁻¹³ Their widespread availability and good reversibility in many solvents has made them of interest particularly in the field of redox flow batteries. However, to date no investigations have been conducted of these complexes in TECs.

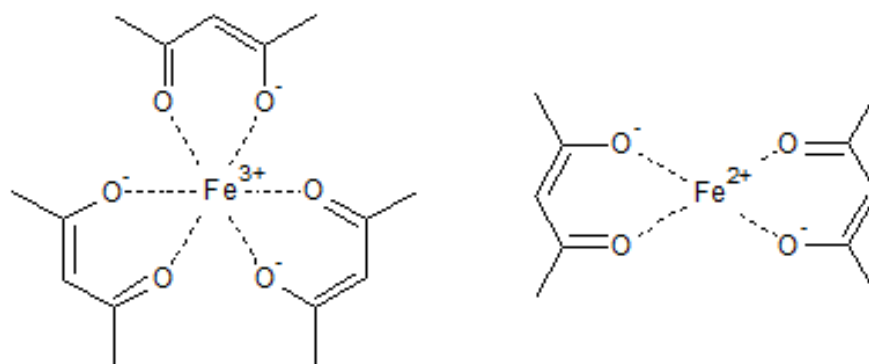
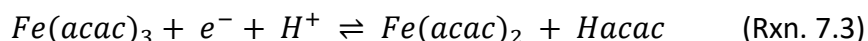
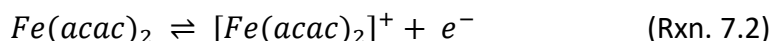


Fig. 7.1: The chemical structures of $Fe(acac)_3$ (left) and $Fe(acac)_2$ (right).

The complication of thermoelectrochemical measurements for these two species lies in the fact that these complexes do not readily interchange between these two species. For example, in organic media the $Fe(acac)_3$ reduction generally involves the addition of an electron resulting in the formation of $Fe(acac)_3^-$. Rather

than the removal of one acac ligand to form $Fe(acac)_2$. The $Fe(acac)_2$ oxidation, likewise, does not gain an additional acac ligand. These pathways are outlined in reactions 7.1 to 7.3.



However, in the context of TECs a single redox couple is generally required, since two different reactions occurring at the electrodes can lead to additional complications and unstable potentials at the electrodes. In addition, the exchange of a ligand may enhance the entropy change associated with the reaction.

The free ligand, acetylacetone, generally exists on its own in two forms as either a diketone or enol, both of which are a protonated form of the ligand. Base is therefore often added during the synthesis of acac complexes in order to deprotonate the ligand and assist in the complex formation. Since [tea][TFAc] acts as a buffer, it was thought that this may therefore allow access to both the protonated and deprotonated forms to exist in solution, thus allowing for the direct conversion between the pairs of complexes.

In this chapter, the electrochemical and thermoelectrochemical analysis has been conducted on several metal acac complexes dissolved in several ILs, where solubility and stability allows. The aim is to investigate if these complexes can

make improvements on the Seebeck coefficients and power outputs of existing systems. It is hoped that the exchange of the acac ligand will enable a higher entropy change of the reaction, and thus provide a high S_e for the system.

7.2 Experimental

7.2.1 Chemicals

Analytical grade $V(acac)_3$ (97%, Aldrich), $VO(acac)_2$ (98%, Aldrich), $Fe(acac)_2$ (97%, Aldrich) and $Fe(acac)_3$ (97%, Aldrich) were used as obtained. The reagents used for the IL synthesis were trifluoroacetic acid (99%, Aldrich) and triethylamine ($\geq 99.5\%$, Aldrich).

The PIL was synthesised as outlined in section 3.1, by the addition 1 M acid solution dropwise to 1 M base with a 5% molar excess of the base. The solution was then stored in a glove box under a N_2 atmosphere to maintain dryness. The water content for the stock solutions was established to be <100 ppm by Karl-Fischer titration.

7.2.2 Electrochemical studies

The solubility of two redox states of four metal acetylacetonate complexes, $Co(acac)_{2/3}$, $Fe(acac)_{2/3}$, $Mn(acac)_{2/3}$ and $V(acac)_2/VO(acac)_3$ were investigated in the protic ionic liquid [tea][TFAc]. Of these only $Fe(acac)_{2/3}$ and $V(acac)_2/VO(acac)_3$ dissolve at a total concentration of 0.1 M. Electrochemical and

thermoelectrochemical studies were therefore carried out for both $\text{Fe}(\text{acac})_{2/3}$ and $\text{V}(\text{acac})_2/\text{VO}(\text{acac})_3$ in $[\text{tea}][\text{TFAc}]$.

Cyclic voltammetry for the $\text{Fe}(\text{acac})_{2/3}$ solutions was carried out inside a nitrogen filled glove box. For the $\text{V}(\text{acac})_3/\text{VO}(\text{acac})_2$ solutions and the blanks, the voltammograms were conducted in dried $[\text{tea}][\text{TFAc}]$ which was purged for each solution for half an hour using a dried Ar gas line prior to each set of measurements being carried out. The cell consisted of a 1 mm or 50 μm diameter Pt WE, a Pt wire CE, and an Ag wire RE. Measurements were recorded either using a CHI700D or CHI760B Potentiostat.

TEC measurements were conducted using a two-electrode U-shaped cell as outlined in Chapter 3. This consisted of two Pt disk electrodes separated by 10 cm and kept at different temperatures. Measurements were carried out on benchtop with no additional inert atmosphere. A CH700D Potentiostat was used to record OCP and current/voltage measurements.

7.3 Results and discussion

7.3.1 Electrochemical Studies of Iron acetylacetonates

Figures 7.2 and 7.3 shows voltammograms for 10 mM $\text{Fe}(\text{acac})_2$ (red) and $\text{Fe}(\text{acac})_3$ in the presence and absence of additional acetylacetone. In the absence of additional acetylacetone in Fig. 7.2, there are two reductions present for each of the complexes. The $\text{Fe}(\text{acac})_3$ reduction at approximately 0.4 V also appears to be present for $\text{Fe}(\text{acac})_2$ with good overlap of the oxidation and reduction, particularly at the microelectrode. The reduction at around -0.6 V is only present for $\text{Fe}(\text{acac})_3$ with an additional oxidation wave also observed at 0.1 V. There is also a small reduction at -0.1 V for $\text{Fe}(\text{acac})_2$ although the no additional oxidation reaction is present in this case.

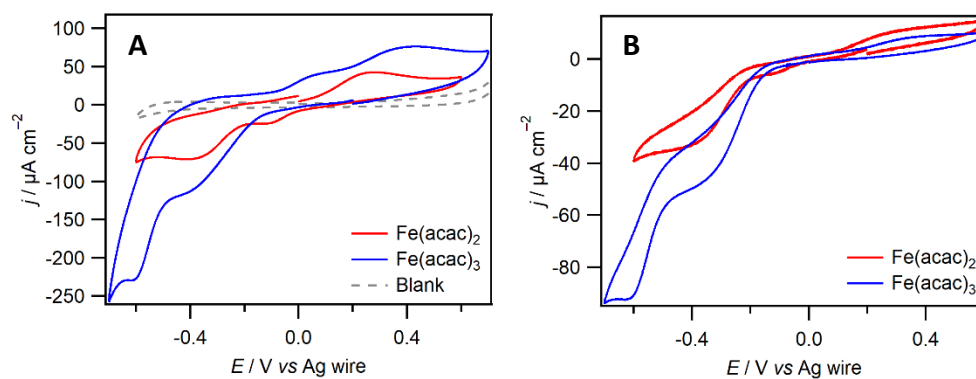


Fig. 7.2: Cyclic voltammograms of 10 mM $\text{Fe}(\text{acac})_2$ (red) and 10 mM $\text{Fe}(\text{acac})_3$ (blue) dissolved in $[\text{tea}][\text{TFAc}]$. A blank voltammogram of only $[\text{tea}][\text{TFAc}]$ (grey) also shown. The cycles were recorded at 50 mV s^{-1} using a 0.1 mm Pt WE (A) or $25 \mu\text{m}$ Pt microdisk electrode (B).

Fig. 7.3 shows the voltammetry of $\text{Fe}(\text{acac})_2$ and $\text{Fe}(\text{acac})_3$ in the presence of additional acetylacetone. For $\text{Fe}(\text{acac})_3$, the voltammetry is similar to the absence of excess acetylacetone in Fig. 7.2, which suggests that the reactions are not significantly changing. However, the second reduction dominates, with the first

barely visible. For $\text{Fe}(\text{acac})_2$, the voltammetry is similar to the $\text{Fe}(\text{acac})_3$ voltammetry in the absence of the excess acetylacetonone, which therefore suggests that the solutions are similar at this point.

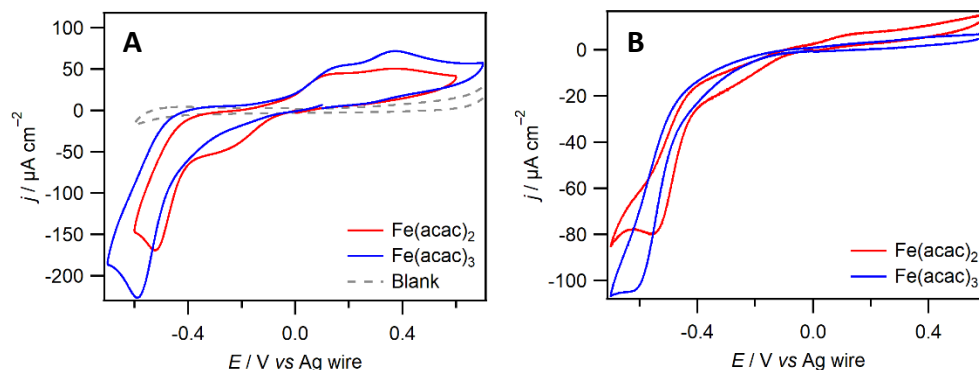


Fig. 7.3: Cyclic voltammograms of 10 mM $\text{Fe}(\text{acac})_2$ (red) and 10 mM $\text{Fe}(\text{acac})_3$ (blue) dissolved in $[\text{tea}][\text{TFAc}]$ with an additional 0.1 M acetylacetonone. A blank voltammogram of $[\text{tea}][\text{TFAc}]$ in the presence of 0.1 M acetylacetonone (grey) also shown. Cycles were recorded at 50 mV s^{-1} using a 0.1 mm diameter Pt WE (A) or 25 μm radius Pt microdisk electrode (B).

A comparison of these two solutions therefore suggests that in the absence of excess acac, the $\text{Fe}(\text{acac})_2$ reaction proceeds according to Rxn. 7.2. This is to be expected since there is an absence of any excess acac. When an excess of acac is then added to this solution this results in the $\text{Fe}(\text{acac})_2$ complex gaining another acac ligand. It is unclear, however, if this $\text{Fe}(\text{acac})_2$ is readily forming $[\text{Fe}(\text{acac})_3]^-$ or whether the ligand is only being gained during the oxidation of this species as in Rxn. 7.3. However, further analysis would be required of these systems, particularly as they reach zero current at the same point.

From chronoamperometric measurements at the microelectrode a total of one electron is passed over the two reductions, thus implying two different pathways are occurring for the reduction of $\text{Fe}(\text{acac})_3$ rather than consecutive reductions of the species. Likewise, in the presence of excess acetylacetonone both $\text{Fe}(\text{acac})_2$ and $\text{Fe}(\text{acac})_3$ are reduced by a total of one electron. In the absence of excess acetylacetonone less than one electron is passed per molecule, which shows that not all of the molecules are reduced. This may therefore suggest that both reactions 7.2 and 7.3 are occurring in these liquids.

7.3.2 Electrochemical Studies of Vanadium acetylacetonates

Fig. 7.4 shows voltammograms for 20 mM of $\text{V}(\text{acac})_3$ or $\text{VO}(\text{acac})_2$ dissolved in [tea][TFAc]. It was found that 10 mM of the species was not significant enough to observe any significant redox waves, so the concentration of each species was increased to 20 mM. In both cases a single redox reaction is observed at potentials just shy of the positive solvent window.

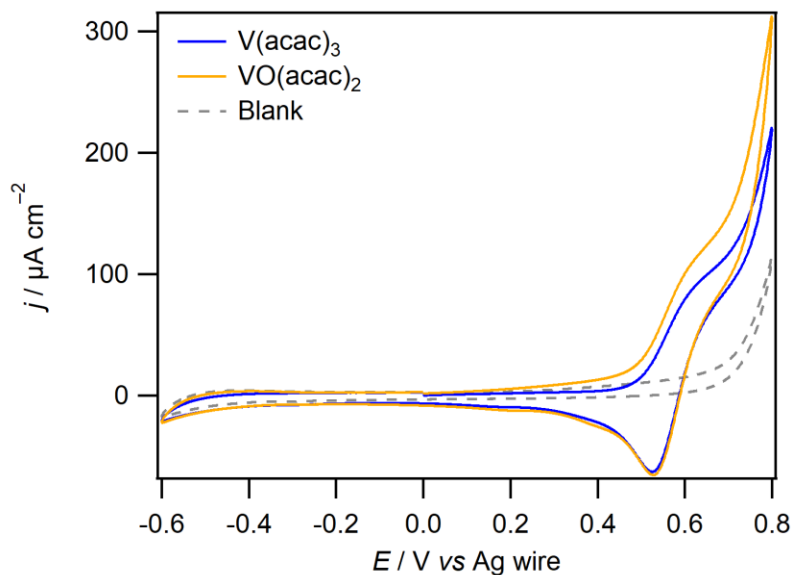


Fig. 7.4: Cyclic voltammograms of 20 mM $\text{V}(\text{acac})_3$ (blue) and 20 mM $\text{VO}(\text{acac})_2$ (yellow), with pure [tea][TFAc] (grey) also shown. The cycles were recorded at 50 mV s^{-1} using a 0.1 mm Pt WE.

The overlap of the two species and the baseline, which is the same in each case, suggests that in both cases the redox species exist in the same reduced state in the solution. A comparison with vanadium dissolved in other ILs, such as in Fig. 2.4 from Ejigu et al.¹ shows similarities to the oxidation of $\text{V}(\text{acac})_3$ to $\text{V}(\text{acac})_3^+$, comparable to that observed in Rxn. 7.2. However there would be insufficient ligands to form this species from $\text{VO}(\text{acac})_2$. The exact identity of the redox reactions is therefore difficult to establish.

The closeness to this solvent window means that calculations of the diffusion coefficients and number of electrons transferred is not possible in this solution.

7.3.3 Thermoelectrochemical studies of acetylacetonates

Thermoelectrochemical measurements were taken of a 50:50 mix of $\text{Fe}(\text{acac})_{2/3}$ in the presence and absence of additional acac. Measurements of $\text{V}(\text{acac})_2/\text{VO}(\text{acac})_3$ in the absence of additional acac were also measured. For $\text{Fe}(\text{acac})_{2/3}$, in the absence of acac, reliable measurements could be taken up to $\Delta T = 30^\circ\text{C}$, above which the potential began to drift. With excess acac present, the potential became unstable even at $\Delta T = 30^\circ\text{C}$. For $\text{V}(\text{acac})_2/\text{VO}(\text{acac})_3$ the measurements were reasonably stable up to 50°C . The results for these are shown in figures 7.5 and 7.6.

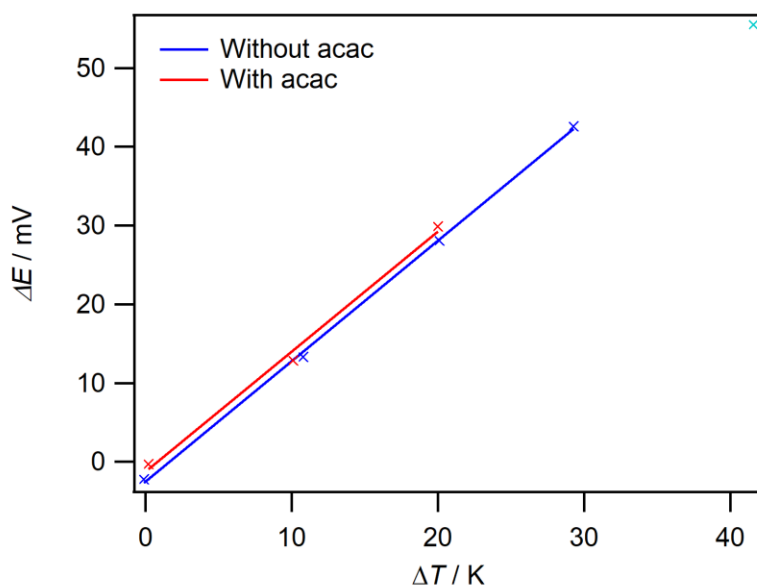


Fig. 7.5: Graph of potential difference vs temperature difference for a $0.1 \text{ M Fe}(\text{acac})_{2/3}$ in $[\text{tea}][\text{TFAc}]$ in the presence (red) and absence (blue) of 50 mM excess acac.

For $\text{Fe}(\text{acac})_{2/3}$ in Fig. 7.5, the solution produces a S_e value of 1.53 mV K^{-1} both in the presence and absence of additional acac, which is comparable to that of $[\text{Fe}(\text{CN})_6]^{3-/4-}$ at the same concentration. However, the instability at temperatures above 30°C limits the maximum observed stable potential. The redox reactions

occur quite close to the negative potential window, as observed in figures 7.2 and 7.3. It is therefore possible that at higher temperatures this affects the redox reactions, meaning a stable equilibrium is not reached.

Due to the instabilities of the $\text{Fe}(\text{acac})_{2/3}$ system, current/voltage measurements were only measured for the species in the absence of additional acac at $\Delta T = 30\text{ }^\circ\text{C}$. However, the current drawn was very small and a constant current could not be drawn from the system with no steady state value being reached. This therefore meant that reliable power measurements for this system could ultimately not be calculated. This likely arises from the lack of a true equilibrium reaction being clear in the solutions.

For $\text{V}(\text{acac})_3/\text{VO}(\text{acac})_2$ in Fig. 7.6, the solutions produce a lower S_e value of -0.56 mV K^{-1} , which is much smaller than for the $\text{Fe}(\text{acac})_{2/3}$ system. S_e is also negative for this system, rather than positive for the $\text{Fe}(\text{acac})_{2/3}$ system indicating a negative entropy change associated with the reduction reaction. The switch from a positive to a negative entropy, as well as the significant decrease in the size of the entropy suggests that very different reactions are occurring in each liquid.

Although S_e was smaller in this case, the system displayed improved stability in the established OCP meaning results could be obtained up to $\Delta T = 50\text{ }^\circ\text{C}$. However, there is a large deviation in the data points from the best fit line, suggesting that the equilibrium potential is difficult to reach. The reason for the higher stability is unclear since again the voltammetry for this species, as seen in

Fig. 7.4 shows that although there is overlap in the redox waves, and the redox reaction is close to the positive potential window. This was observed to severely affect the thermal stability of $I^-/[I_3]^-$ in this liquid, and a similar response may be expected here.

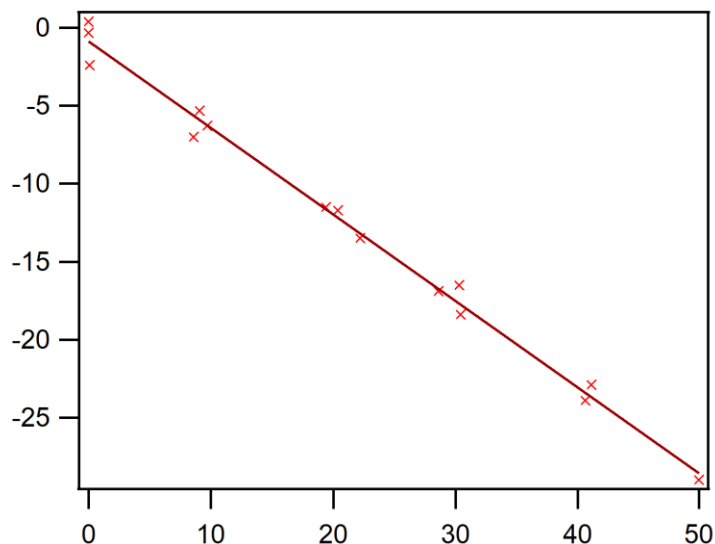


Fig. 7.6: Graph of potential difference vs temperature difference for a 0.1 M $V(acac)_3/VO(acac)_2$ in $[tea][TFAc]$.

Power measurements were attempted for this system at $\Delta T = 30$ and 50 °C, however the current was too small to be detected and reliable results were therefore not obtainable. This likely arises from the equilibrium state of the two species as observed in the voltammetry in Fig. 7.4, which shows that the solution is mostly made up of the reduced state of the species.

7.4 Conclusions

Electrochemical and thermoelectrochemical measurements have been conducted for $\text{Fe}(\text{acac})_{2/3}$ and $\text{V}(\text{acac})_3/\text{VO}(\text{acac})_2$ in $[\text{tea}][\text{TFAc}]$. The results of the voltammetry show irreversible electrochemistry occurring in each case. However, the voltammetry suggests some similarities in the redox states of the different species when dissolved in the solution. It is difficult to draw further conclusions from the voltammetry without further studies on the system.

Thermoelectrochemical measurements reveal that the $\text{Fe}(\text{acac})_{2/3}$ solution has a high S_e of 1.53 mV K^{-1} . Comparable to that of $[\text{Fe}(\text{CN})_6]^{3-/4-}$ at the same concentration. For the $\text{V}(\text{acac})_3/\text{VO}(\text{acac})_2$ solution, S_e was much lower at just -0.56 mV K^{-1} . A stable current could not be drawn from either system, meaning that power measurements could not be conducted for the systems. Ultimately this means that despite the promising S_e these systems in themselves are unviable for application in TECs.

7.5 References

1. A. Ejigu, et al., *Electrochem. Commun.*, 2015, **54**, 55-59.
2. S.-H. Shin, et al., *Rsc Advances*, 2013, **3**, 9095-9116.
3. A. Z. Weber, et al., *J. Appl. Electrochem.*, 2011, **41**, 1137-1164.
4. M. H. Chakrabarti, et al., *Electrochim. Acta*, 2007, **52**, 2189-2195.
5. Q. Liu, et al., *Electrochem. Commun.*, 2009, **11**, 2312-2315.

6. T. Herr, et al., *Electrochim. Acta*, 2013, **113**, 127-133.
7. A. A. Shinkle, et al., *J. Power Sources*, 2014, **248**, 1299-1305.
8. D. Zhang, et al., *J. Power Sources*, 2012, **203**, 201-205.
9. Q. Liu, et al., *Electrochem. Commun.*, 2010, **12**, 1634-1637.
10. A. E. S. Sleightholme, et al., *J. Power Sources*, 2011, **196**, 5742-5745.
11. F.-Q. Xue, et al., *Electrochim. Acta*, 2008, **53**, 6636-6642.
12. M. Mahdavian, M. M. Attar, *Corros. Sci.*, 2009, **51**, 409-414.
13. M. H. Chakrabarti, et al., *Int. J. Electrochem. Sci.*, 2013, **8**, 9652-9676.

Chapter 8

Conclusions and Future Work

8.1 Conclusions

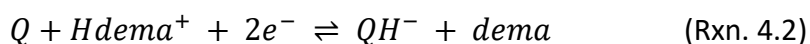
The present work presents several redox couples for use in TECs, largely focusing on the use of these in PILs. The redox couples are $I^-/[I_3]^-$, Q/QH_2 , $Fe(acac)_{2/3}$ and $V(acac)_3/VO(acac)_2$. The work also compares the performance of the first two redox couples in water. In addition, comparisons against aqueous $[Fe(CN)_6]^{3-/4-}$ are drawn, with this system generally being considered the benchmark for TECs.

The $I^-/[I_3]^-$ redox couple is widely used as a comparison in TECs across a range of solvents, due to its widespread solubility and reversibility. The other three redox couples were selected as the additional chemical step may help to increase the entropy change of the redox reaction, leading to higher Seebeck coefficients.

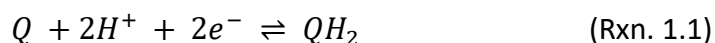
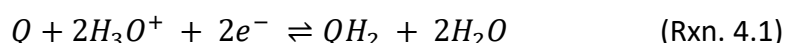
Along with thermoelectric studies, electrochemical investigations using voltammetry and chronoamperometry have been used to understand these systems. A further in-depth study into the electrochemistry of Q/QH_2 in PILs was conducted in order to understand the role that protons in the liquid play in reactions involving proton transfer, such as the Q/QH_2 reactions.

In chapter 4, the results of the Q/QH₂ electrochemistry reveal very different electrochemistry in [dema][TfO] and [tea][TFAc]. The difference in these two situations lies in the strength of the acid involved in the reaction, which leads to changes in the labile proton in the PIL.

The cyclic voltammetry of Q and QH₂ in [dema][TfO] collectively shows three successive redox reactions. It is proposed that the most negative redox reaction involves the reduction of Q to QH⁻, taking the proton from the protonated base according to the reaction:



The second and third redox reactions are proposed to both be the result of the reduction of Q to QH₂. The difference between these two is postulated to be due to the source of the protons with the more negative reduction drawing protons from hydronium ions, while the most positive reduction involves protons coming from the parent acid of the PIL according to the equations:



In the presence of excess acid only Rxn. 1.1 remains, due to this becoming the dominant source of protons. In the presence of base Rxn. 4.2 is the main reaction to remain, due to the depletion of the more acidic proton sources. However, an

additional reduction reaction is observed at lower potentials which is suggested may be due to the reduction of Q to Q^{2-} , although more investigation is required.

In [tea][TFAc] the redox reaction behaves similarly to that observed in buffered aqueous media, with a single two-electron redox reaction occurring, which corresponds to the reduction of Q to QH_2 and vice versa, as in Rxn. 1.1. When adding either acid or base to this solution only small changes occur with no change in the redox reaction.

Chapter 5 investigates the $I^-/[I_3]^-$ redox couple in several PILs as well as one AIL and water. The IL systems produce a lower Seebeck coefficients than the aqueous system, and all show a far lower S_e than for the benchmark system, $[Fe(CN)_6]^{3-/4-}$. Two of the ILs showed good thermoelectric stability at high temperatures, with stable potentials being measured up to a temperature difference of 100 °C. This higher temperature lead to $I^-/[I_3]^-$ in [dmba][TfO] providing the highest potential difference of 54.9 mV.

The power outputs for the IL systems were also significantly below that of the aqueous system, which in turn was lower than that achieved for the $[Fe(CN)_6]^{3-/4-}$ redox couple in water. Although the highest potential difference was established in [dmba][TfO], the power output of this system was still below that observed for aqueous $I^-/[I_3]^-$. This reflected the higher viscosity of the PIL, which leads to lower diffusion coefficients for the redox species.

Chapters 6 and 7 investigate the performance of Q/QH₂, Fe(acac)_{2/3} and V(acac)₃/VO(acac)₂ in [tea][TFAc]. In addition, the Q/QH₂ redox couple was investigated in water. The Fe(acac)_{2/3} system showed the highest Seebeck coefficient of the present study, with a value of 1.53 mV K⁻¹ observed both in the presence and absence of additional acac ligand. However, the power output from this system was poor with no steady current able to be drawn.

The aqueous Q/QH₂ showed a higher S_e than aqueous I⁻/[I₃]⁻ at comparable concentrations. Despite this higher S_e value the maximum power output was observed to be 8.2 nW cm⁻² for this system at a concentration of 25 mM. This compares to 2.6 μW cm⁻² for I⁻/[I₃]⁻ at a concentration of 20 mM. The power output for this aqueous is insignificant compared to the value of 150 μW cm⁻² for aqueous [Fe(CN)₆]^{3-/4-}, and solubility limits prevent significant improvement of this value.

Overall, the present work shows that the potential of these systems for employment in TECs is limited. Neither the acac complexes nor the quinones were shown to perform well in these devices with power outputs severely limited. The I⁻/[I₃]⁻ redox couple also performed poorly in comparison to the benchmark [Fe(CN)₆]^{3-/4-} system.

The use of ILs allowed higher temperatures and potential differences to be obtained for some of these experiments. However, the power output of these systems was still severely limited due to the high viscosities of these liquids.

Although the thermoelectric performance of these systems was limited, a good knowledge was gained from the electrochemical studies of both the $I^-/[I_3]^-$ and Q/QH_2 systems. The $I^-/[I_3]^-$ studies showed these species being stable up to higher temperatures in a range of ILs and provided an understanding of how the temperature increases influence these reactions.

However, the most promising studies came from the electrochemical analysis of Q and QH_2 in PILs. The study provides a good understanding of how these molecules behave in the two PILs used and allows for further work to be built in this foundation.

8.2 Future Work

For the thermoelectrochemical work all the systems fall below the performance of the benchmark $[Fe(CN)_6]^{3-/4-}$. Of the analytes investigated, $I^-/[I_3]^-$ shows the most room for further investigation with one possibility being to vary the concentration of the species in the ILs. The performance of $I^-/[I_3]^-$ in these ILs is unlikely to match that observed in water. However, this may provide some useful insight into whether Grothuss-like mechanisms readily occur in these systems with this type of interaction expected decrease at lower concentrations.

Another direction for this could be to investigate other redox couples. The majority of studies to date have focused on metal complexes, and investigating some organic compounds could be an option. (2,2,6,6-Tetramethylpiperidin-1-

yl)oxyl (TEMPO) is one which shows good reversible electrochemistry in water and therefore may present a good option.

The most promising work is on the electrochemical studies of Q and QH₂ in chapter 4. While providing a good foundation, this work provides a lot of scope for further investigation on the electrochemistry of these species in PILs. To further this work a wider range of acid strengths could be used with the electrochemical responses investigated. Particular focus could be paid to acids with strengths that lie between that of the acids used in the present study. This would enable a closer study of the transition between buffered and unbuffered systems.

In addition to this, another direction could be to investigate the use of stronger bases in the PIL. This would enable a closer study of the Q/QH⁻ redox couple, since a stronger base should then fully deprotonate the reduced species. In addition, a closer look at the base interactions with a more gradual addition of base to [dema][TfO] may provide a better insight into the interactions between that and the quinone species.

The Q/QH₂ study in [tea][TfO] could also be expanded, with further investigations on the influence of acid, base and water on this system. This would enable further confirmation of whether the conclusions drawn from the [dema][TfO] system are valid.